

Supplementary Information for

**Profiling of basal and ligand-dependent GPCR activities by means of a polyvalent
cell-based high-throughput platform**

Manel Zeghal¹, Geneviève Laroche¹, Julia Douglas Freitas¹, Rebecca Wang¹, Patrick M.
Giguère^{1,2*}

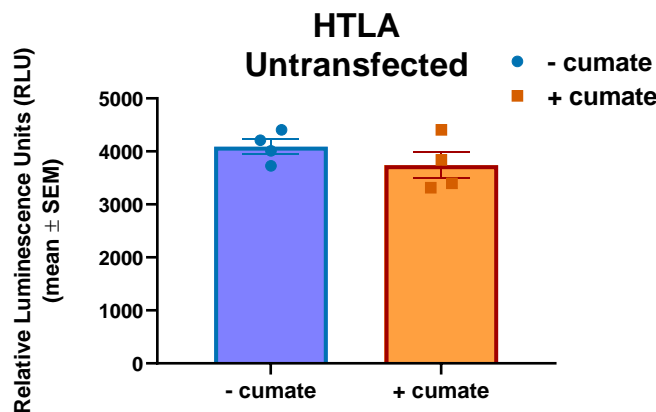
¹ Department of Biochemistry, Microbiology and Immunology, University of Ottawa, Ottawa, ON, K1H8M5, Canada

² Brain and Mind Research Institute, University of Ottawa, Ottawa, ON, K1H8M5, Canada

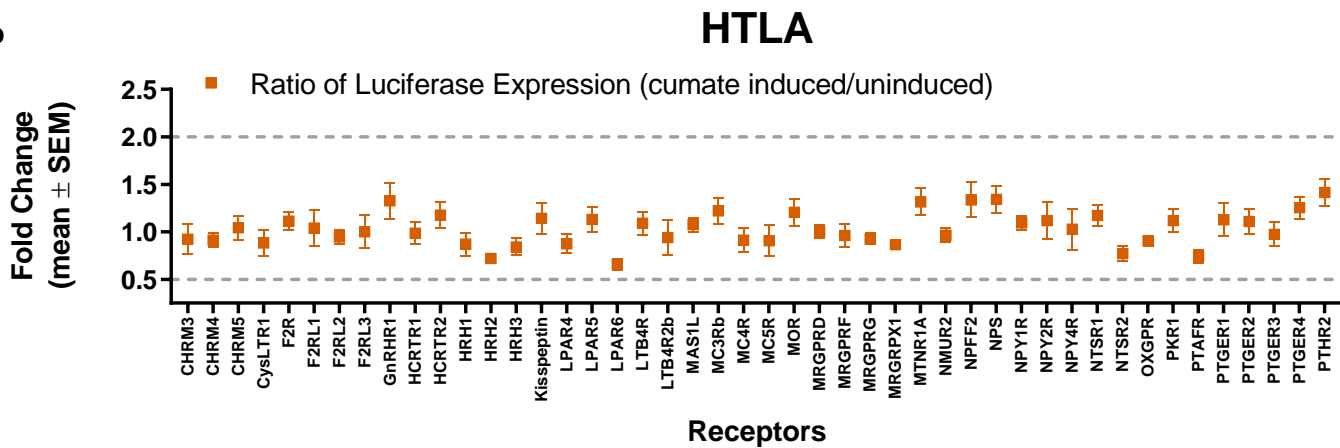
*Correspondence to Patrick M. Giguère. Email: patrick.giguere@uottawa.ca

Supplemental Figures

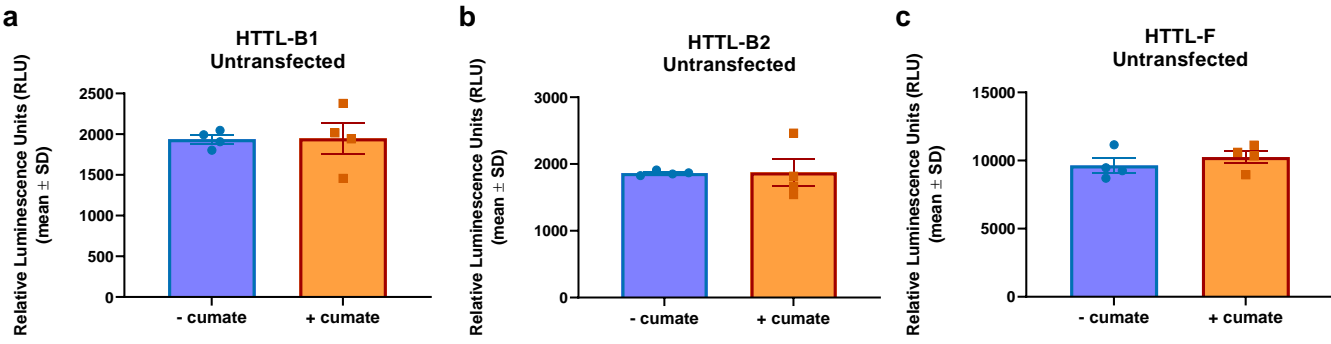
a



b

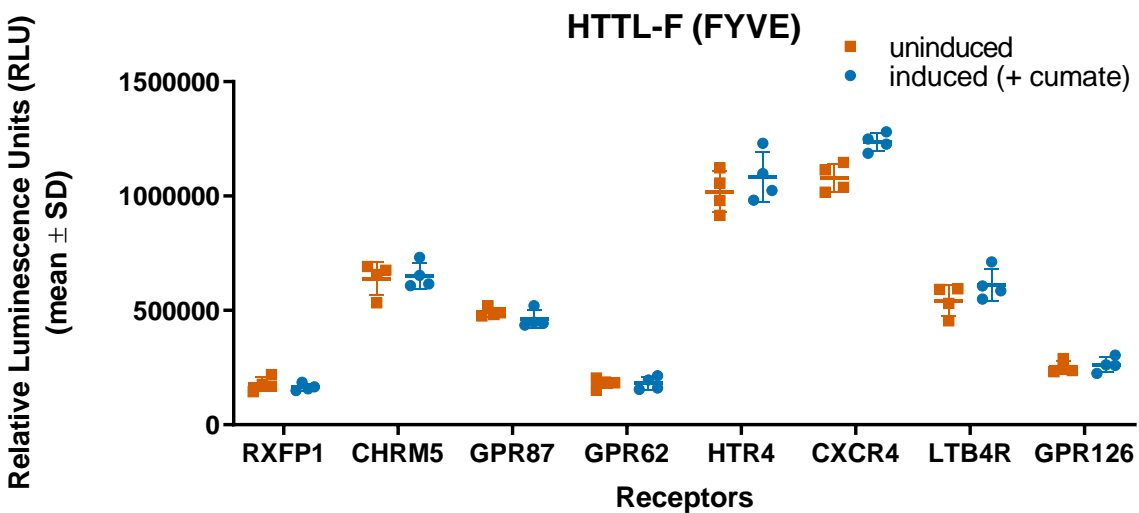
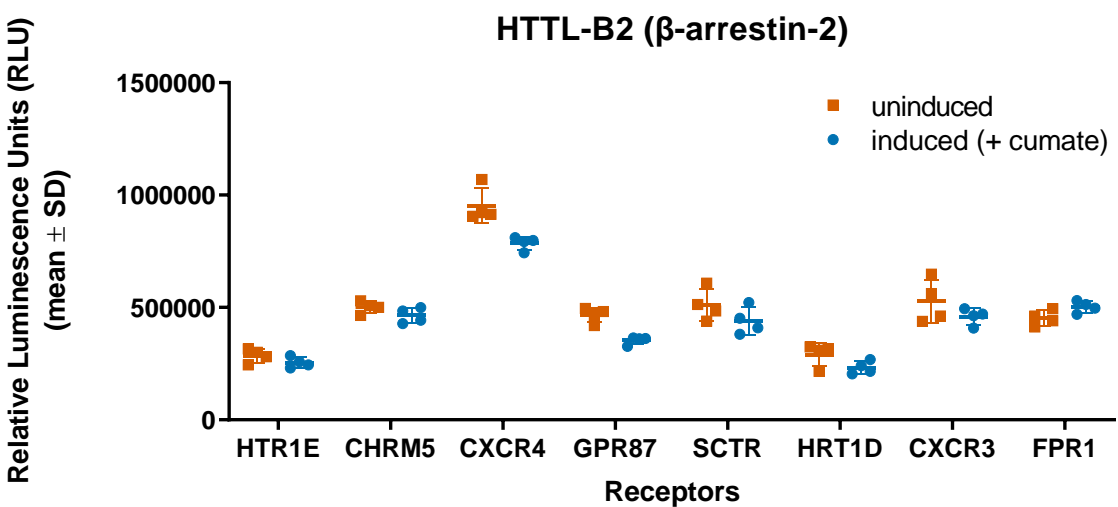
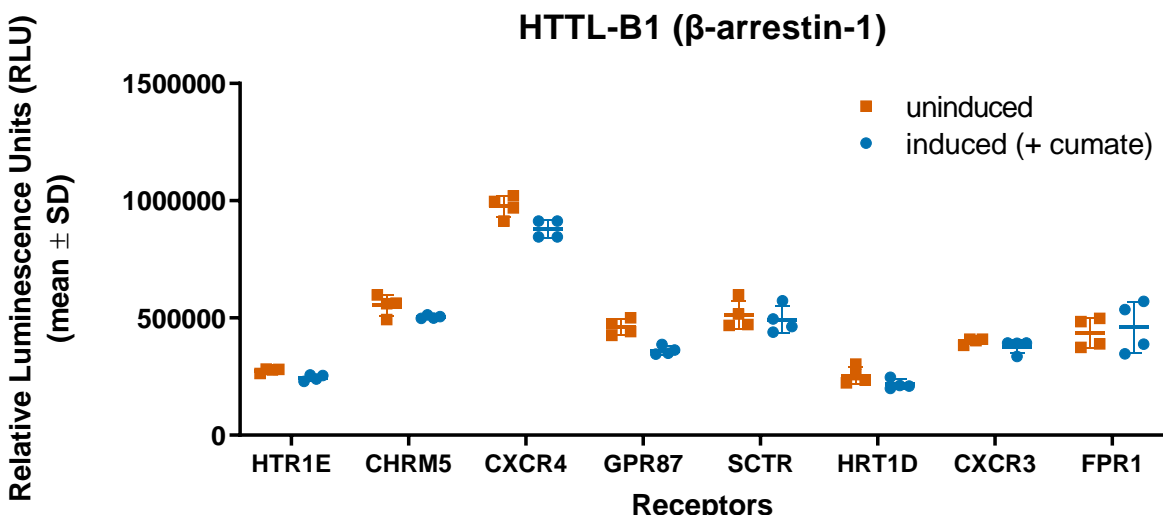


Supplementary Figure 1. Assessment of the effect of cumate in the PRESTO-Tango (cumate-independent system). To confirm that cumate itself does not possess any agonistic or antagonistic properties in a cumate-independent system, HTLA cells from the PRESTO-Tango platform were plated in the presence and absence of cumate (30 μ g/mL) (a) and were transfected with a panel of diverse GPCR Tango constructs (b). 96 hours following its initial addition, fold changes in basal arrestin recruitment were calculated between the wells in the absence or presence of cumate. Data are presented as mean values, with error bars representing SEM (Supplementary Fig 1A: n = 12, with 3 technical replicates from 4 biological samples; Supplementary Fig 1B: n = 4, with 4 technical replicates from one biological sample). Generic receptor codes refer to the GPCR-Tango constructs.



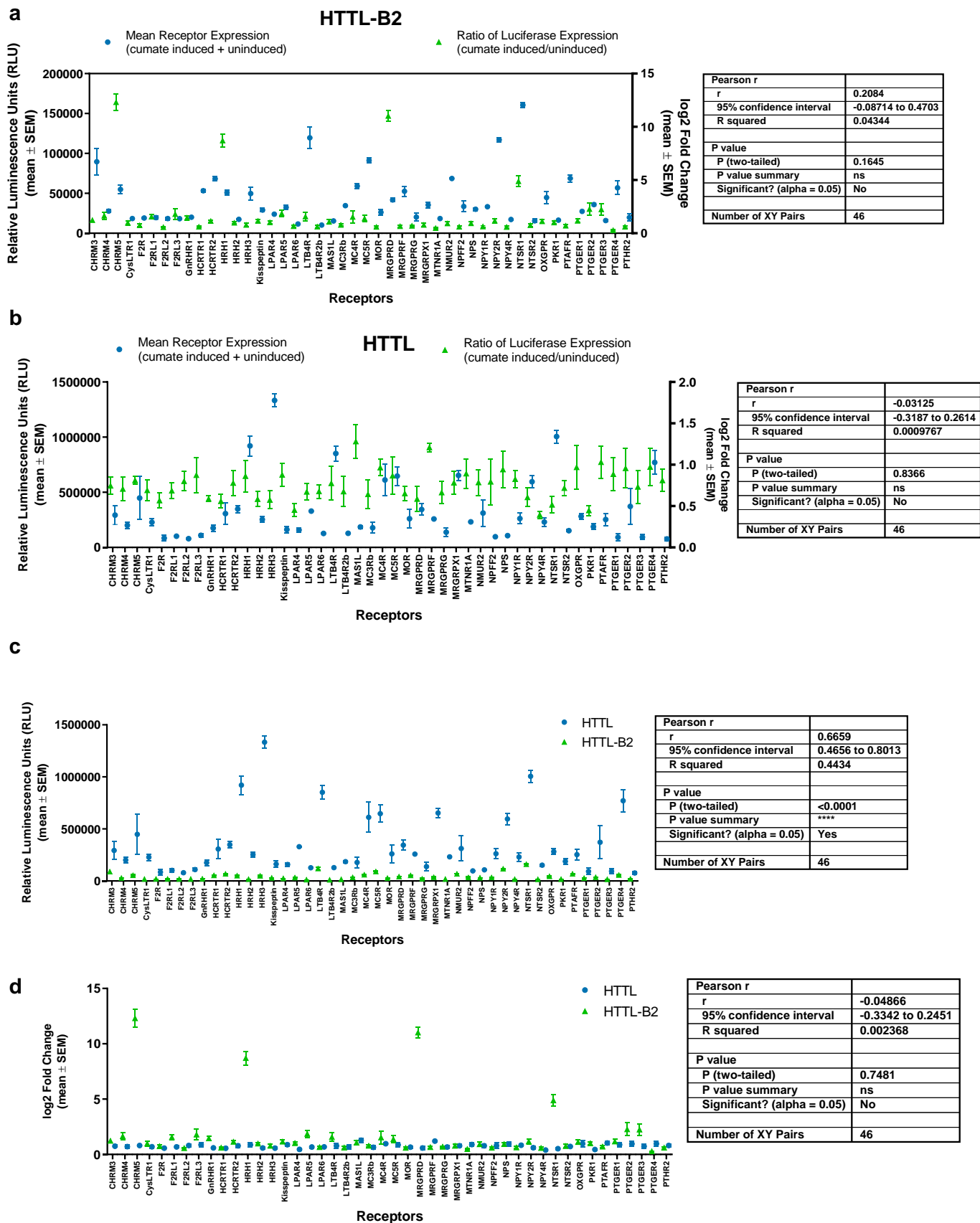
Supplementary Figure 2. Baseline signal of Tango-Trio cell lines. (A-C) HTTL-B1, HTTL-B2, and HTTL-F cells were plated in the presence or absence of cumate (30 µg/mL), which was maintained throughout (totalling approximately 72 hours). As per standard protocol, cells were serum starved for the last 24 hours of the experiment, and luminescence was subsequently read to compare the differences in baseline signal of untransfected cells. Data are presented as mean values, with error bars representing SD ($n = 12$, with 3 technical replicates from 4 biological samples).

Supplementary Figure 3. Changes in baseline signals and fold windows due to cumate induction. HTTL-B1, HTTL-B2 and HTTL-F cells were plated in increasing concentrations of cumate (0, 0.625, 1.25, 2.5, 5, 10, 20, and 40 μ g/mL), which was maintained throughout the entire experiment, and were transfected with select GPCRs: HTR4 (a), CHRM5 (b), and NMBR (c) in HTTL-F; NTSR1 (d), PTGER4 (e), MC4R (f), FPR2 (g), and SSTR2 (h) in HTTL-B2; HTR1E (i), HTR1D (j), ADRA2C (k), and MTNR1B (l) in HTTL-B1. Transfected cells were stimulated with the receptor specific agonist and dose-response curves were built using XY analysis for non-linear regression curve and the 3-parameters dose-response stimulation function, followed by baseline correction. Data are presented as mean values, with error bars representing SEM ($n = 3$, with three technical replicates from one biological sample). Generic receptor codes refer to the GPCR-Tango constructs.

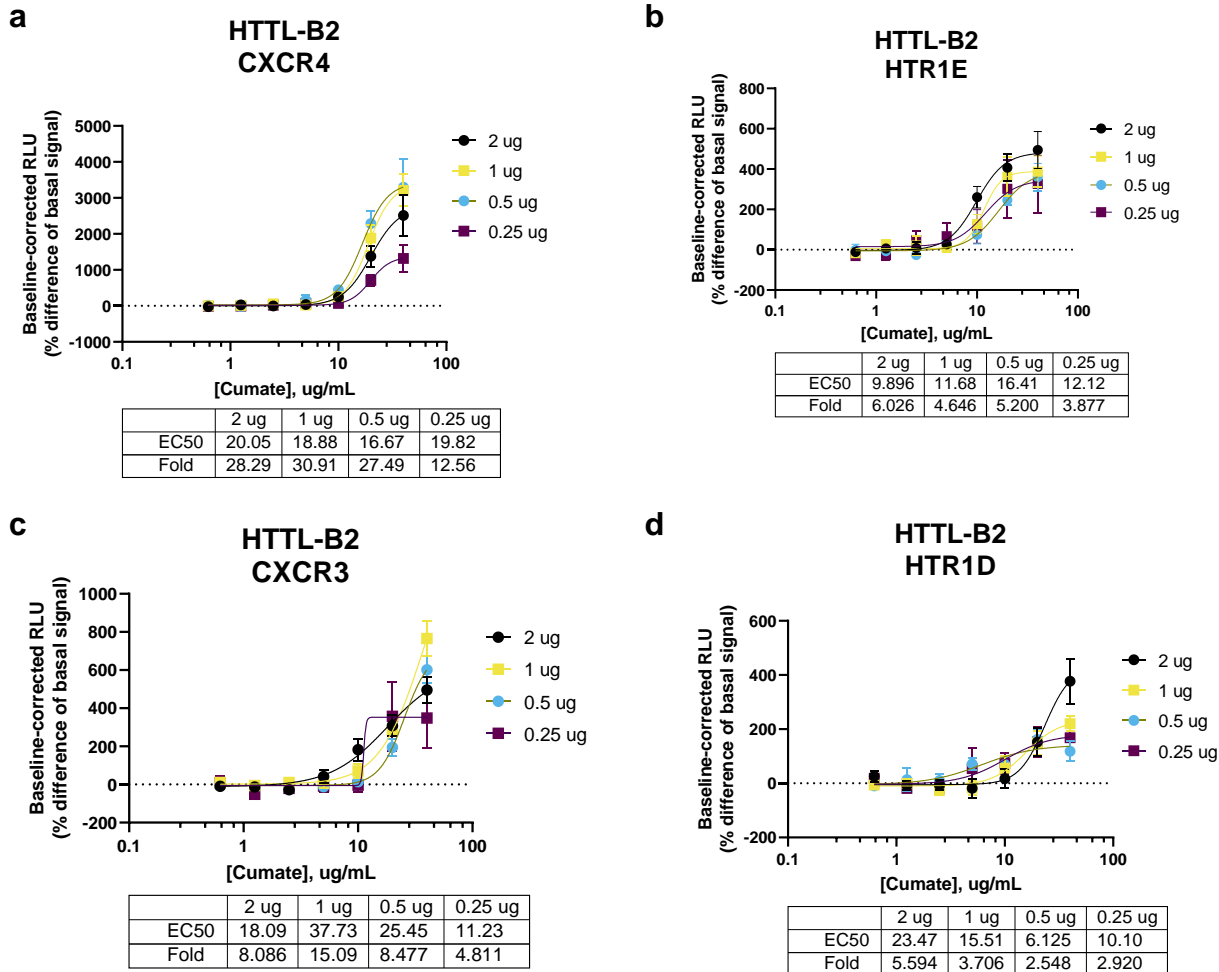


Supplementary Figure 4. Receptor surface expression following cumatate induction of fusion protein expression

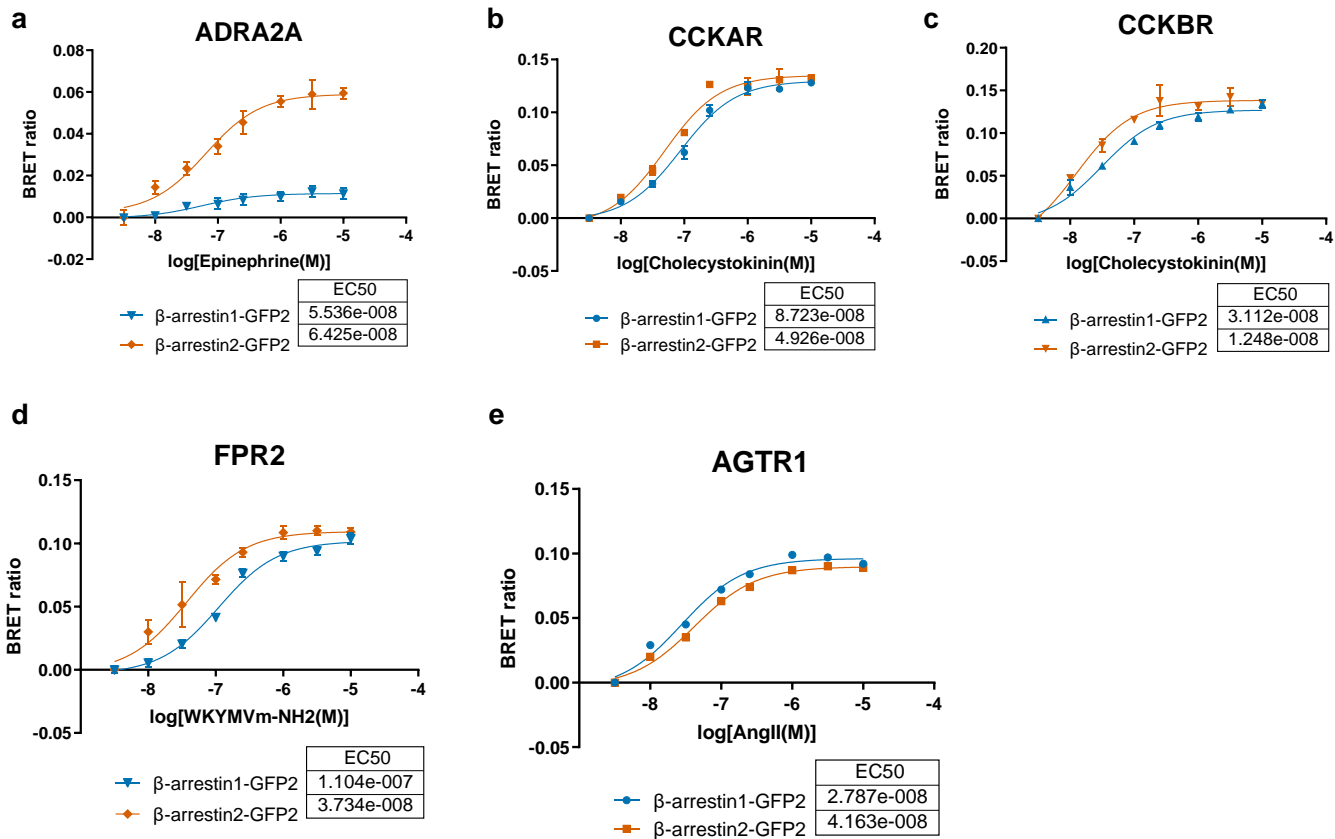
HTTL-B1, HTTL-B2 and HTTL-F were plated in the presence or absence of cumate (30 µg/mL) and were transfected with a select number of positive GPCR hits from the constitutive HTS. ELISA experiments were subsequently carried out on transfected cells to determine receptor surface expression. Data are presented as mean values, with error bars representing SD (n = 4, with four technical replicates from one biological sample). Generic receptor codes refer to the GPCR-Tango constructs.



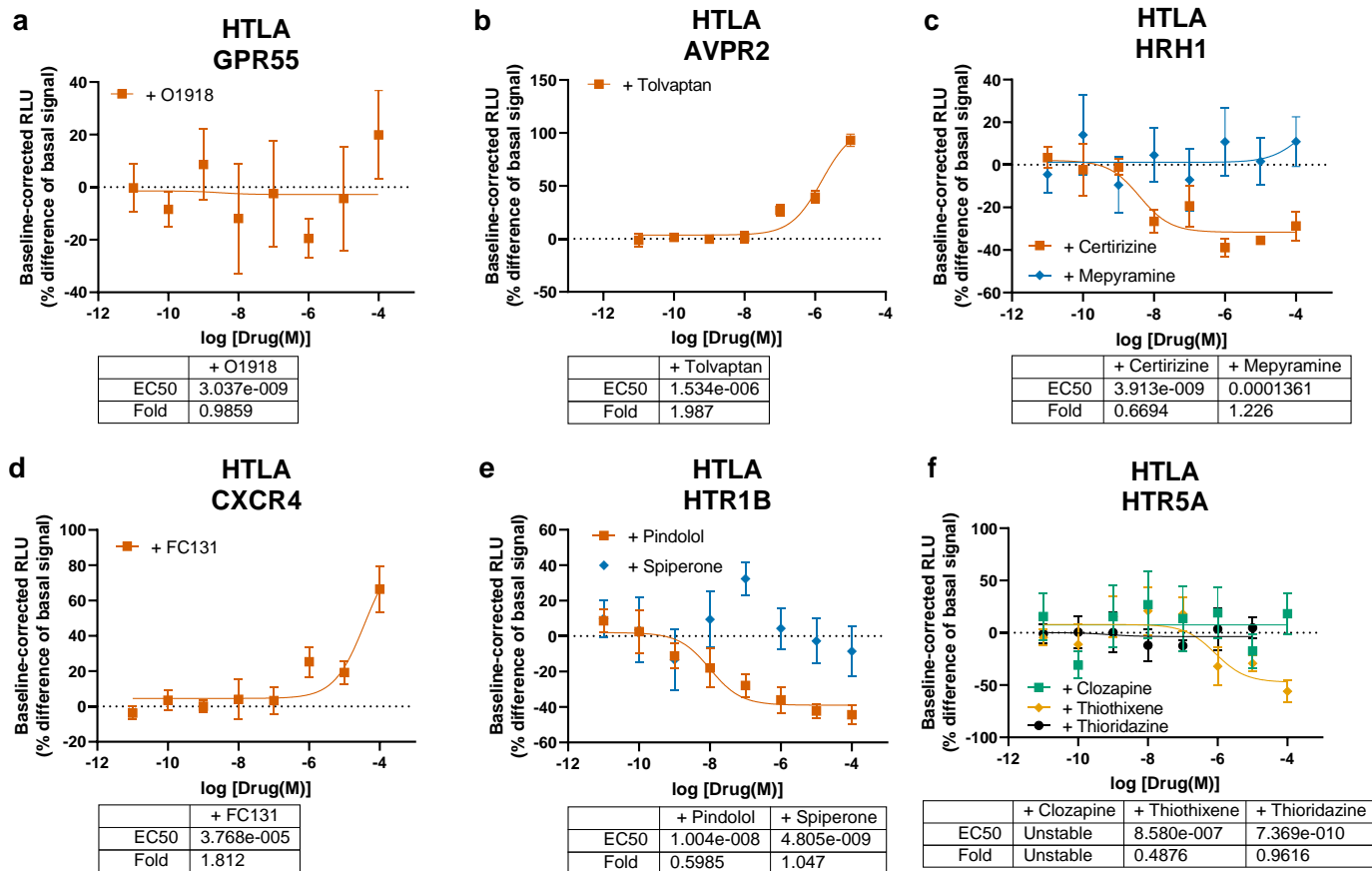
Supplementary Figure 5. Comparison of receptor expression and constitutive activity across panel of GPCRs. HTTL-B2 (a) and HTTL (b) were plated in the presence or absence of cumate (30 µg/mL) and were transfected with a panel of GPCRs with a varying range of constitutive activities. ELISA experiments were subsequently carried out on transfected cells to determine receptor surface expression, and log₂ fold changes in constitutive arrestin recruitment were calculated between the wells in the absence or presence of cumate. Mean receptor expression (c) and log₂ fold changes in constitutive arrestin recruitment (d) were also compared between the HTTL and HTTL-B2 cell lines. Pearson correlation coefficients (r) and corresponding p values (two-tailed) were computed between data sets using GraphPad Prism. Data are presented as mean values, with error bars representing SEM (n = 4, with four technical replicates from one biological sample). Generic receptor codes refer to the GPCR-Tango constructs.



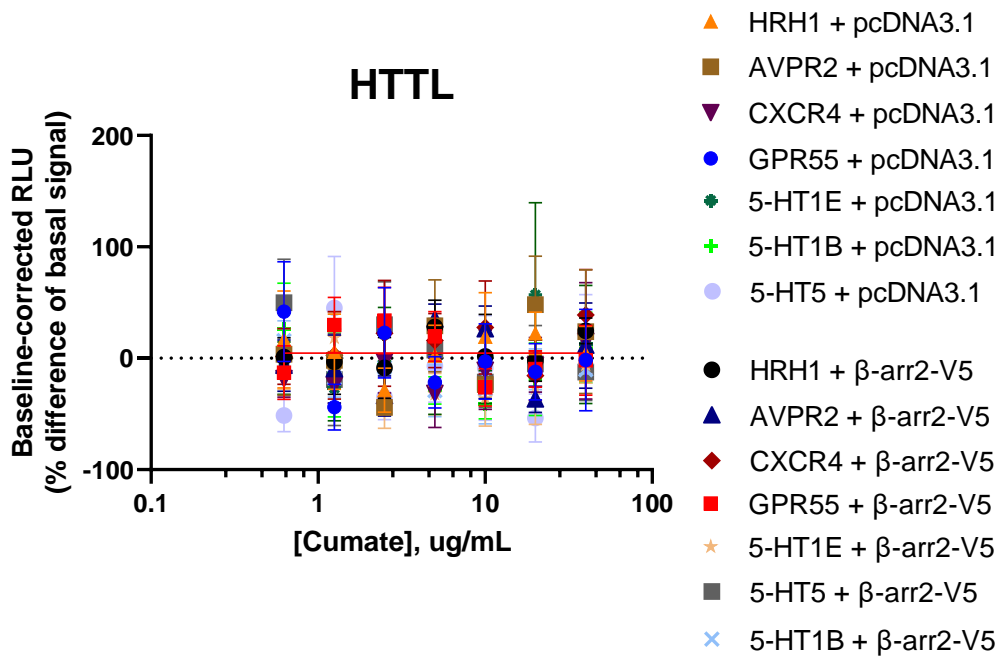
Supplementary Figure 6. Titration of GPCR Tango DNA and consequent effects on constitutive activity. HTTL-B2 cells were seeded in 6-well plates and transfected with various amount of CXCR4 (a), HTR1E (b), CXCR3 (c), and HTR1D (d) Tango DNA, ranging from 0.25 ug – 2 ug total per well. Transfected cells were stimulated with cumate, and dose- response curves were built using XY analysis for non-linear regression curve and the 4-parameters dose-response stimulation function, followed by baseline correction. Data are presented as mean values, with error bars representing SEM ($n = 3$, with three technical replicates from one biological sample). Generic receptor codes refer to the GPCR-Tango constructs.



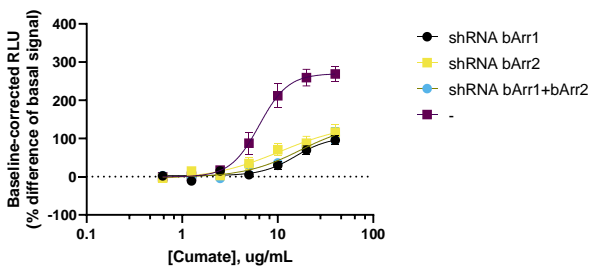
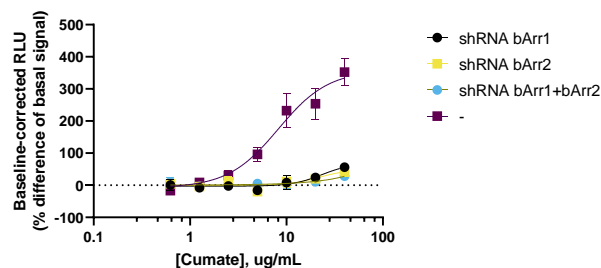
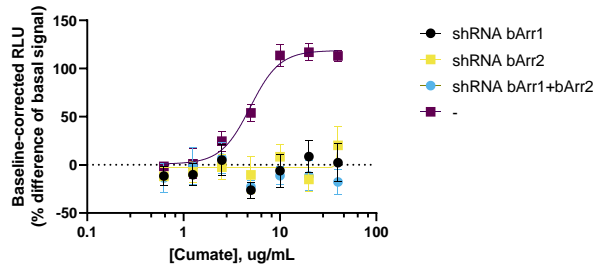
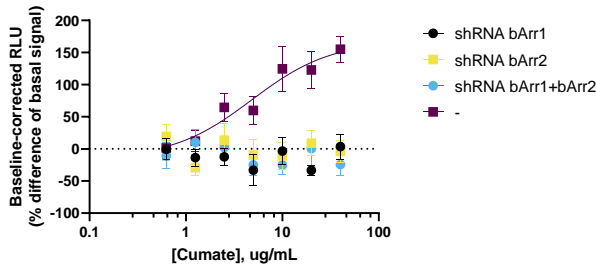
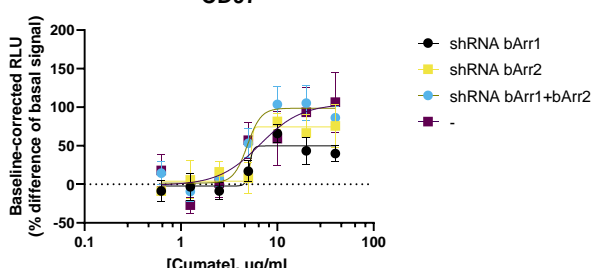
Supplementary Figure 7. Orthogonal determination of arrestin isoform selectivity using BRET2. HEK293T cells were transfected with β -arrestin1/2-GFP2, as well as the following GPCRs: ADRA2A (a), CCKAR (b), CCKBR (c), FPR2 (d), AGTR1 (e). Following transfection, cells were stimulated with serial dilutions of selective agonist, and read with 405 nm (RLuc8-Coelenterazine 400a) and 500 nm (GFP2) emission filters. Dose-response curves were built using XY analysis for non-linear regression curve and the 3-parameters dose-response stimulation function, followed by baseline correction. Data are presented as mean values, with error bars representing SEM ($n = 2$, with two technical replicates from one biological sample). Generic receptor codes refer to the GPCR-Rluc8 constructs.



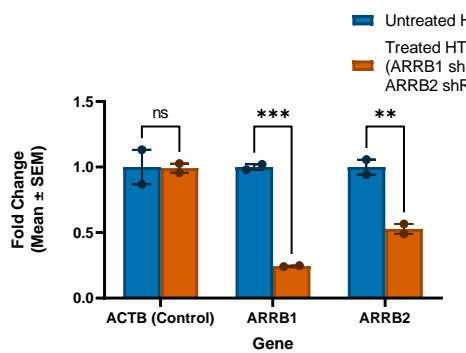
Supplementary Figure 8. Orthogonal characterization of select inverse agonists and antagonists using PRESTO-Tango. HTLA cells were transfected with GPCRs exhibiting strong constitutive arrestin recruitment from the primary Tango-Trio screen, serving to validate the findings shown in Figure 7. Transfected cells were stimulated with a dose-response curve using the following inverse agonists/antagonists: O-1918 at GPR55 (a), Tolvaptan at AVPR2 (b), Cetirizine and Mepyramine at HRH1 (c), FC131 at CXCR4 (d), Pindolol and Spiperone at HTR1E (e), and Clozapine, Thiothixene, and Thioridazine at HTR5A (f). Stimulation curves were built using XY analysis for non-linear regression curve and the 3-parameters dose-response stimulation function, followed by baseline correction. Data are presented as mean values, with error bars representing SEM (Supplementary Figs 8a, 8c-f: n = 3, with three technical replicates from one biological sample; Supplementary Fig 8b: n = 6, with three technical replicates from two biological samples). Generic receptor codes refer to the GPCR-Tango constructs.



Supplementary Figure 9. Expression of GPCR-Tango constructs in the absence of TEV protease. HTTL cells were co-transfected with select GPCR constructs (tested with antagonists/inverse agonists from Fig 7), and either β -arrestin-2 (not tagged to TEV protease) or pcDNA3.1 as a control. Transfected cells were stimulated as a cumate dose-response, and stimulation curves were built using XY analysis for non-linear regression curve and the 4-parameters dose-response stimulation function, followed by baseline correction. Data are presented as mean values, with error bars representing SEM ($n = 3$, with three technical replicates from one biological sample). Generic receptor codes refer to the GPCR-Tango constructs.

a**HTTL-F
CHRM5****b****HTTL-F
GPR87****c****HTTL-F
GPR126****d****HTTL-F
VIPR2****e****HTTL-F
CD97****f**

Untreated HTTL-F
Treated HTTL-F
(ARRB1 shRNA +
ARRB2 shRNA)

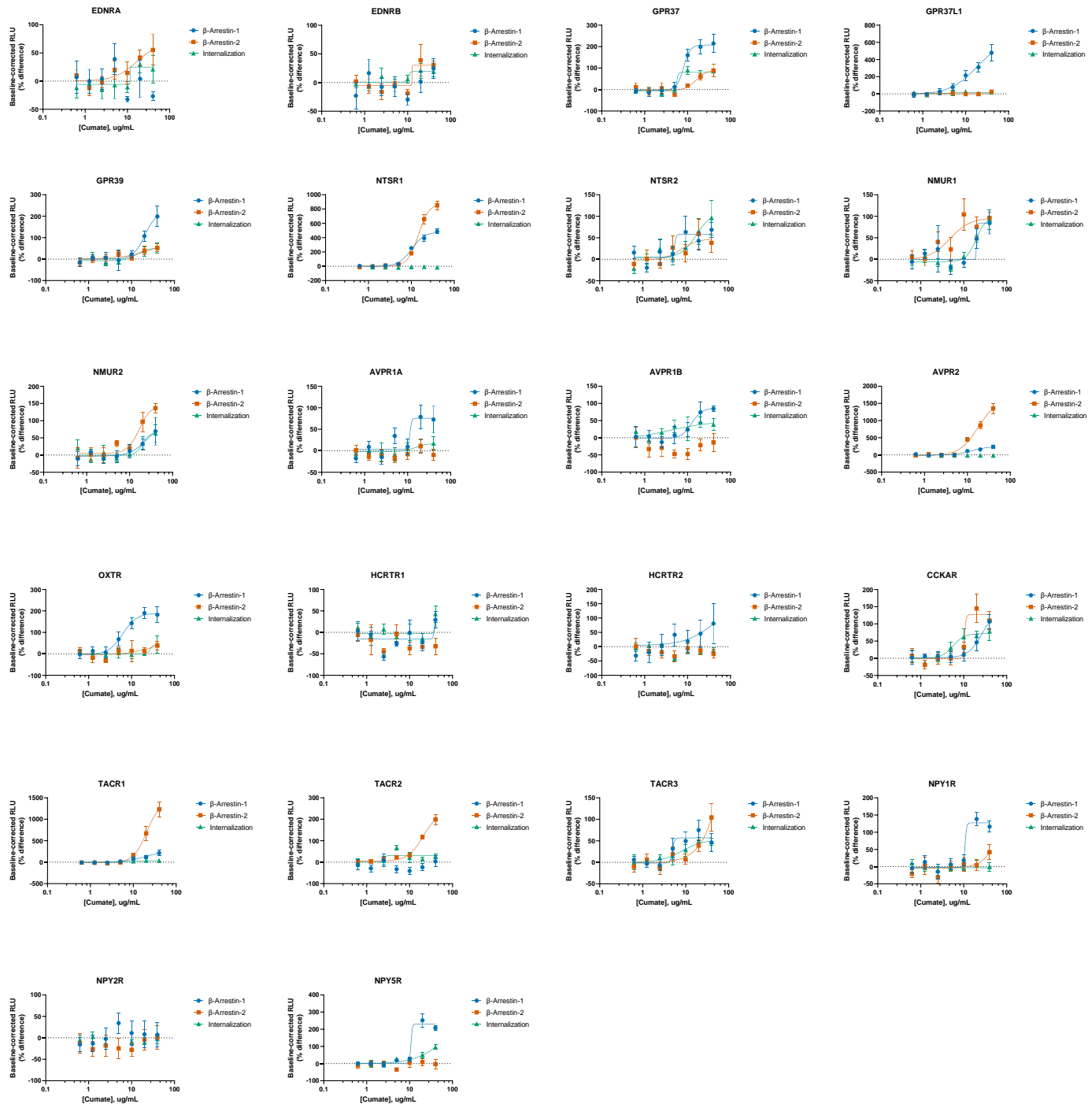


	ACTB (Control)	ARRB1	ARRB2
P value	0.930008	0.000147	0.001847
Mean of Untreated HTTL-F	1.000	1.000	1.000
Mean of Column B	0.9918	0.2444	0.5285
Difference	0.008163	0.7556	0.4715
SE of difference	0.08913	0.08913	0.08913
t ratio	0.09159	8.477	5.290
df	6.000	6.000	6.000
Adjusted P Value	0.930008	0.000442	0.003691

Supplementary Figure 10. Internalization of GPCRs in HTTL-F following β-arrestin-1 and β-arrestin-2 knockdown. Lentiviral β-arrestin-1 and -2 shRNA plasmids were transfected in HEK293T cells, along with psPAX2 and VSV-G vectors. The medium was replaced the following day with complete fresh medium, and lentiviral shRNA medium was collected following 48 hours transfection. For the knockdown experiment, HTTL-F cells were seeded in either complete medium or in the previously prepared lentiviral β-arrestin-1 and -2 shRNA medium (combined at a 1:1 ratio), with infection of cells facilitated with polybrene at 8 µg/mL. HTTL-F cells were transfected with GPCRs demonstrating high constitutive internalization: CHRM5 (a), GPR87 (b), GPR126 (c), VIPR2 (d), and CD97 (e). Transfected cells were stimulated as a cumat dose-response, and stimulation curves were built using XY analysis for non-linear regression curve and the 4-parameters dose-response stimulation function, followed by baseline correction. Data are presented as mean values, with error bars representing SEM ($n = 3$, with three technical replicates from one biological sample), and generic receptor codes refer to the GPCR-Tango constructs. qPCR was performed on untreated and infected HTTL-F cells to confirm sufficient knockdown of β-arrestin-1 and -2 (f). Data are presented as mean values, with error bars representing SEM. Fold change of gene expression and corresponding p values (two-tailed) were assessed with multiple unpaired t test using the FDR method of Benjamini & Yekutieli ($n = 2$, with two technical replicates from one biological sample).



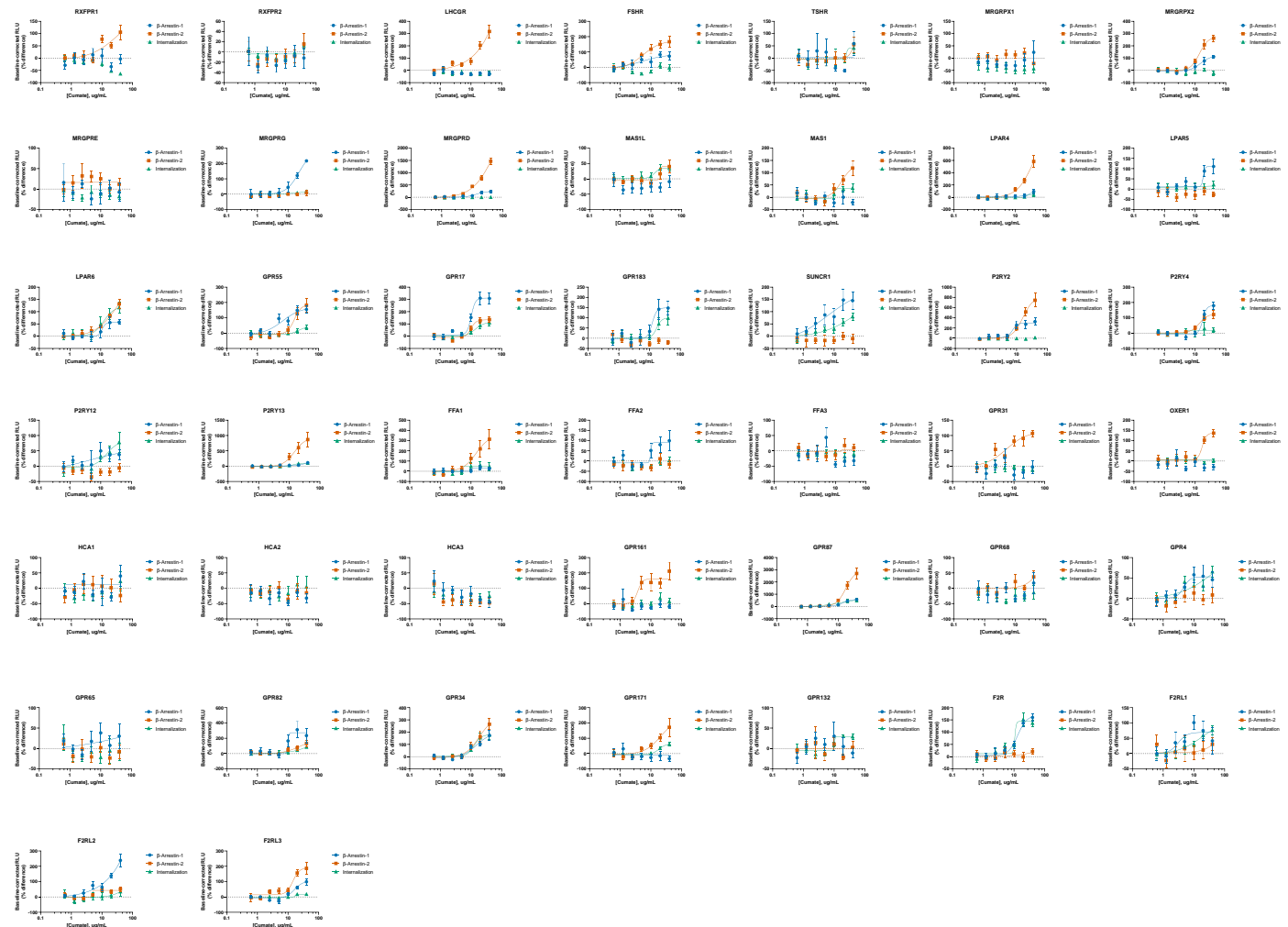
Supplementary Figure 11. Basal profiles of β -arrestin-1 and β -arrestin-2 translocation, and receptor internalization generated using Tango-Trio (Class A, α -branch). To profile basal activities, HTTL-B1, HTTL-B2 and HTTL-F cells were transfected with GPCR Tango constructs. Transfected cells were stimulated with cumate in a dose-dependent manner. Dose-response curves were built using XY analysis for non-linear regression curve and the 4-parameters dose-response stimulation function, followed by baseline correction. Data are presented as mean values, with error bars representing SEM ($n = 3$, with 3 technical replicates from one biological sample). Generic receptor codes refer to the GPCR-Tango constructs.



Supplementary Figure 12. Basal profiles of β -arrestin-1 and β -arrestin-2 translocation, and receptor internalization generated using Tango-Trio (Class A, β -branch). To profile basal activities, HTTL-B1, HTTL-B2 and HTTL-F cells were transfected with GPCR Tango constructs. Transfected cells were stimulated with cumate in a dose-dependent manner. Dose-response curves were built using XY analysis for non-linear regression curve and the 4-parameters dose-response stimulation function, followed by baseline correction. Data are presented as mean values, with error bars representing SEM ($n = 3$, with 3 technical replicates from one biological sample). Generic receptor codes refer to the GPCR-Tango constructs.



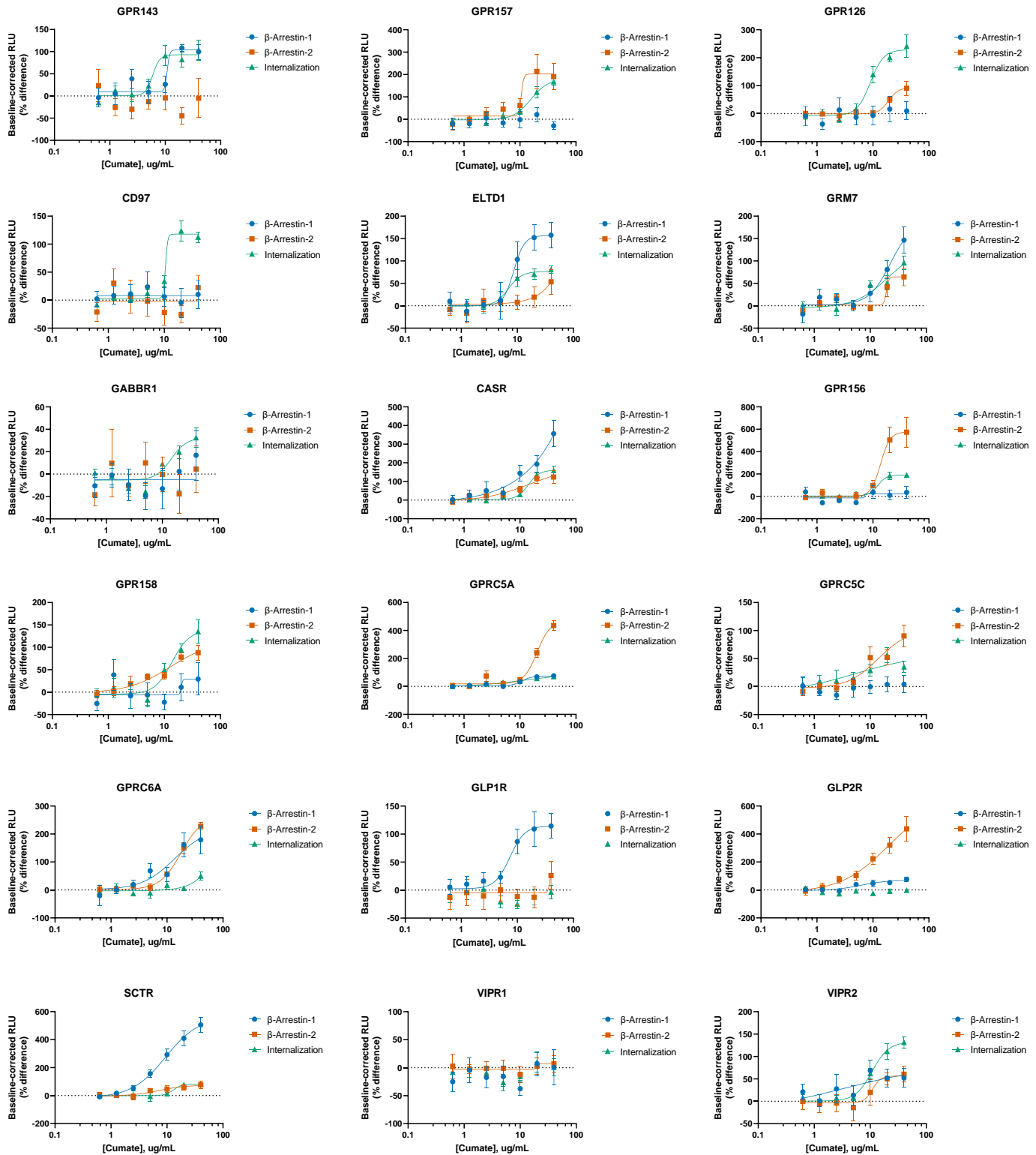
Supplementary Figure 13. Basal profiles of β -arrestin-1 and β -arrestin-2 translocation, and receptor internalization generated using Tango-Trio (Class A, γ -branch). To profile basal activities, HTTL-B1, HTTL-B2 and HTTL-F cells were transfected with GPCR Tango constructs. Transfected cells were stimulated with cumate in a dose-dependent manner. Dose-response curves were built using XY analysis for non-linear regression curve and the 4-parameters dose-response stimulation function, followed by baseline correction. Data are presented as mean values, with error bars representing SEM ($n = 3$, with 3 technical replicates from one biological sample). Generic receptor codes refer to the GPCR-Tango constructs.



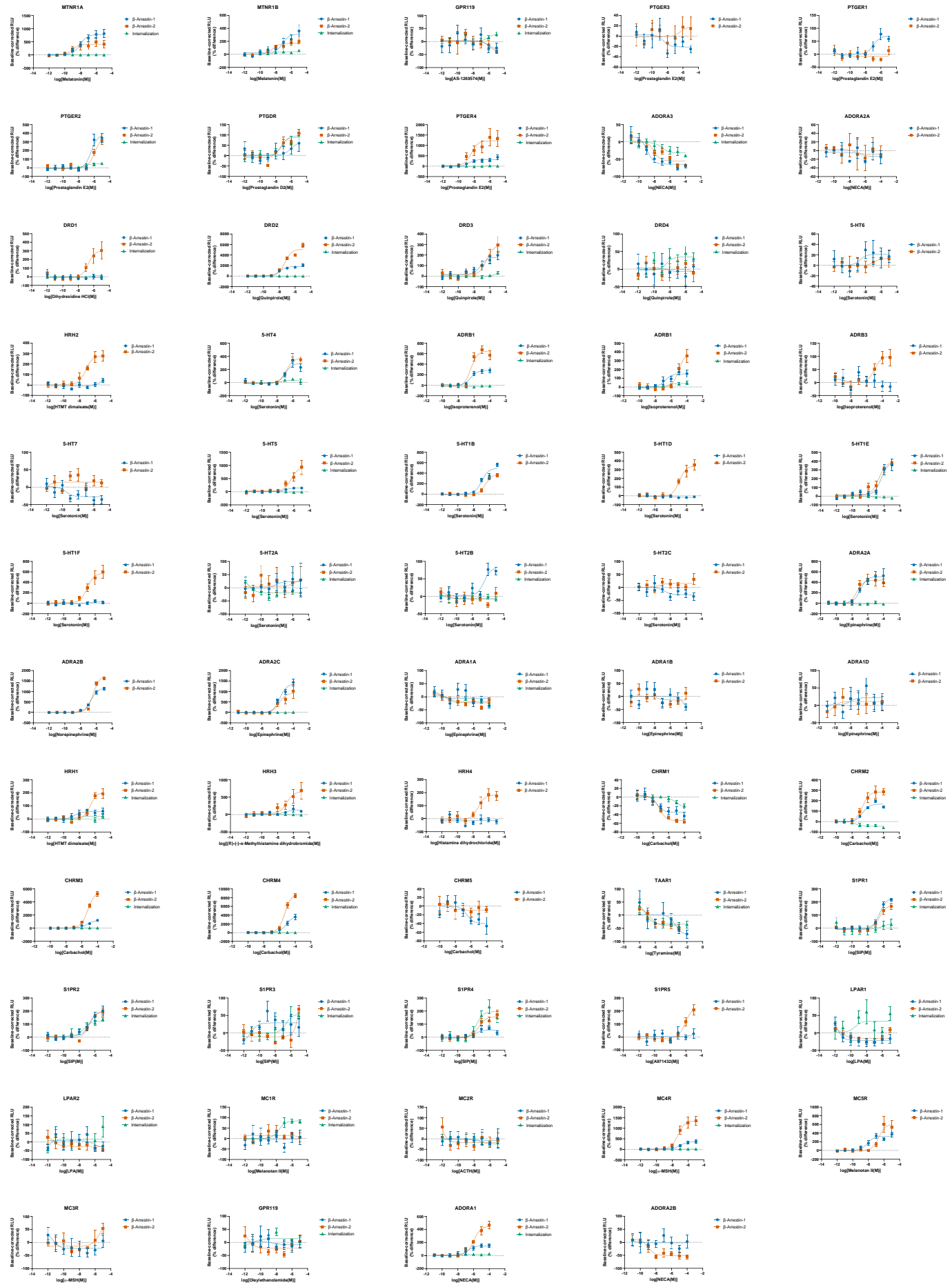
Supplementary Figure 14. Basal profiles of β -arrestin-1 and β -arrestin-2 translocation, and receptor internalization generated using Tango-Trio (Class A, δ -branch). To profile basal activities, HTTL-B1, HTTL-B2 and HTTL-F cells were transfected with GPCR Tango constructs. Transfected cells were stimulated with cumate in a dose-dependent manner. Dose-response curves were built using XY analysis for non-linear regression curve and the 4-parameters dose-response stimulation function, followed by baseline correction. Data are presented as mean values, with error bars representing SEM ($n = 3$, with 3 technical replicates from one biological sample). Generic receptor codes refer to the GPCR-Tango constructs.



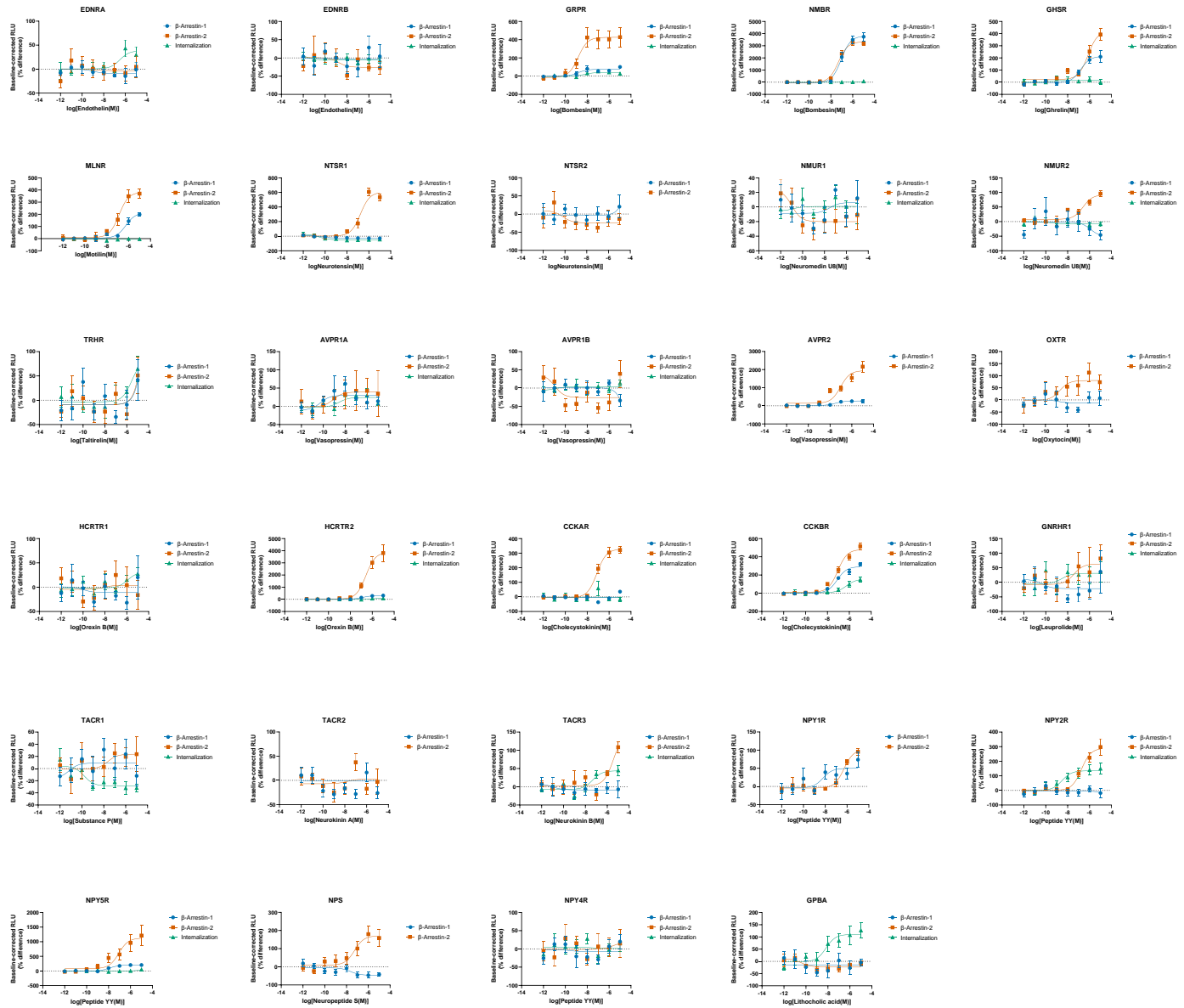
Supplementary Figure 15. Basal profiles of β -arrestin-1 and β -arrestin-2 translocation, and receptor internalization generated using Tango-Trio (Class A, orphan receptors). To profile basal activities, HTTL-B1, HTTL-B2 and HTTL-F cells were transfected with GPCR Tango constructs. Transfected cells were stimulated with cumate in a dose-dependent manner. Dose-response curves were built using XY analysis for non-linear regression curve and the 4-parameters dose-response stimulation function, followed by baseline correction. Data are presented as mean values, with error bars representing SEM ($n = 3$, with 3 technical replicates from one biological sample). Generic receptor codes refer to the GPCR-Tango constructs.



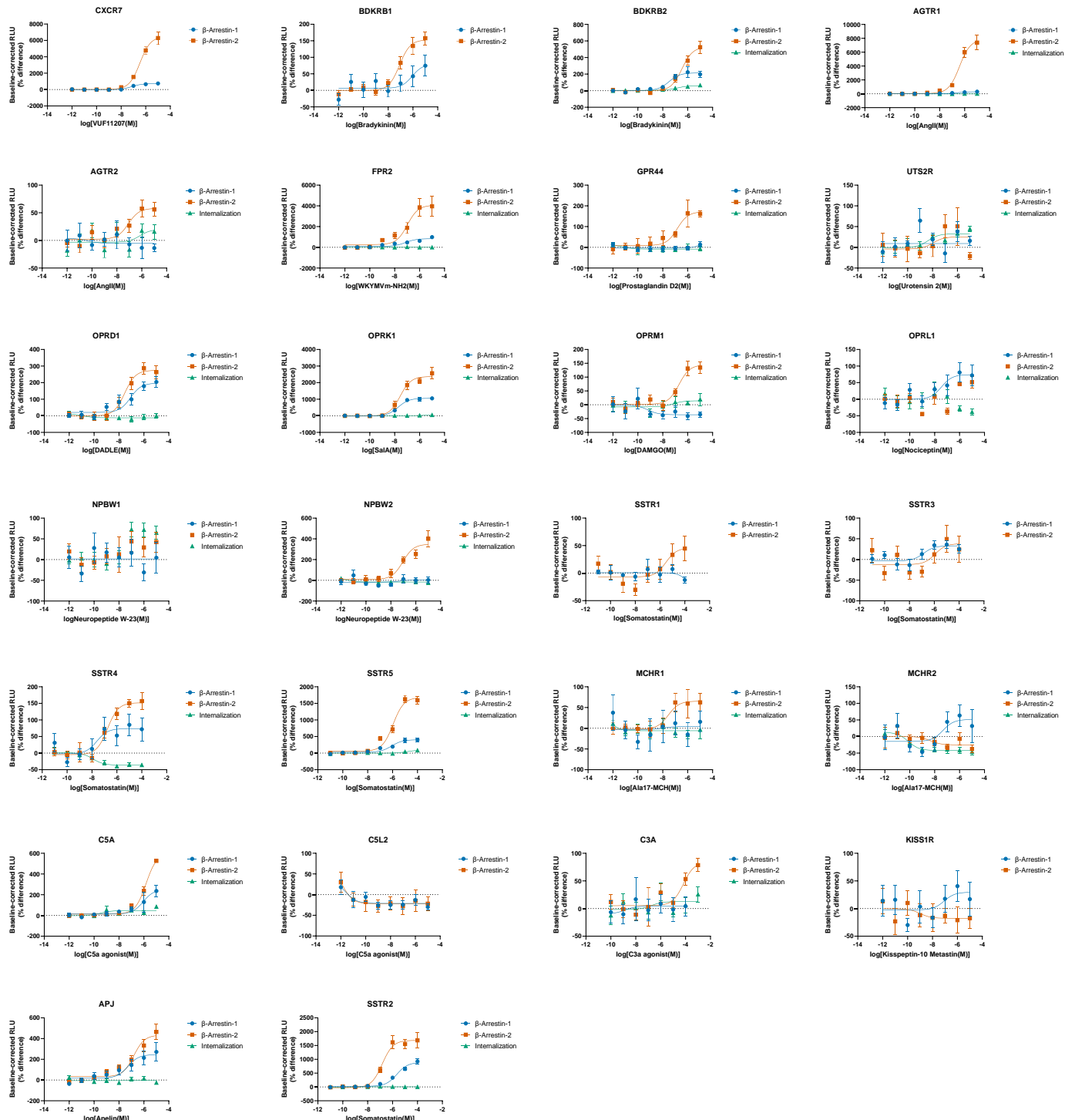
Supplementary Figure 16. Basal profiles of β -arrestin-1 and β -arrestin-2 translocation, and receptor internalization generated using Tango-Trio (Class B/C). To profile basal activities, HTTL-B1, HTTL-B2 and HTTL-F cells were transfected with GPCR Tango constructs. Transfected cells were stimulated with cumate in a dose-dependent manner. Dose-response curves were built using XY analysis for non-linear regression curve and the 4-parameters dose-response stimulation function, followed by baseline correction. Data are presented as mean values, with error bars representing SEM ($n = 3$, with 3 technical replicates from one biological sample). Generic receptor codes refer to the GPCR-Tango constructs.



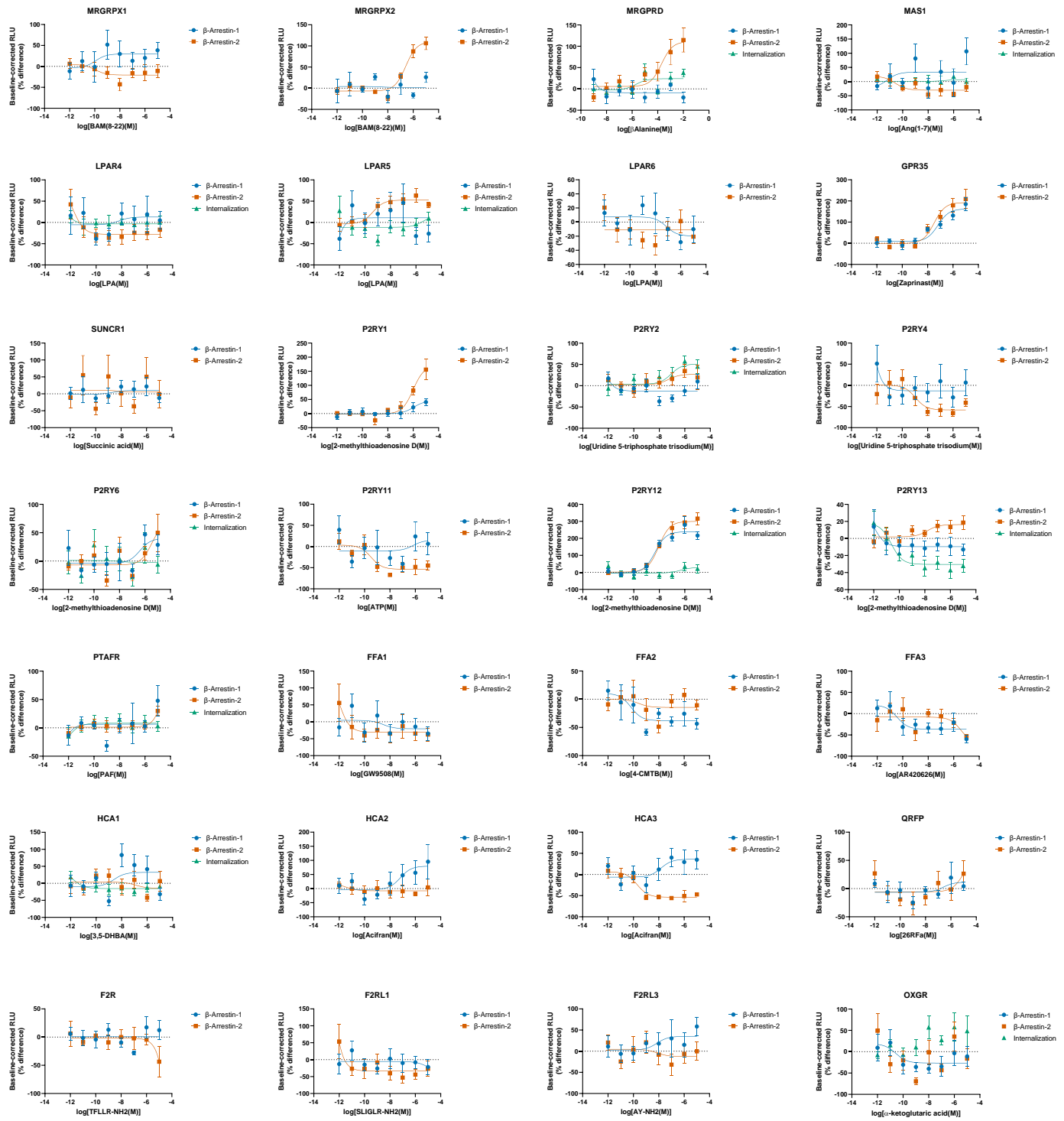
Supplementary Figure 17. Agonist-induced profiles of β -arrestin-1 and β -arrestin-2 translocation, and receptor internalization generated using Tango-Trio (Class A, α -branch). To quantify agonist-dependent activities, HTTL-B1, HTTL-B2 and HTTL-F cells were plated in cumate-containing (30 μ g/mL) medium and transfected with non-orphan GPCR Tango constructs. Transfected cells were stimulated with the receptor-specific agonist, and dose-response curves were built using XY analysis for non-linear regression curve and the 3-parameters dose-response stimulation function, followed by baseline correction. Data are presented as mean values, with error bars representing SEM ($n = 3$, with 3 technical replicates from one biological sample). Generic receptor codes refer to the GPCR-Tango constructs.



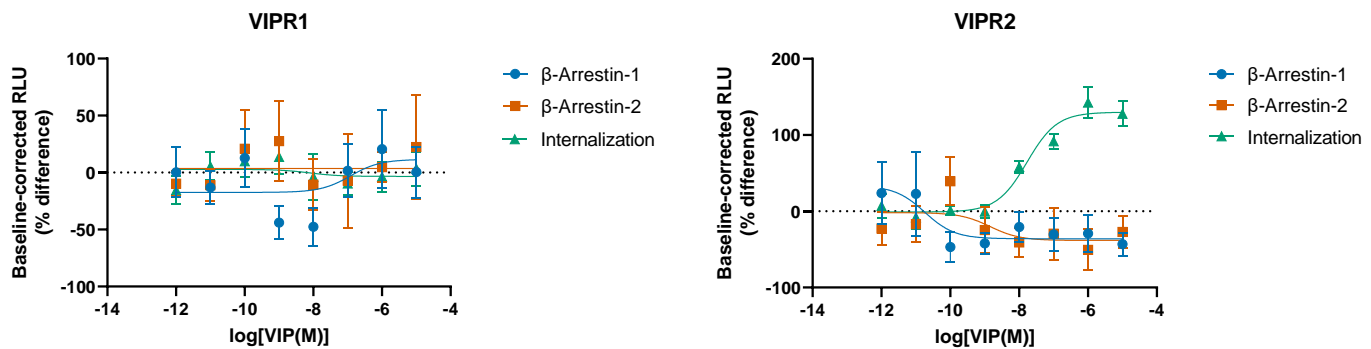
Supplementary Figure 18. Agonist-induced profiles of β -arrestin-1 and β -arrestin-2 translocation, and receptor internalization generated using Tango-Trio (Class A, β -branch). To quantify agonist-dependent activities, HTTL-B1, HTTL-B2 and HTTL-F cells were plated in cumate-containing (30 μ g/mL) medium and transfected with non-orphan GPCR Tango constructs. Transfected cells were stimulated with the receptor-specific agonist, and dose-response curves were built using XY analysis for non-linear regression curve and the 3-parameters dose-response stimulation function, followed by baseline correction. Data are presented as mean values, with error bars representing SEM ($n = 3$, with 3 technical replicates from one biological sample). Generic receptor codes refer to the GPCR-Tango constructs.



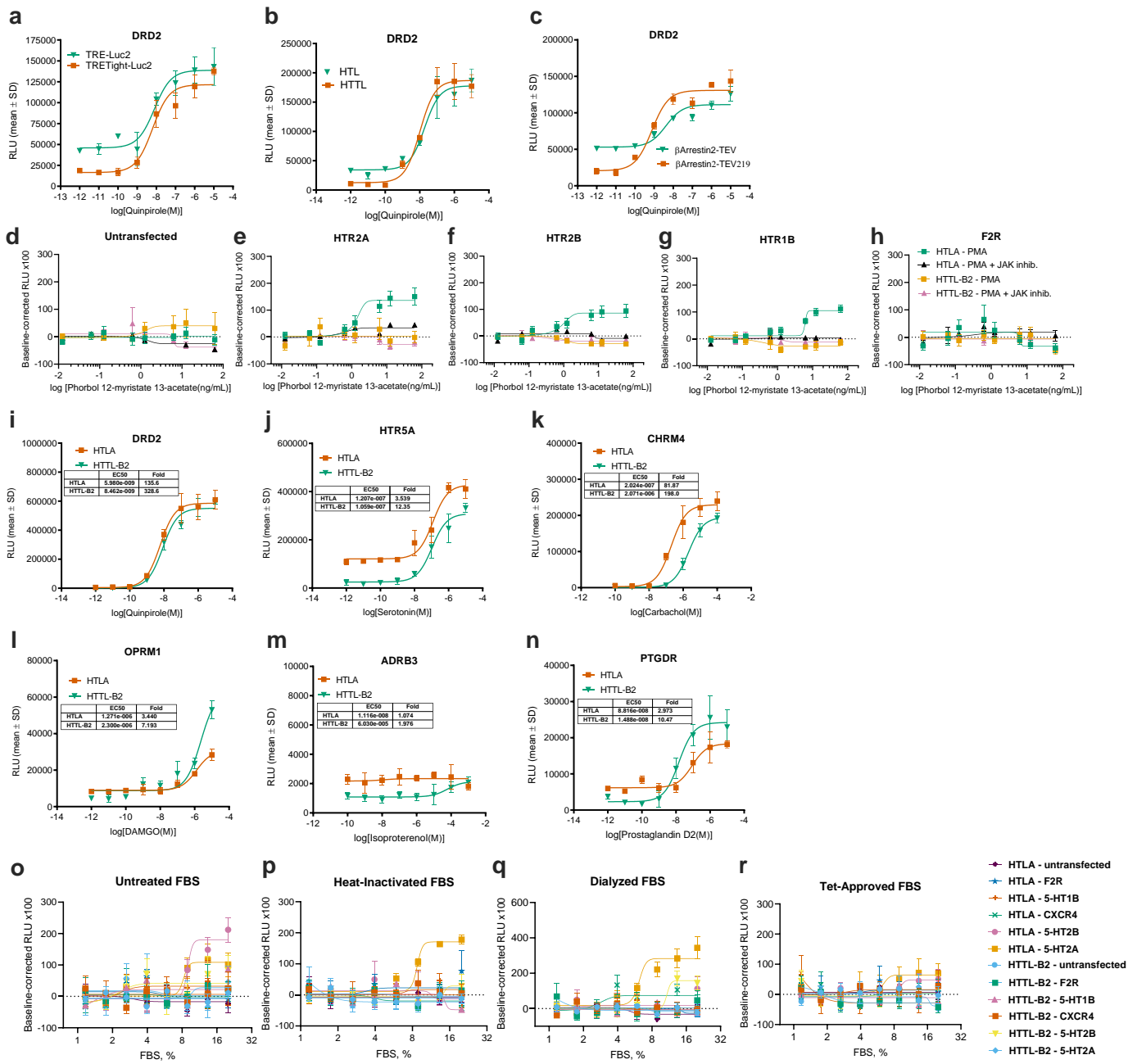
Supplementary Figure 19. Agonist-induced profiles of β -arrestin-1 and β -arrestin-2 translocation, and receptor internalization generated using Tango-Trio (Class A, γ -branch). To quantify agonist-dependent activities, HTTL-B1, HTTL-B2 and HTTL-F cells were plated in cimate-containing (30 μ g/mL) medium and transfected with non-orphan GPCR Tango constructs. Transfected cells were stimulated with the receptor-specific agonist, and dose-response curves were built using XY analysis for non-linear regression curve and the 3-parameters dose-response stimulation function, followed by baseline correction. Data are presented as mean values, with error bars representing SEM ($n = 3$, with 3 technical replicates from one biological sample). Generic receptor codes refer to the GPCR-Tango constructs.



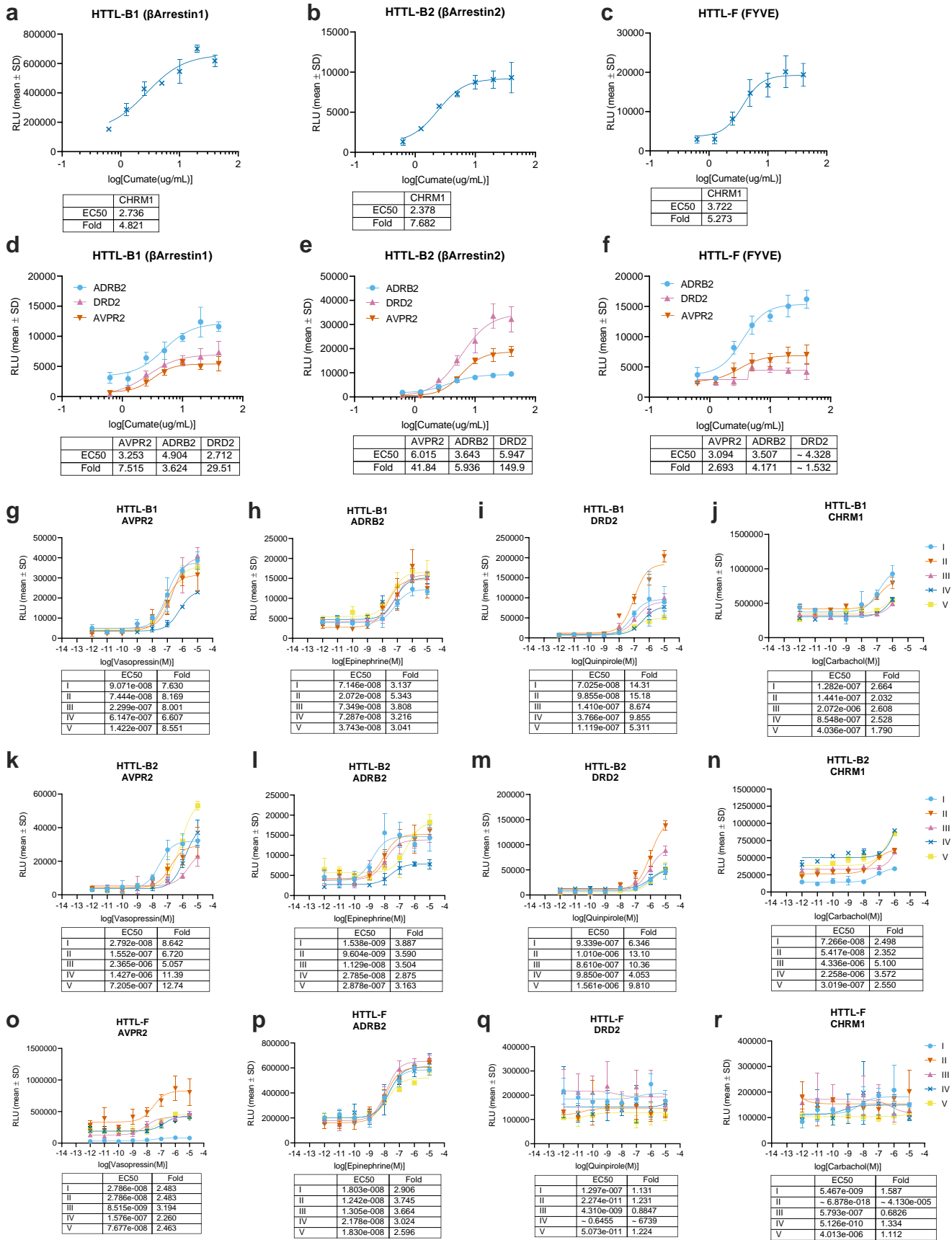
Supplementary Figure 20. Agonist-induced profiles of β -arrestin-1 and β -arrestin-2 translocation, and receptor internalization generated using Tango-Trio (Class A, δ -branch). To quantify agonist-dependent activities, HTTL-B1, HTTL-B2 and HTTL-F cells were plated in cimate-containing (30 μ g/mL) medium and transfected with non-orphan GPCR Tango constructs. Transfected cells were stimulated with the receptor-specific agonist, and dose-response curves were built using XY analysis for non-linear regression curve and the 3-parameters dose-response stimulation function, followed by baseline correction. Data are presented as mean values, with error bars representing SEM ($n = 3$, with 3 technical replicates from one biological sample). Generic receptor codes refer to the GPCR-Tango constructs.



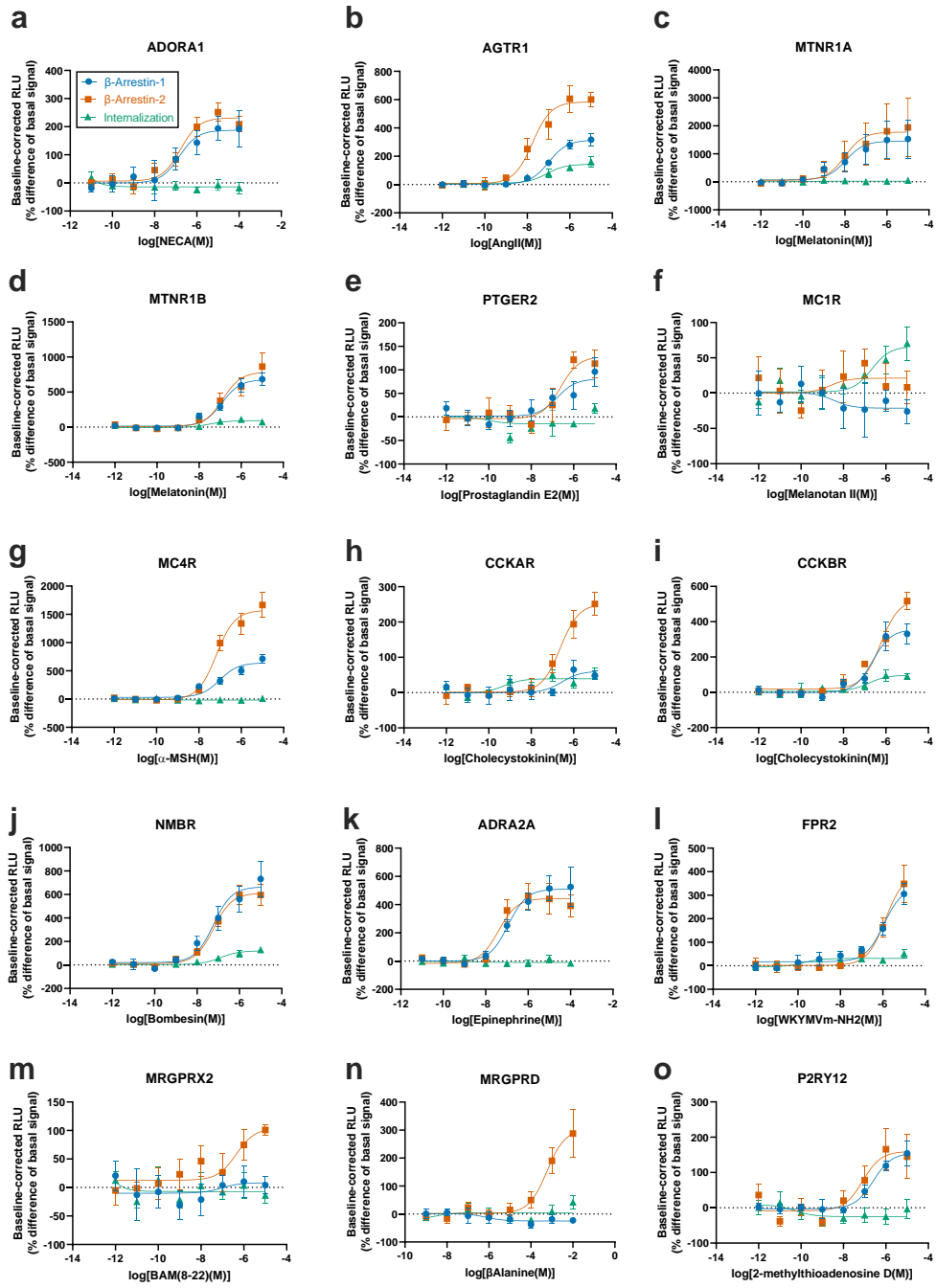
Supplementary Figure 21. Agonist-induced profiles of β -arrestin-1 and β -arrestin-2 translocation, and receptor internalization generated using Tango-Trio (Class B/C). To quantify agonist-dependent activities, HTTL-B1, HTTL-B2 and HTTL-F cells were plated in cumate-containing (30 μ g/mL) medium and transfected with non-orphan GPCR Tango constructs. Transfected cells were stimulated with the receptor-specific agonist, and dose-response curves were built using XY analysis for non-linear regression curve and the 3-parameters dose-response stimulation function, followed by baseline correction. Data are presented as mean values, with error bars representing SEM ($n = 3$, with 3 technical replicates from one biological sample). Generic receptor codes refer to the GPCR-Tango constructs.



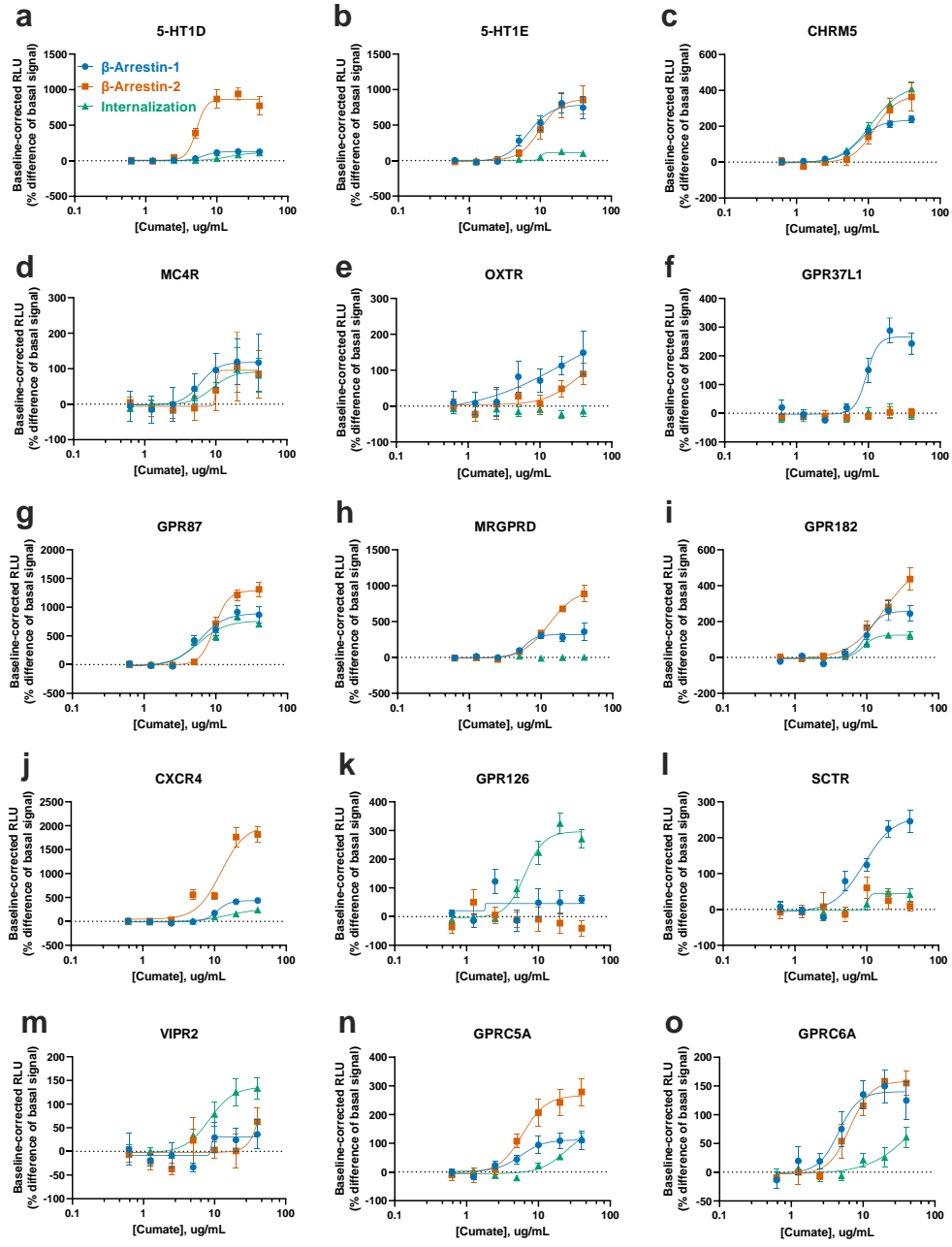
Supplementary Figure 22. Optimization of the dynamic range, sensitivity, and specificity of the Tango-Trio platform - independent biological replicate of the main manuscript Figure 1. (A-R) Data are representative of 2 biological replicates, with 3 technical replicates each.



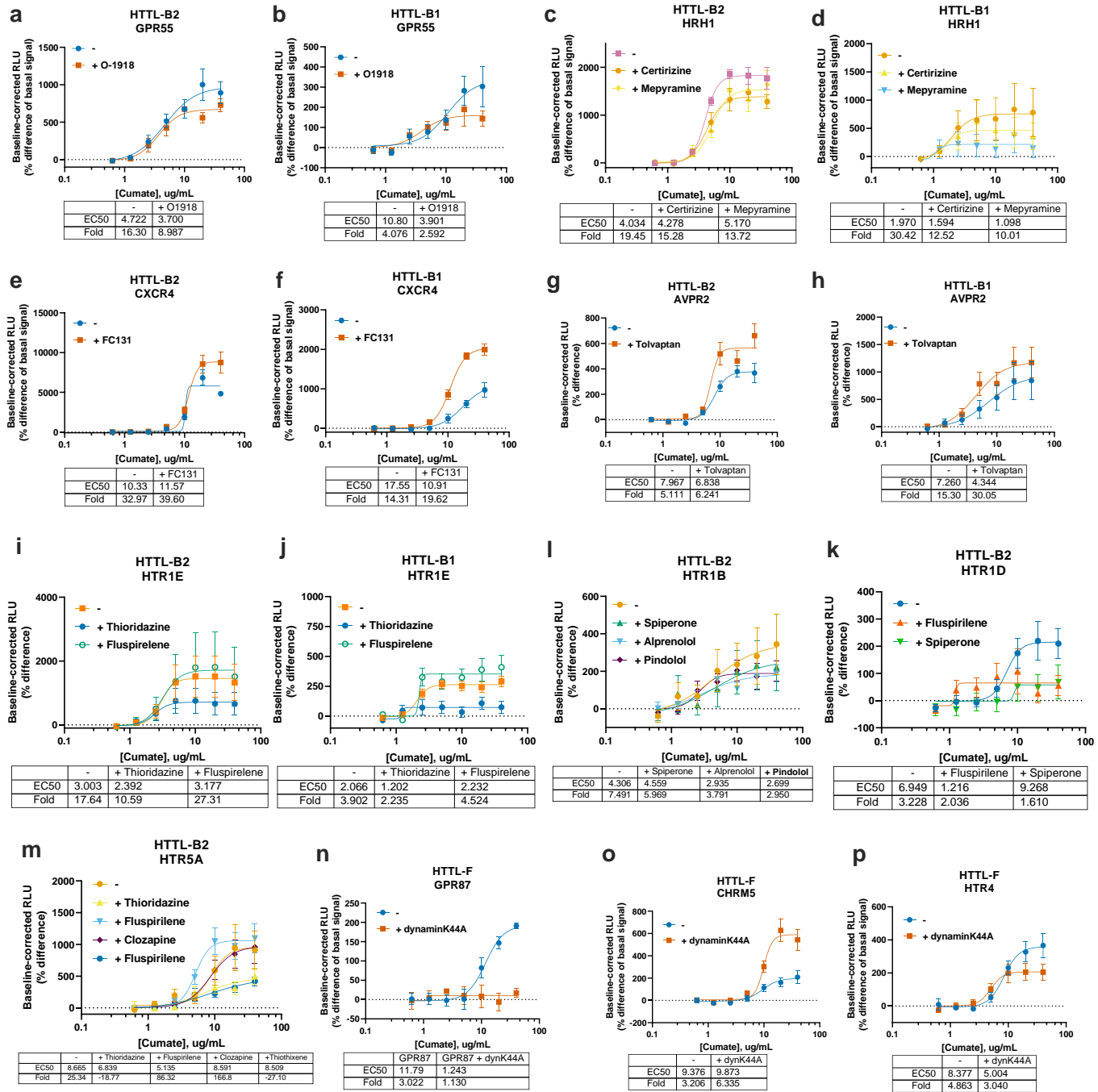
Supplementary Figure 23. Dose-response and time-course verification of climate-induced expression - independent biological replicate of the main manuscript Figure 2. (A-R) Data are representative of 2 biological replicates, with 3 technical replicates each.



Supplementary Figure 24. Validation of compiled positive hits from agonist-dependent HTS in dose response - independent biological replicate of the main manuscript Figure 5. (A-O) Data are representative of 2 biological replicates, with 3 technical replicates each.



Supplementary Figure 25. Validation of compiled positive hits from basal activity HTS in dose-response - independent biological replicate of the main manuscript Figure 6. (A-O) Data are representative of 2 biological replicates, with 3 technical replicates each.



Supplementary Figure 26. Applications and further investigations into basal activities revealed by Tango-Trio - independent biological replicate of the main manuscript Figure 7. (A-P) Data are representative of 2 biological replicates, with 3 technical replicates each.

Supplemental Tables

Supplementary Table 1. Comparison of the pharmacological parameters extracted from EMTA and Tango-Trio. Absolute pEC50 and Emax values of β -arrestin-1/2 activity at GPCRs stimulated with common ligands were extracted from EMTA (Avet et al. 2022) and Tango-Trio studies. Tango-Trio pEC50 data was extracted from the non-linear least-squares regression analysis using the sigmoidal dose-response function (3-parameters modeled using $Y=Bottom + (Top-Bottom)/(1+10^{((LogEC50-X))})$) and Emax values from the baseline correction as percentage difference using $100^* (Value-Baseline)/Baseline$), both provided in GraphPad Prism 9.5.1. ($n = 3$, with three technical replicates from one biological sample). Generic receptor codes refer to the GPCR-Tango constructs.

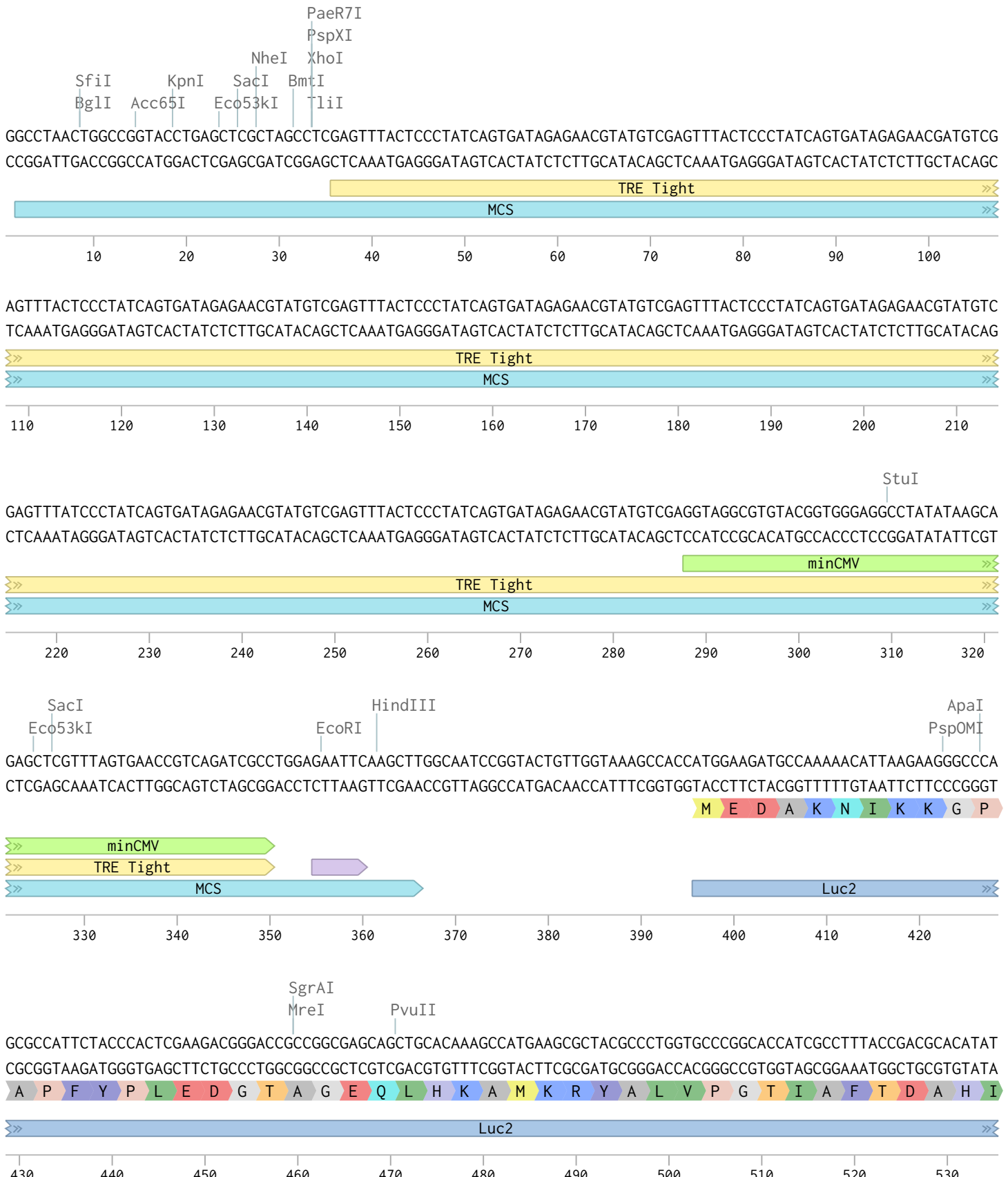
		pEC50				Emax (in % of vehicle response for EMTA & % difference from baseline for Tango-Trio)			
Receptor (Gene Name)	Ligand	βArrestin1 /GRK2	βArrestin1	βArrestin2 /GRK2	β-Arrestin2	βArrestin1 /GRK2	βArrestin1	βArrestin2 /GRK2	β-Arrestin2
		EMTA	Tango-Trio	EMTA	Tango-Trio	EMTA	Tango-Trio	EMTA	Tango-Trio
HTR1B	Serotonin	7.6	6.96	7.685	6.49	36.35	490	57.78	393.4
HTR1D	Serotonin		7.66		6.89		-14.78		347.9
HTR2A	Serotonin	6.709	8.22	7.028	5.76	518.1	24.81	778.6	29.24
HTR2B	Serotonin	7.809	6.5	8.168	11.31	171.6	80.54	247.2	-26.67
HTR2C	Serotonin	7.995	8.76	8.456	9.33	1564	-28.38	705	14.12
AGTR1	Angiotensin II	8.64	6.62	8.84	6.41	207.8	289.2	220.6	7802
CCKAR	Cholecystokinin	8.329	unstable	8.721	7.11	1374	unstable	1520	332.9
PTGER1	PGE2		6.95		unstable		71.02		unstable
PTGER2	PGE2	6.515	6.38	6.925	5.95	107.8	400.8	100.5	363
PTGER3	PGE2		8.53		6.324		-24.13		19.44
PTGER4	PGE2	8.921	8.62	9.25	8.35	251.5	326.9	146.8	1192
EDNRA	Endothelin-1	8.232	8.9	8.381	8.7	588.1	-8.86	1581	-2.98
GHSR	Ghrelin	8.249	6.81	8.515	6.14	68.41	217.8	169.6	396.8
GNRHR	GnRH		10.32		7.43		-31.52		70.49
GPBAR1	Lithocholic acid		unstable		10.41		unstable		-34.66
LPAR1	O-LPA	7.528	11.93	7.464	11.21	289.4	-90.04	232	-32.09
LPAR2	O-LPA	6.773	6.13	7.078	11.33	715.2	-41.64	938.9	-64.29
MC4R	α-MSH		7.01	7.449	7.28		346.3	76.44	1351
OPRM1	DAMGO	7.099	9.19	7.424	6.7	1008	-35.21	1198	142.9
MTNR1A	Melatonin	8.937	8.03	8.75	9.11	78.64	754.1	157.5	425.5
MTNR1B	Melatonin		7.12		8.38		290		168
OPRL1	Nociceptin	8.249	6.15	8.716	6.17	147.5	73.78	238.1	-50.64
OXTR	Oxytocin	8.091	8.78	8.6	8.67	128.3	-13.08	229.8	82.31
HCRT2	Orexin-A	8.471	6.9	8.558	6.58	852.9	315.7	863.9	3850
P2RY2	UTP	5.235	unstable	5.36	7.29	184.7	unstable	94.68	24.6
F2R	TFLLR-NH2	5.082	unstable	5.177	-2.55	445.5	unstable	469.5	unstable
S1PR1	Sphingosine 1-phosphate	7.269	6.47	7.459	6.5	477	233.6	557.1	182.8
SSTR2	Somatostatin	8.815	5.66	8.918	6.83	2867	866	1820	1714
AVPR1A	AVP	7.743	10.25	7.824	9.08	890.1	40.7	934.7	40.67
AVP2R	AVP	7.603	7.52	7.846	7.03	353.3	258.6	334.2	1804
VIPR1	VIP	9.109	6.92	9.254	unstable	1367	28.97	1060	unstable
NPY1R	NPY		8.2	8.815	6.28		53.76	42.09	106.1
NPY5R	NPY		7.92		7.07		210.3		1046

Supplemental Notes

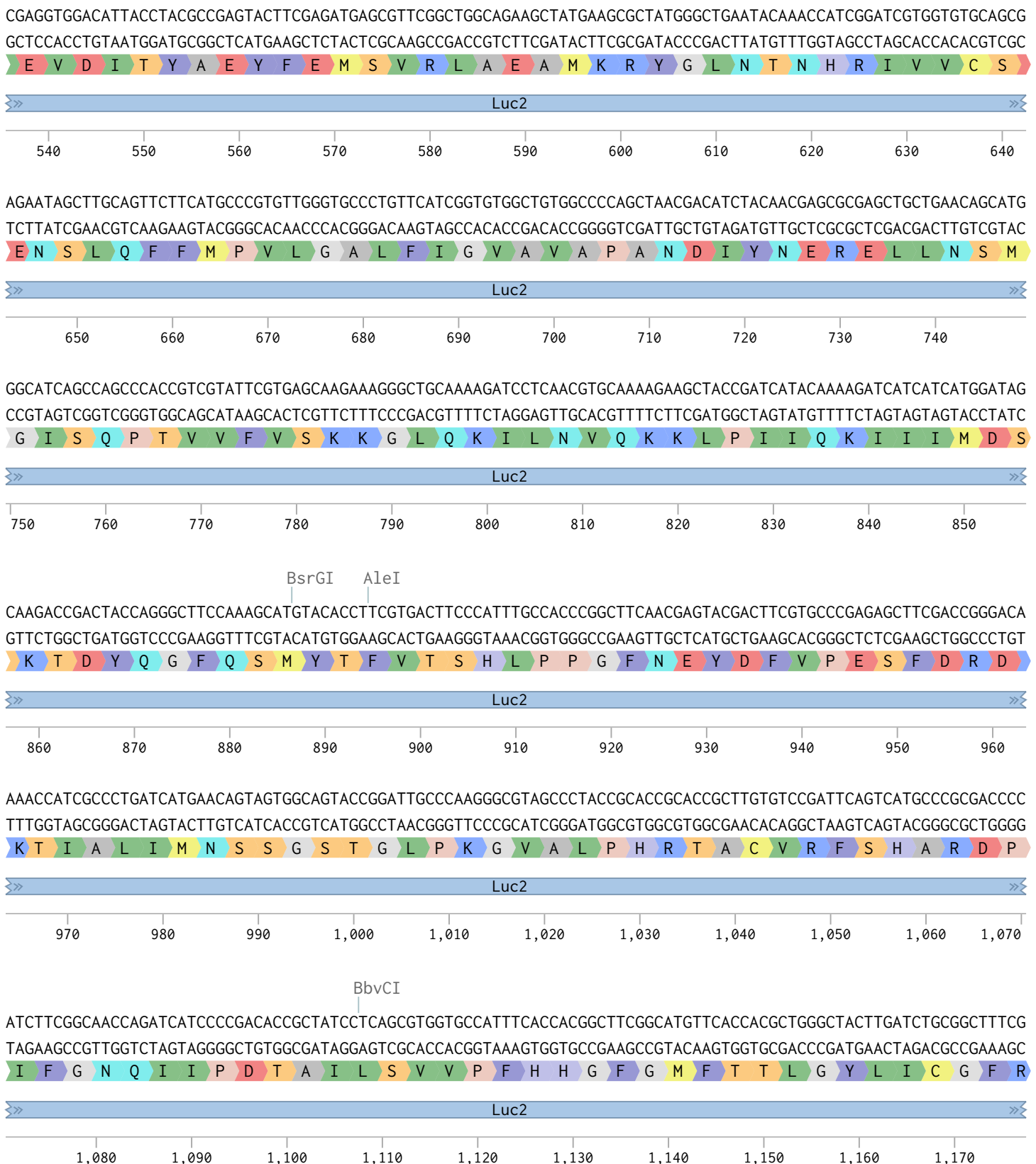
Supplementary Note 1. Sequences of Tango-Trio constructs stably expressed in HTTL, HTTL-B1, HTTL-B2, and HTTL-F cell lines. Information regarding the cloning of the plasmids is provided in the Methods.

(from 1-535 bp)

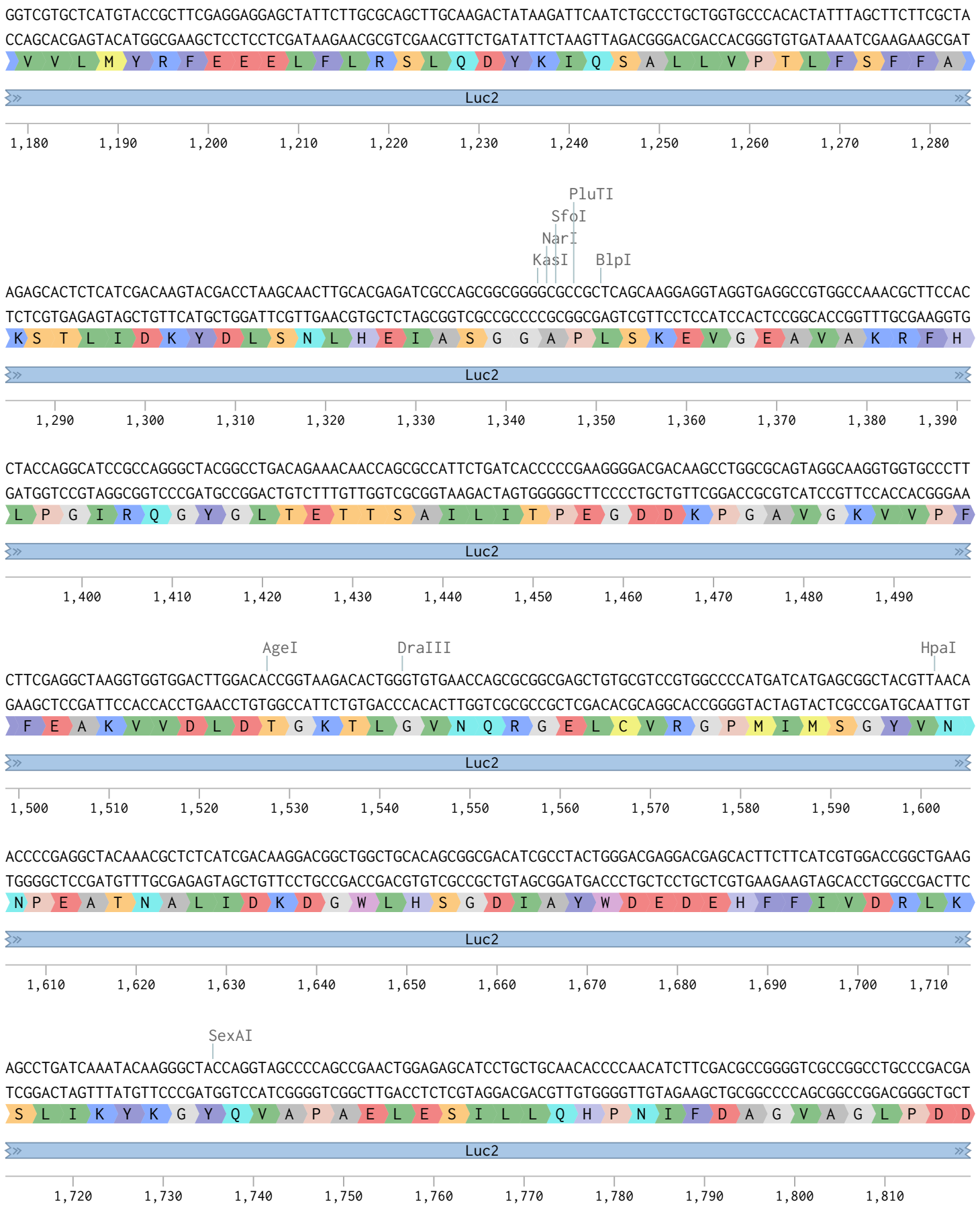
Tight-pNLCol1-Luc2 (6844 bp)



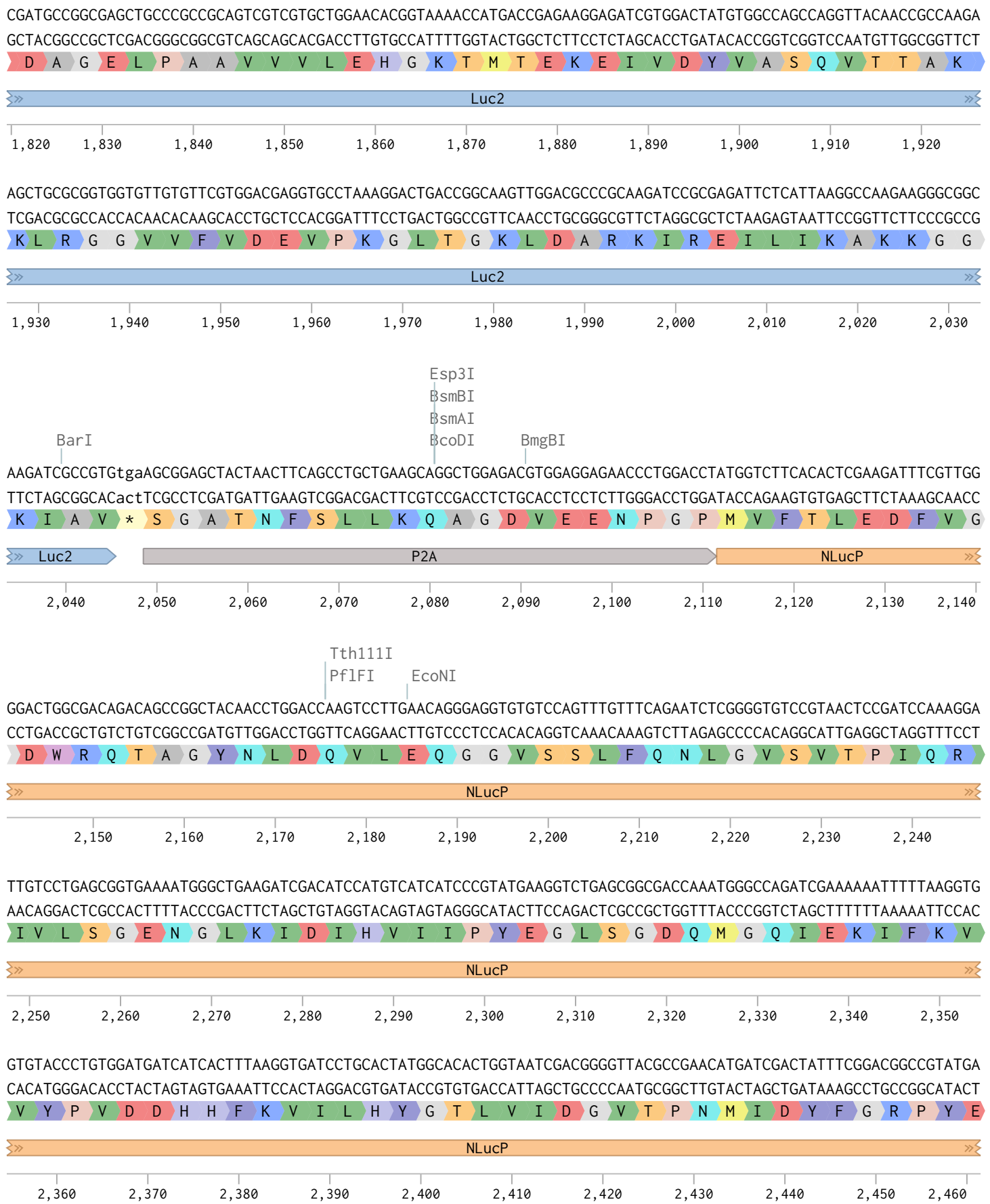
Tight-pNLCoI1-Luc2 (6844 bp) (from 536-1177 bp)



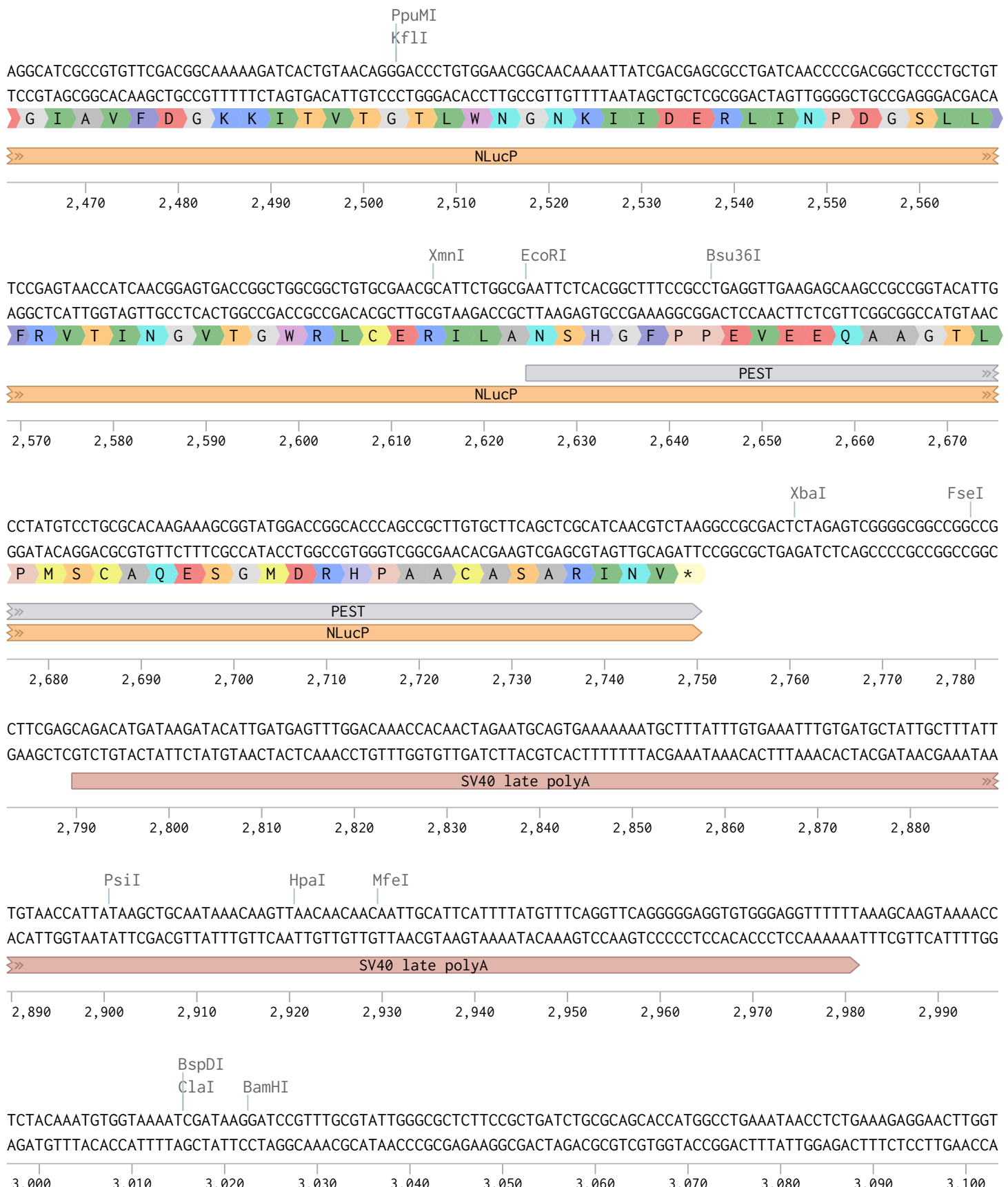
Tight-pNLCol1-Luc2 (6844 bp) (from 1178-1819 bp)



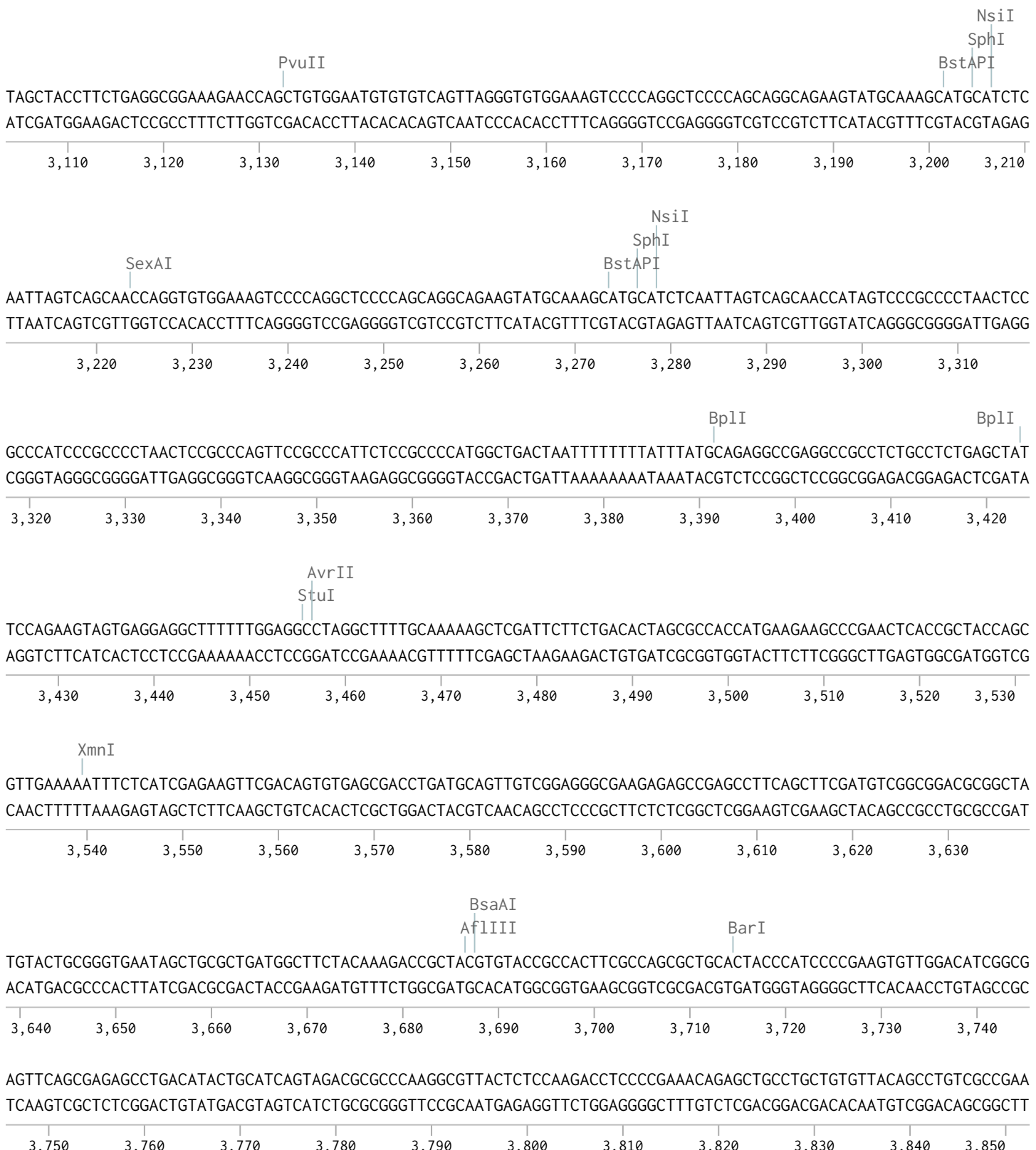
Tight-pNLCol1-Luc2 (6844 bp) (from 1820-2461 bp)



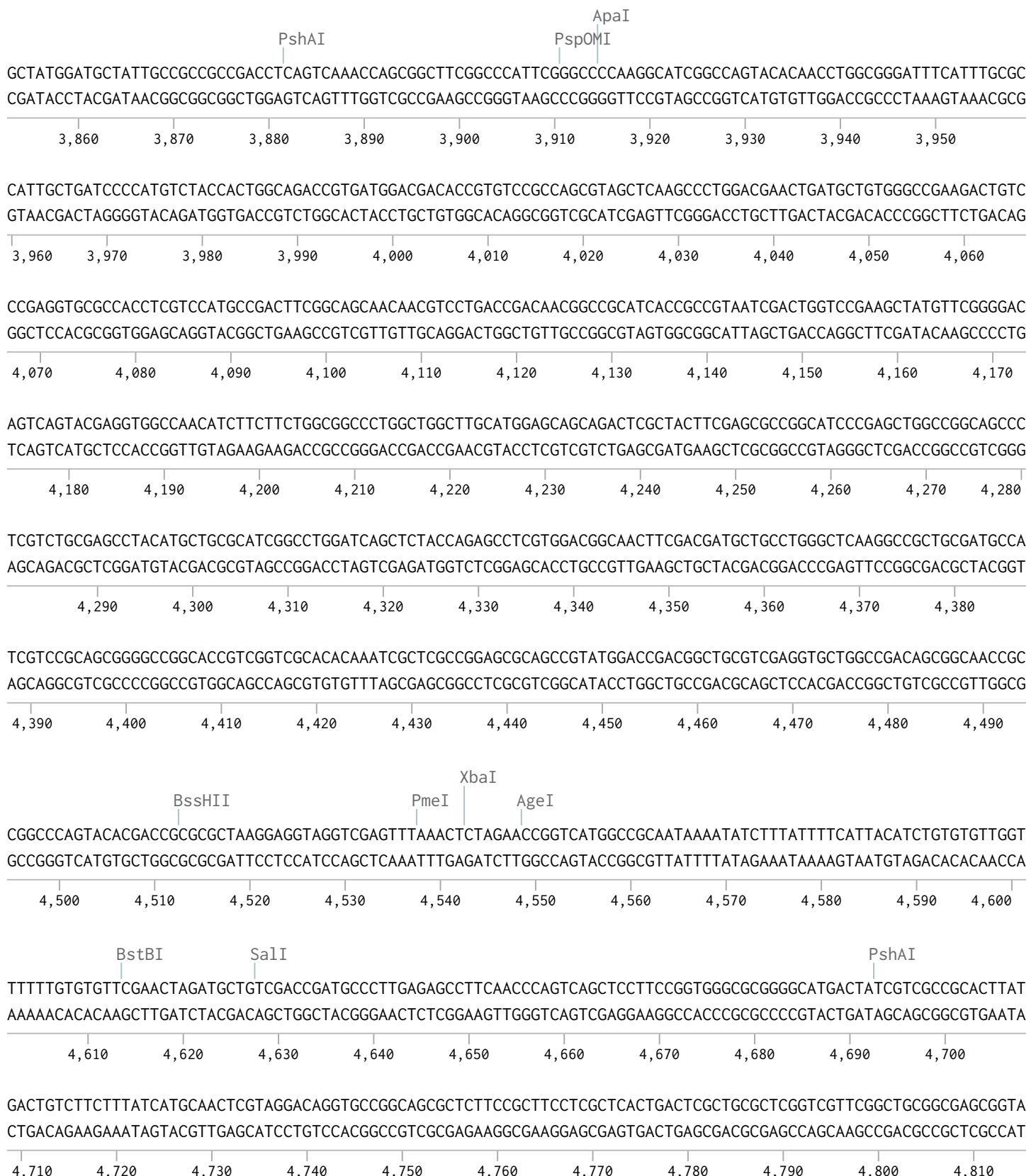
Tight-pNLCoI1-Luc2 (6844 bp) (from 2462-3103 bp)



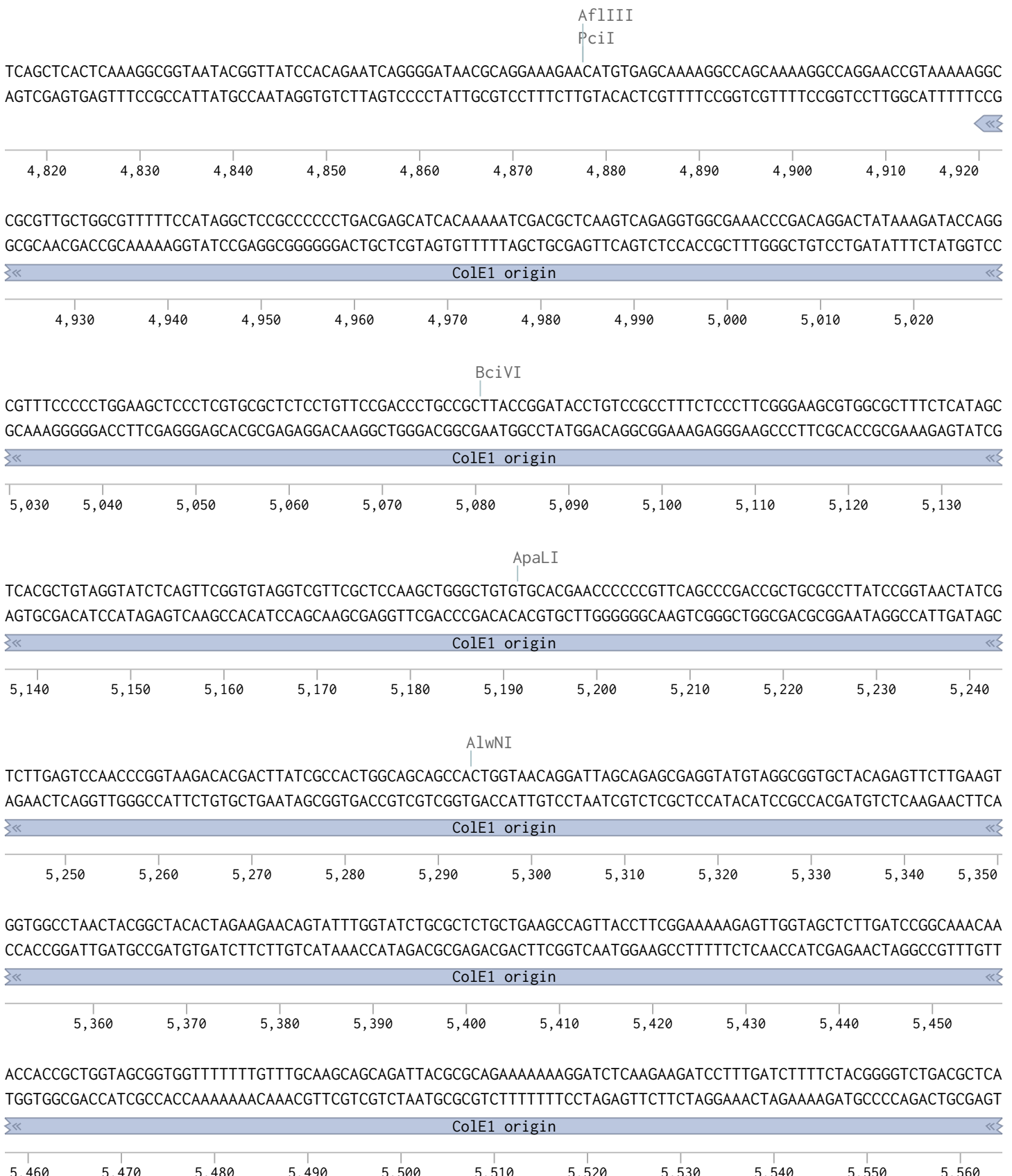
Tight-pNLCol1-Luc2 (6844 bp) (from 3104-3852 bp)



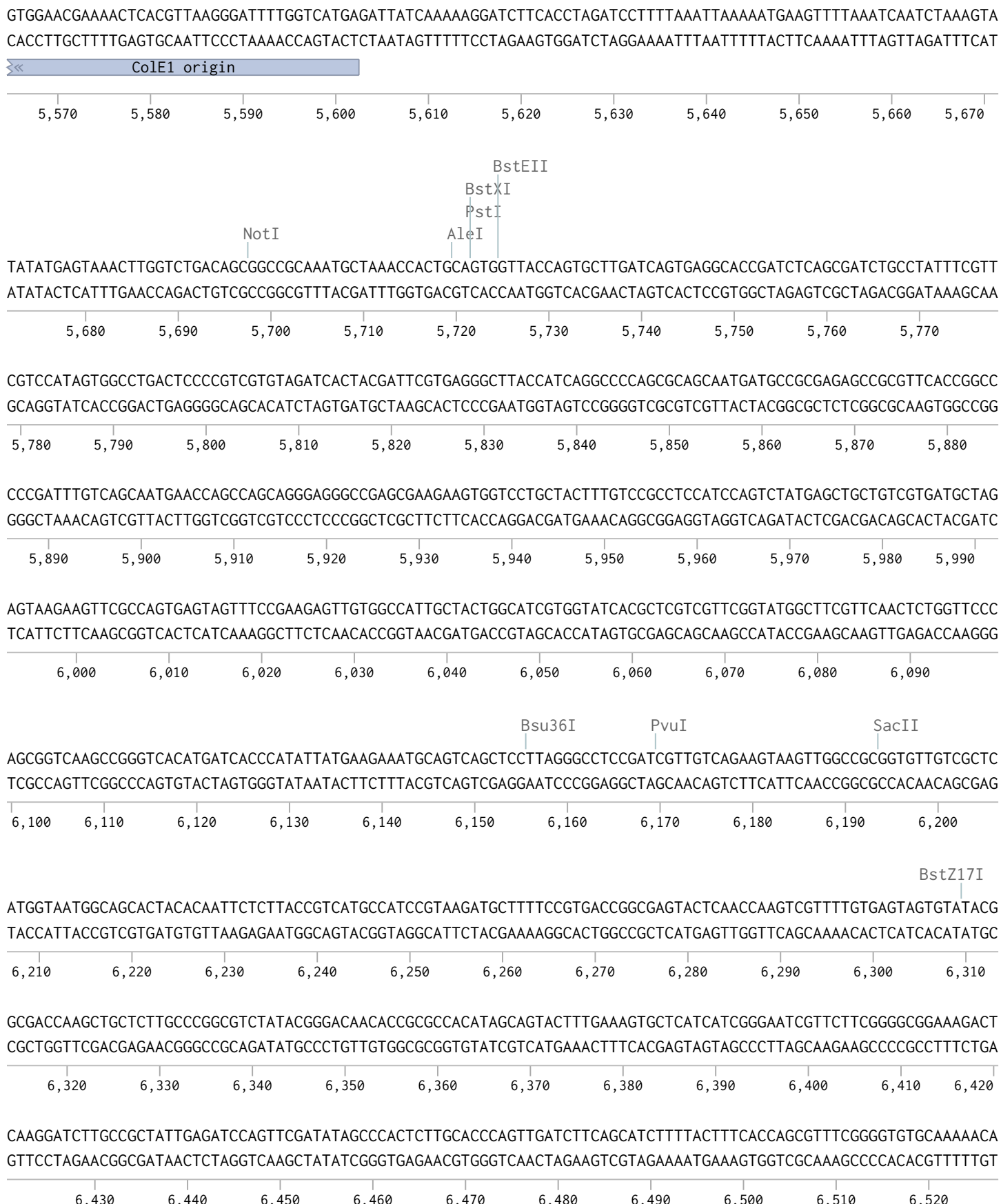
Tight-pNLCol1-Luc2 (6844 bp) (from 3853-4815 bp)



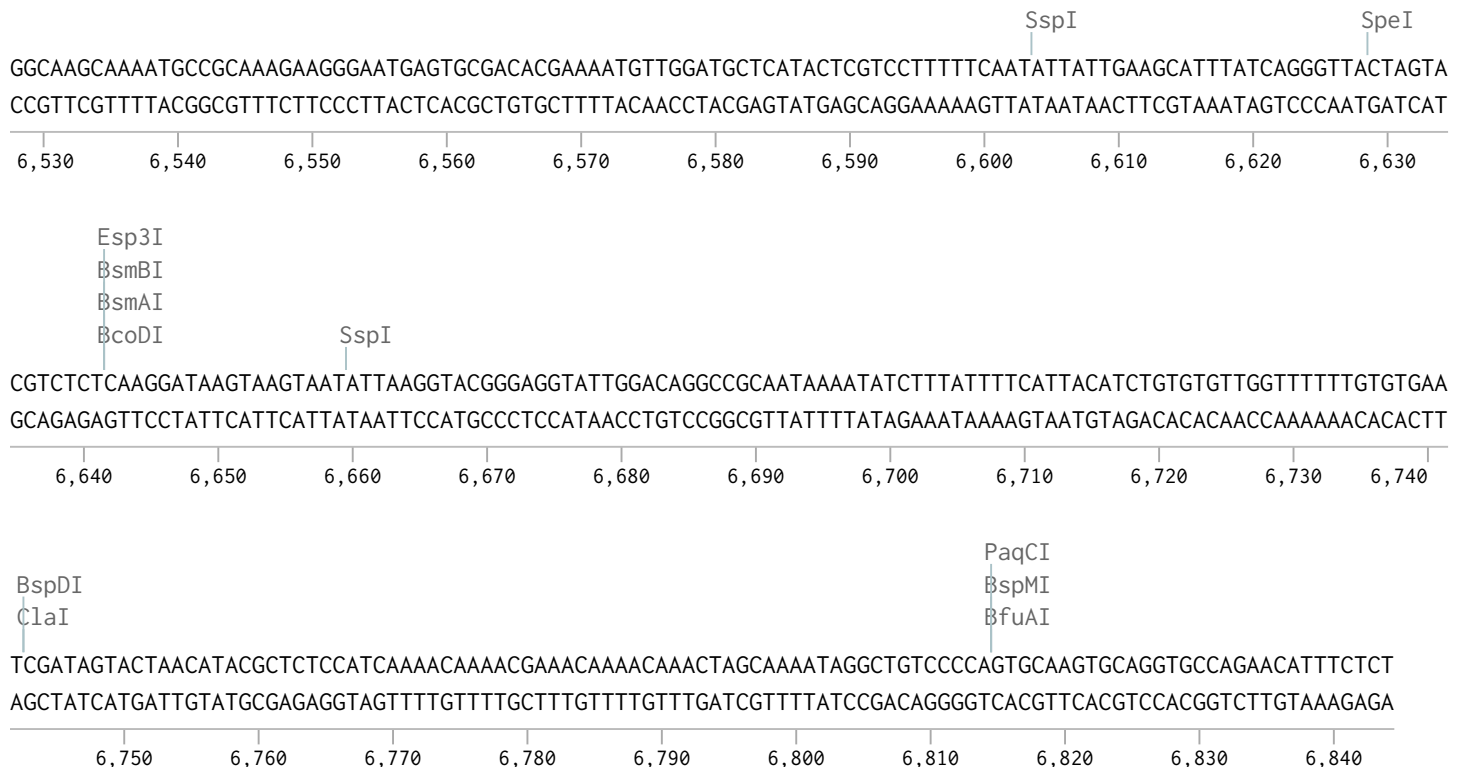
Tight-pNLCol1-Luc2 (6844 bp) (from 4816-5564 bp)



Tight-pNLCol1-Luc2 (6844 bp) (from 5565-6527 bp)

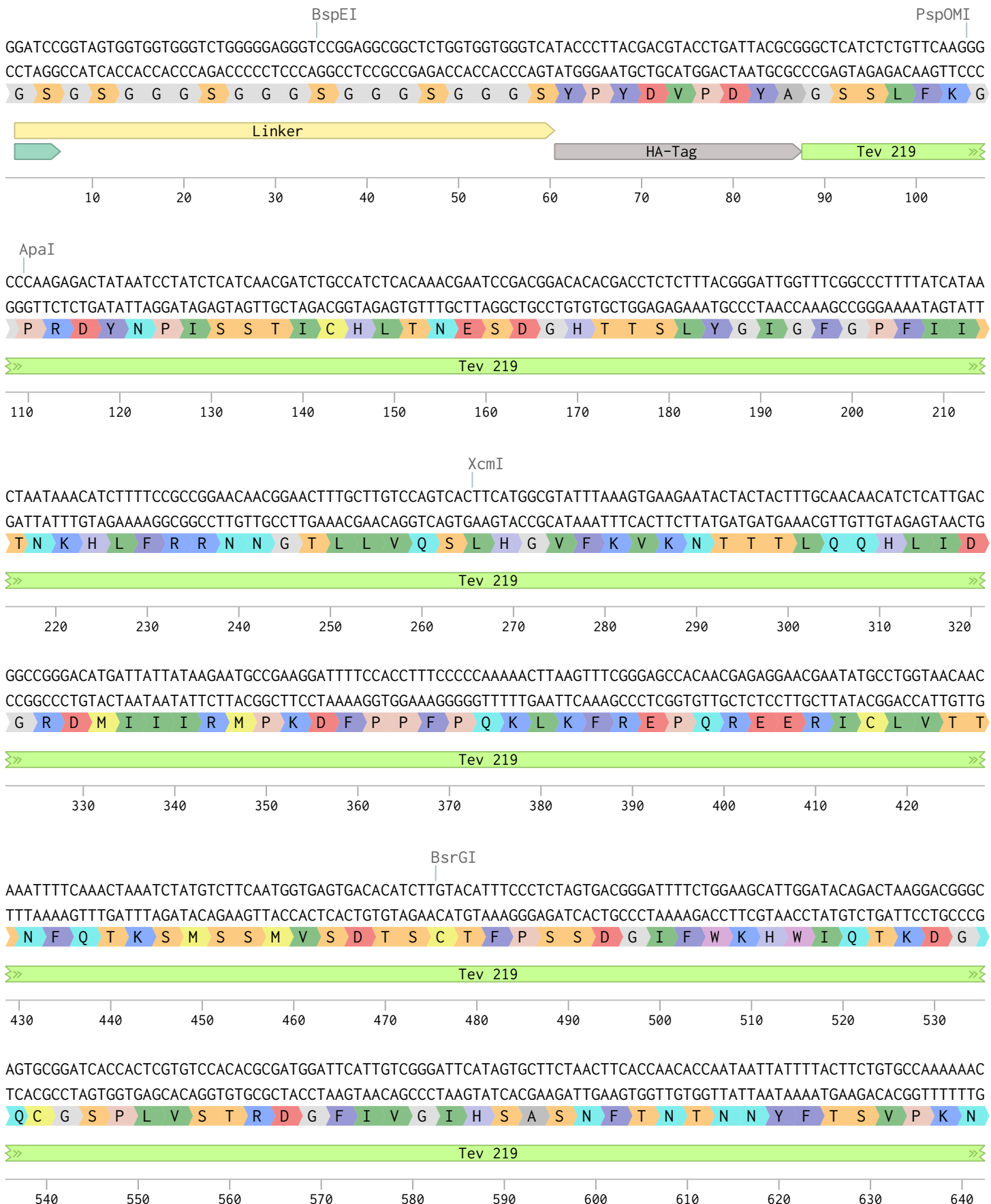


Tight-pNLCol1-Luc2 (6844 bp) (from 6528-6844 bp)



(from 1-642 bp)

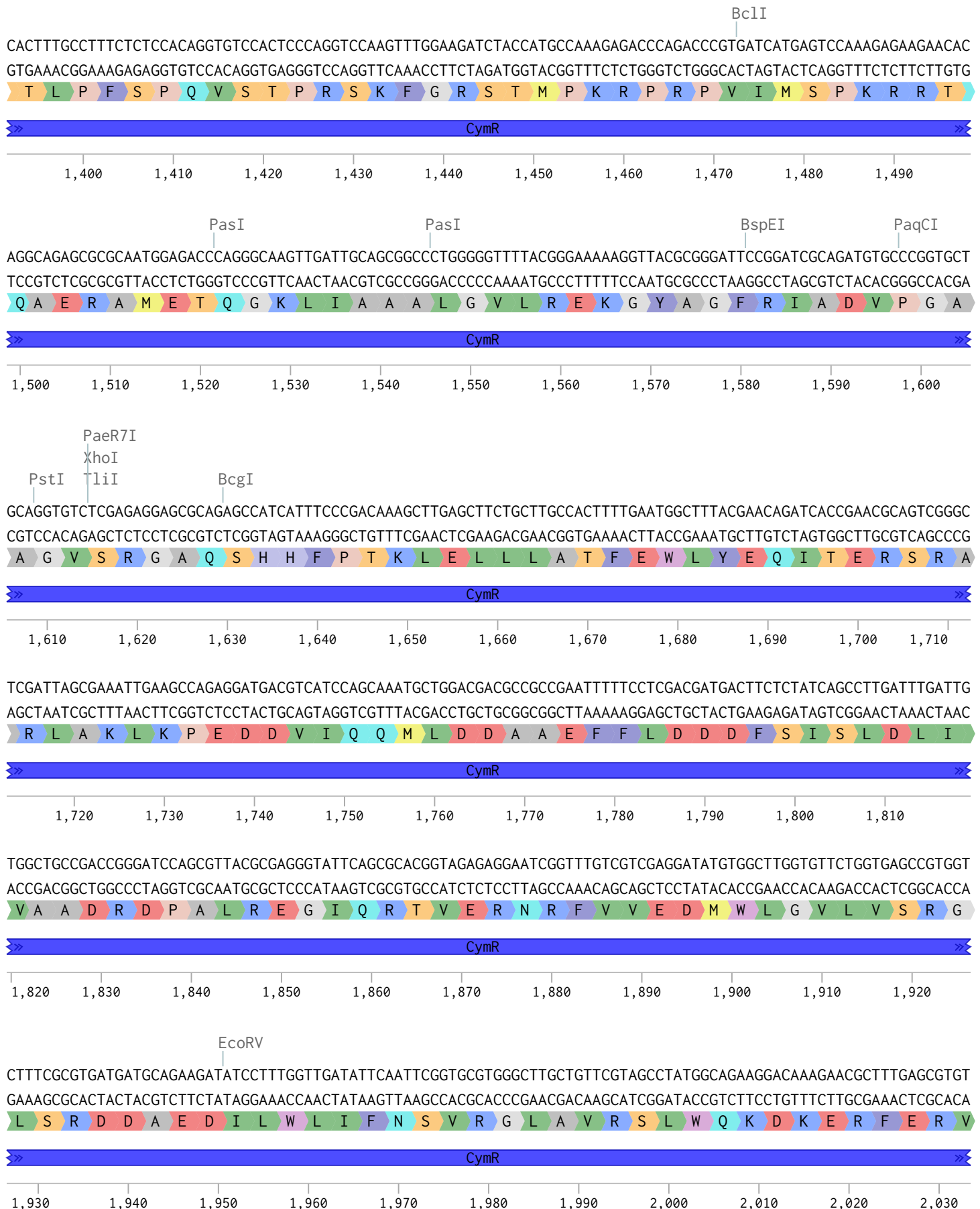
bArr1-HA-TEV219 pCDH-CuO-MCS-EF1 α -CymR-T2A-Bleo...



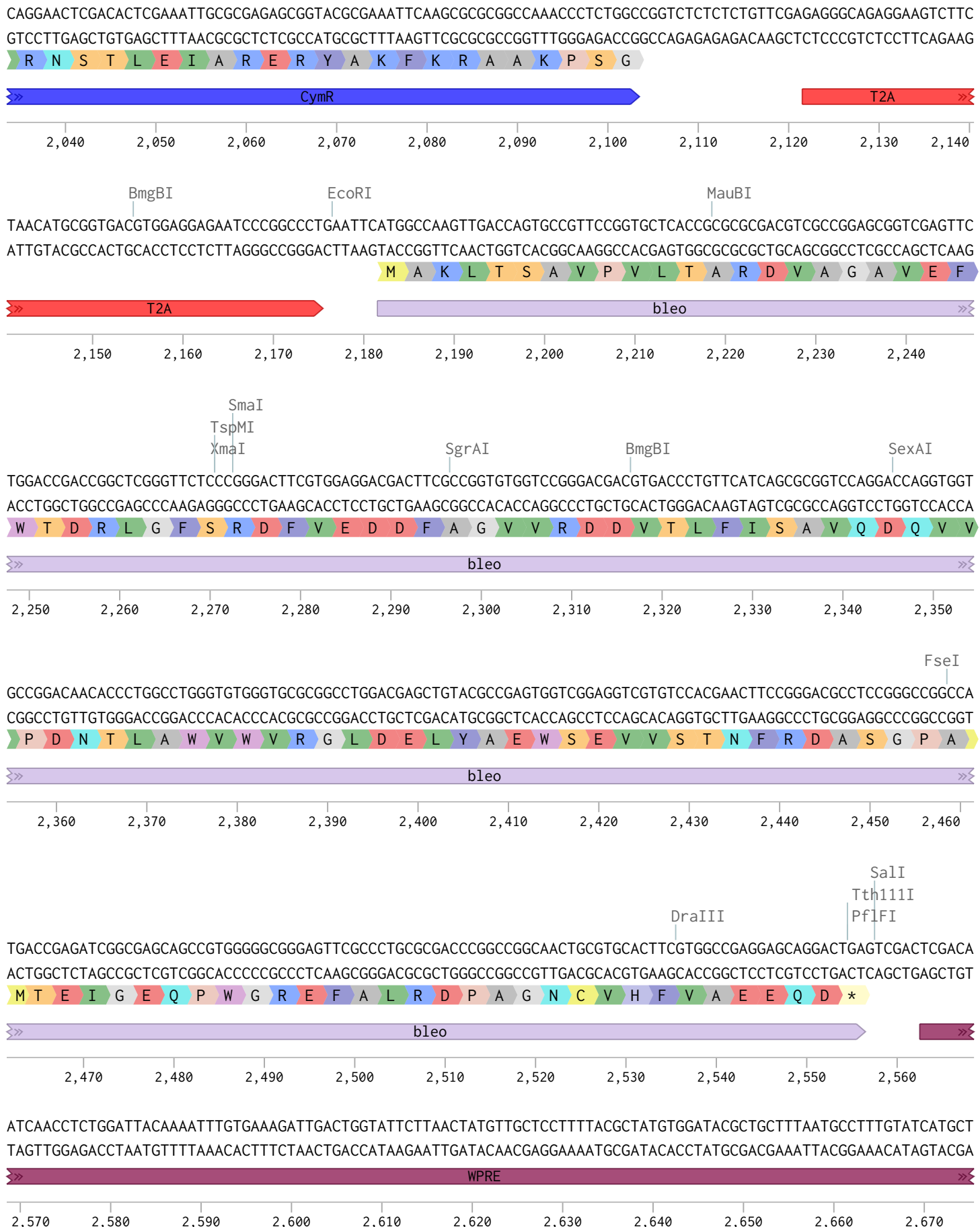
bArr1-HA-TEV219 pCDH-CuO-MCS-EF1 α -CymR-T2A-Bleo3 SparQ (10934 bp)



bArr1-HA-TEV219 pCDH-CuO-MCS-EF1 α -CymR-T2A-Bleo3 SparQ (10934 bp)



bArr1-HA-TEV219 pCDH-CuO-MCS-EF1 α -CymR-T2A-Bleo3 SparQ (10934 bp)



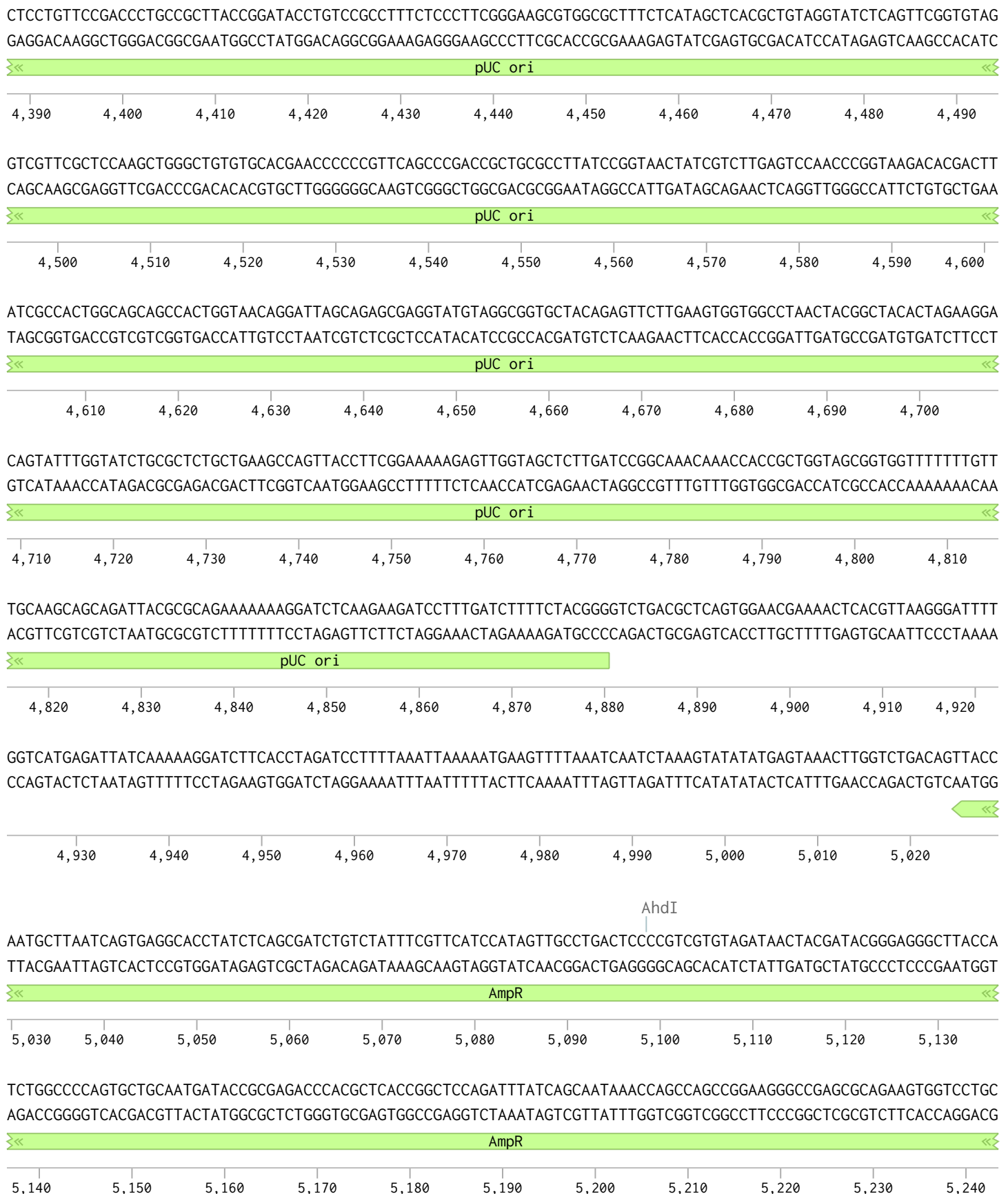
bArr1-HA-TEV219 pCDH-CuO-MCS-EF1 α -CymR-T2A-Bleo3 SparQ (10934 bp)



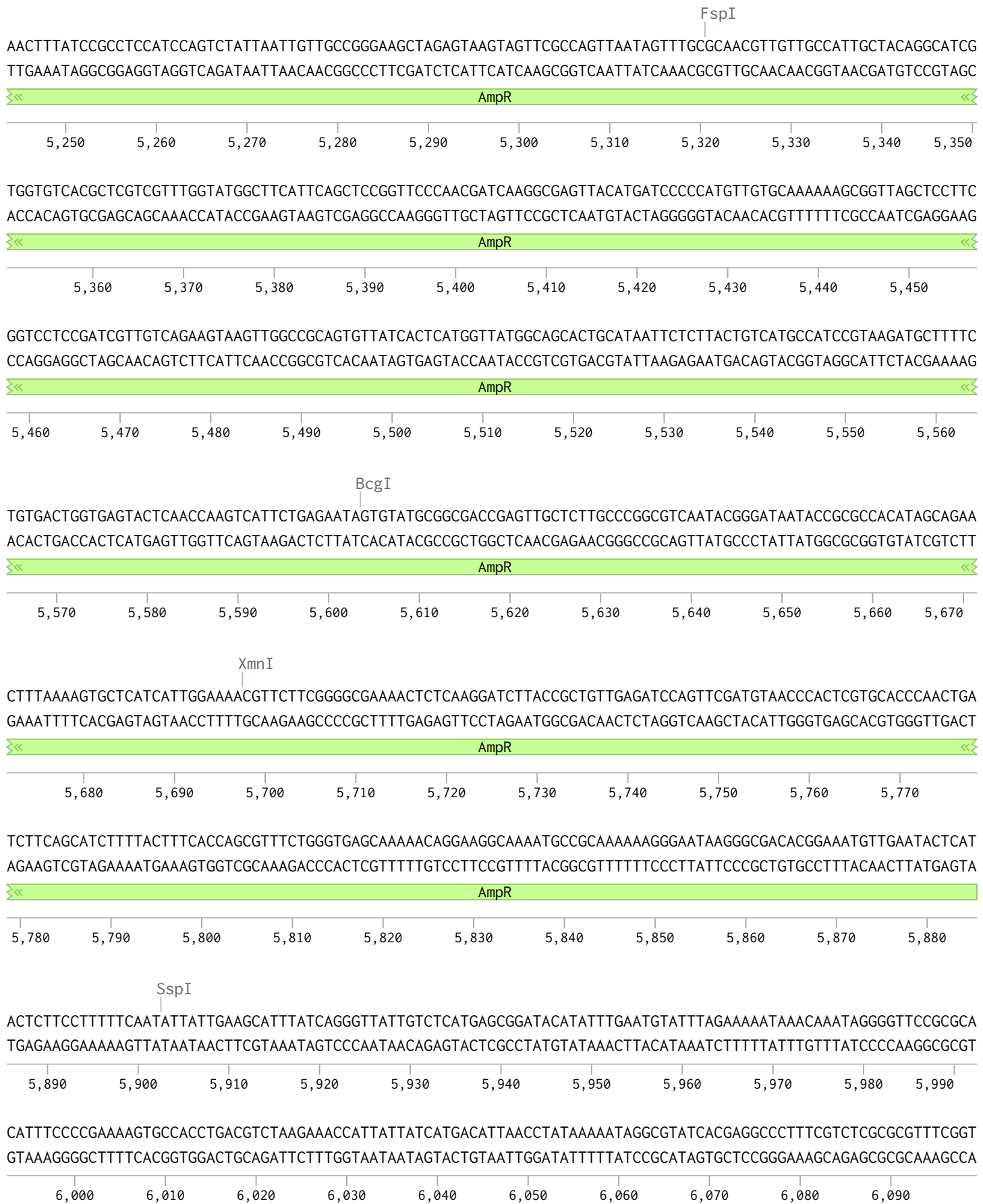
bArr1-HA-TEV219 pCDH-CuO-MCS-EF1 α -CymR-T2A-Bleo3 SparQ (10934 bp)



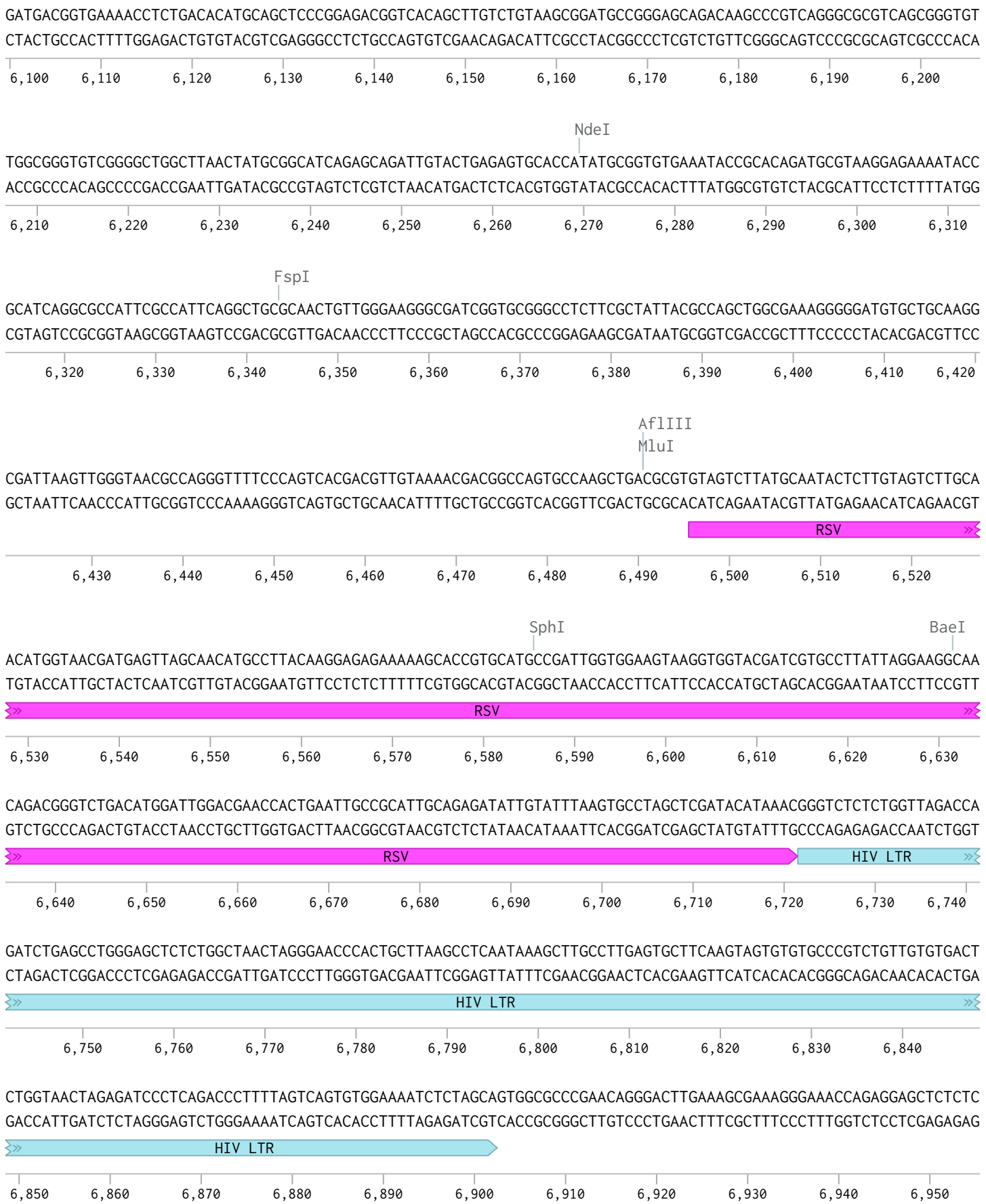
bArr1-HA-TEV219 pCDH-CuO-MCS-EF1 α -CymR-T2A-Bleo3 SparQ (10934 bp)



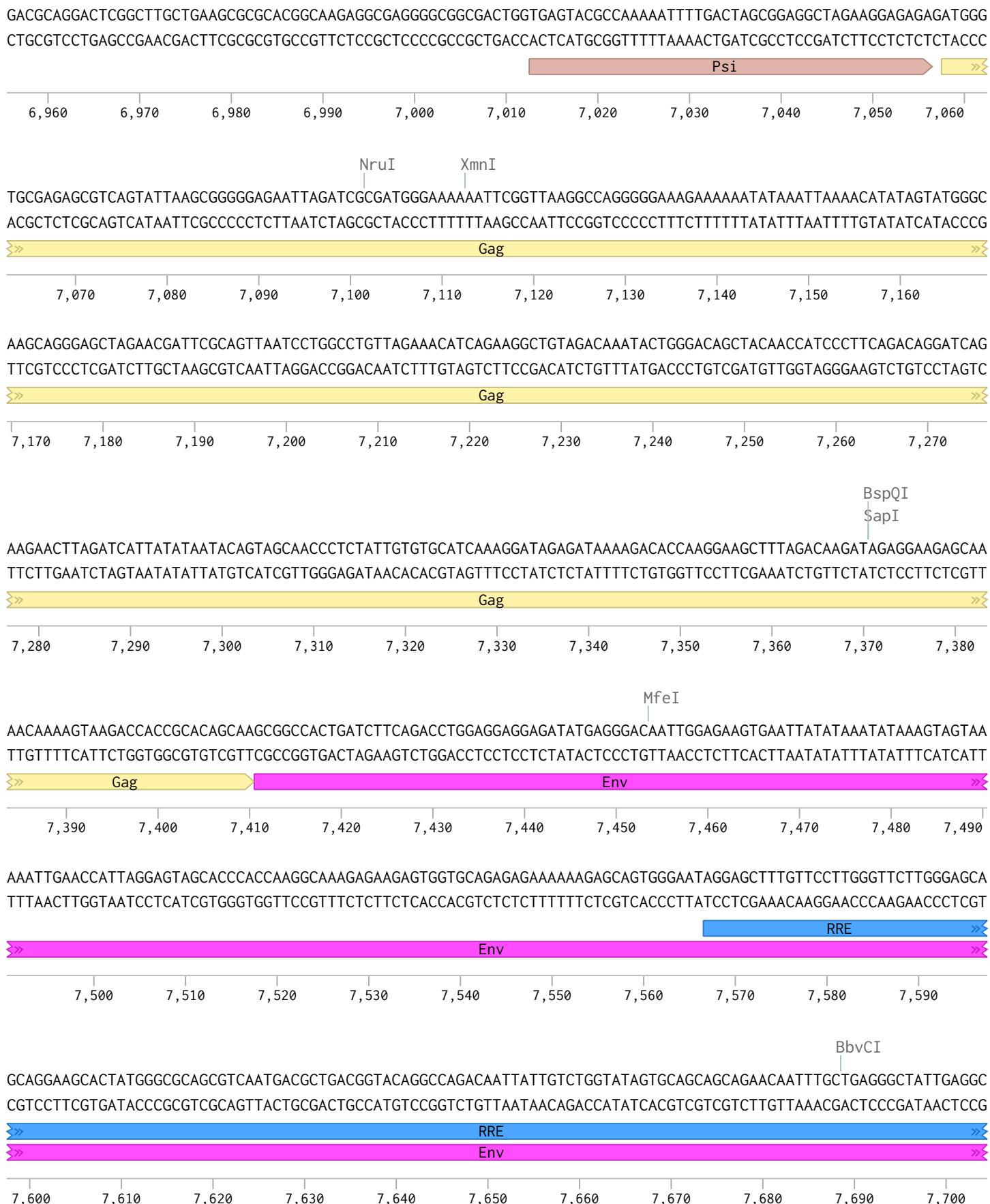
bArr1-HA-TEV219 pCDH-CuO-MCS-EF1 α -CymR-T2A-Bleo3 SparQ (10934 bp)



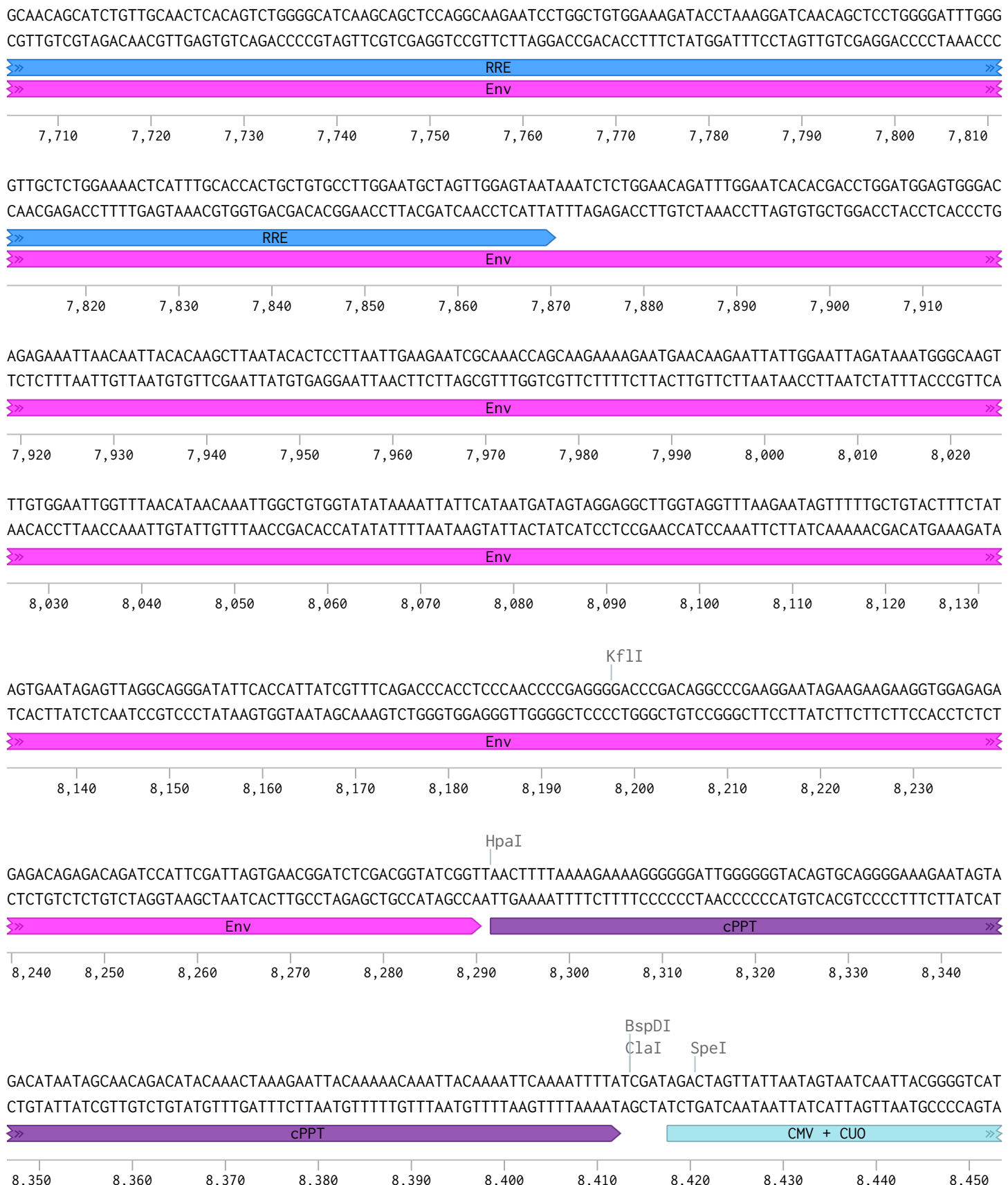
bArr1-HA-TEV219 pCDH-CuO-MCS-EF1 α -CymR-T2A-Bleo3 SparQ (10934 bp)



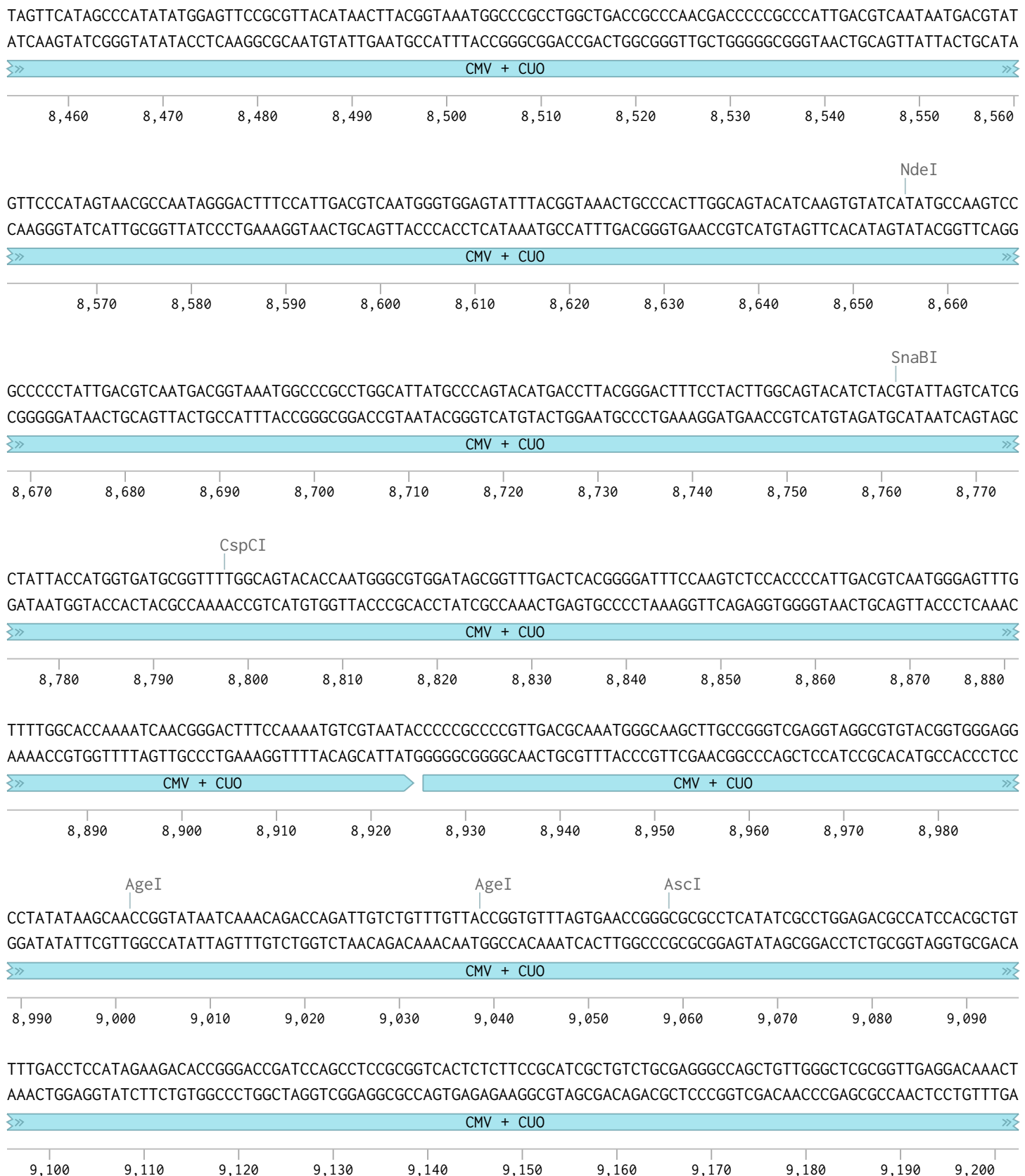
bArr1-HA-TEV219 pCDH-CuO-MCS-EF1 α -CymR-T2A-Bleo3 SparQ (10934 bp)



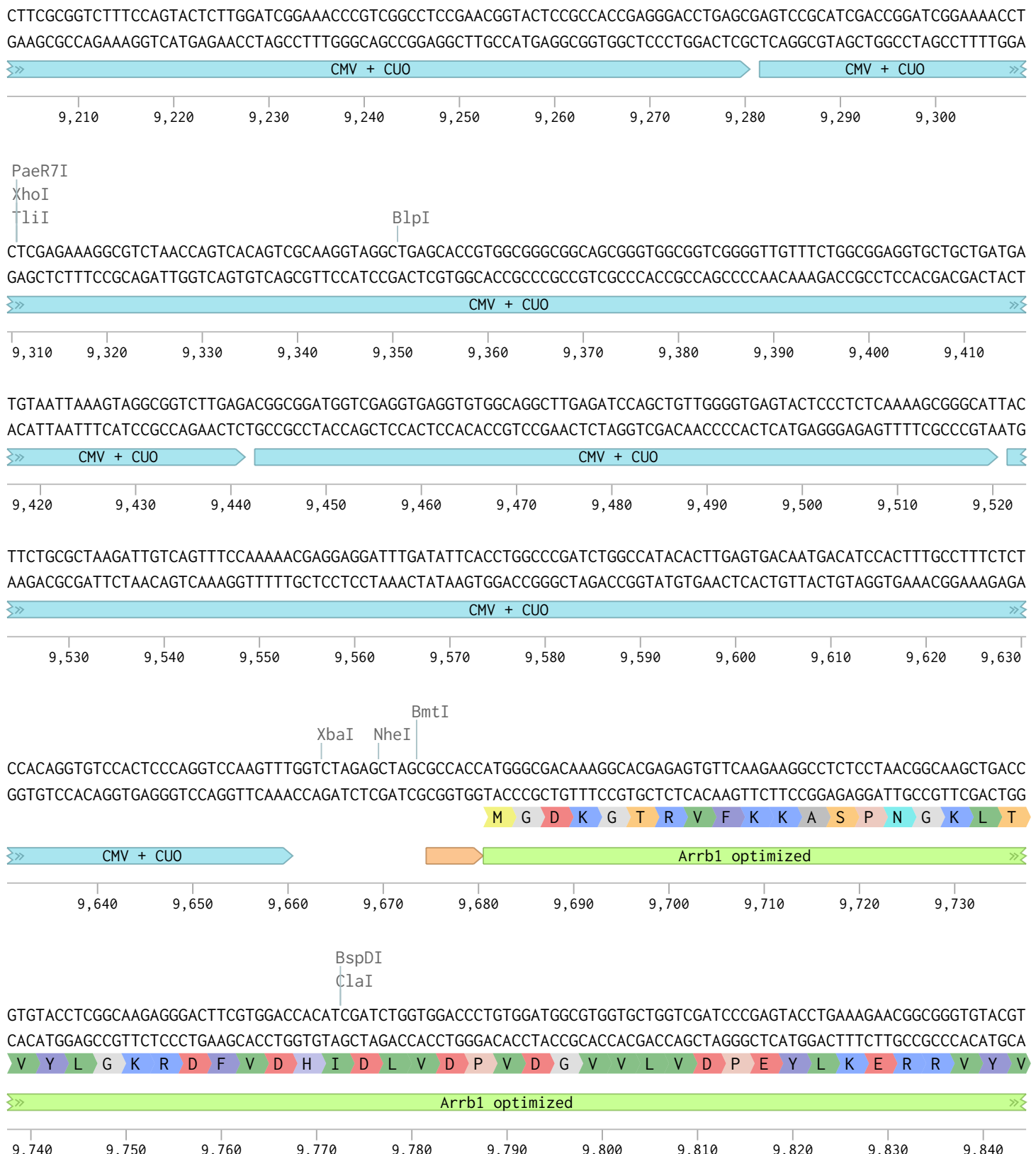
bArr1-HA-TEV219 pCDH-CuO-MCS-EF1 α -CymR-T2A-Bleo3 SparQ (10934 bp)



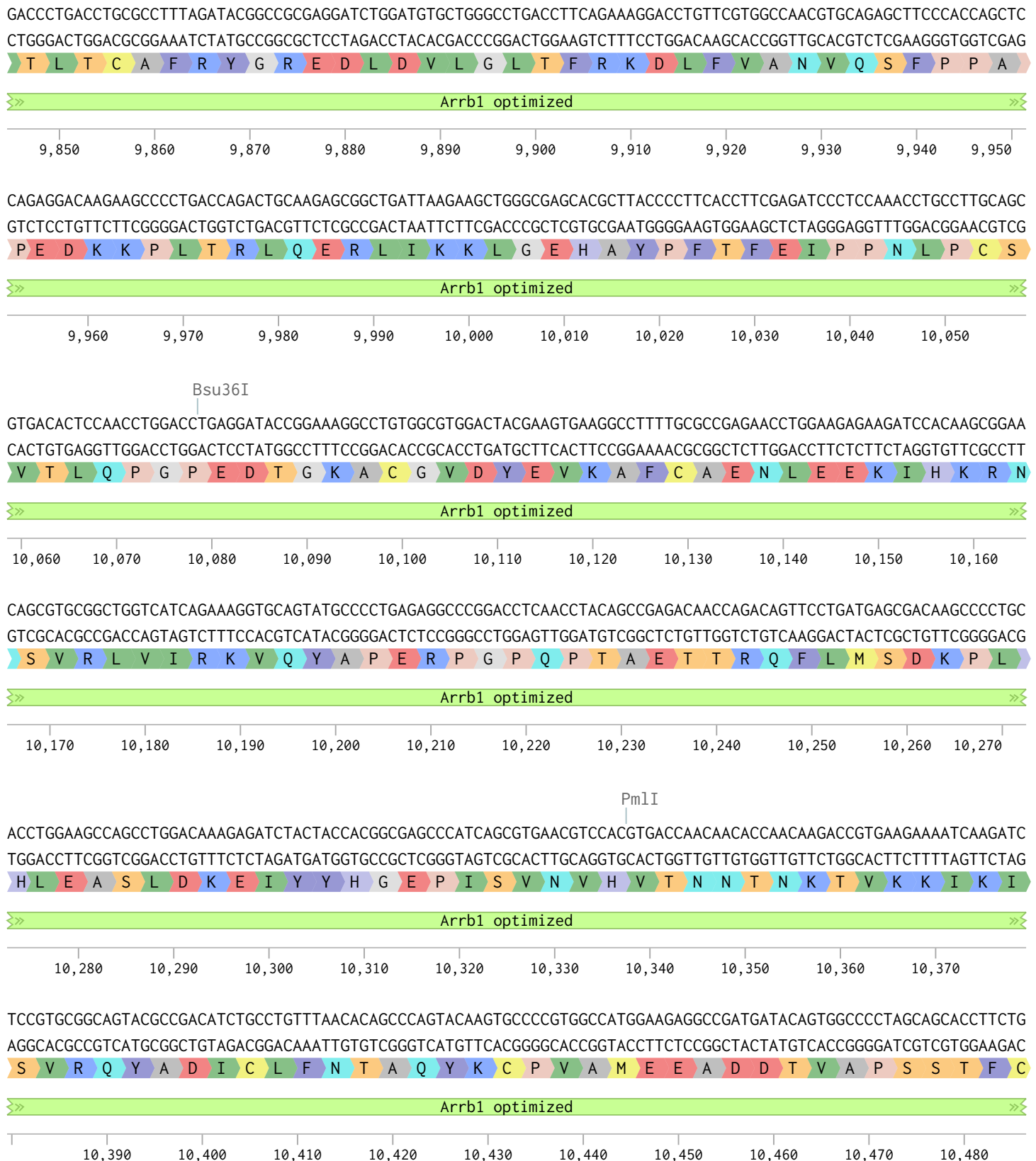
bArr1-HA-TEV219 pCDH-CuO-MCS-EF1 α -CymR-T2A-Bleo3 SparQ (10934 bp)



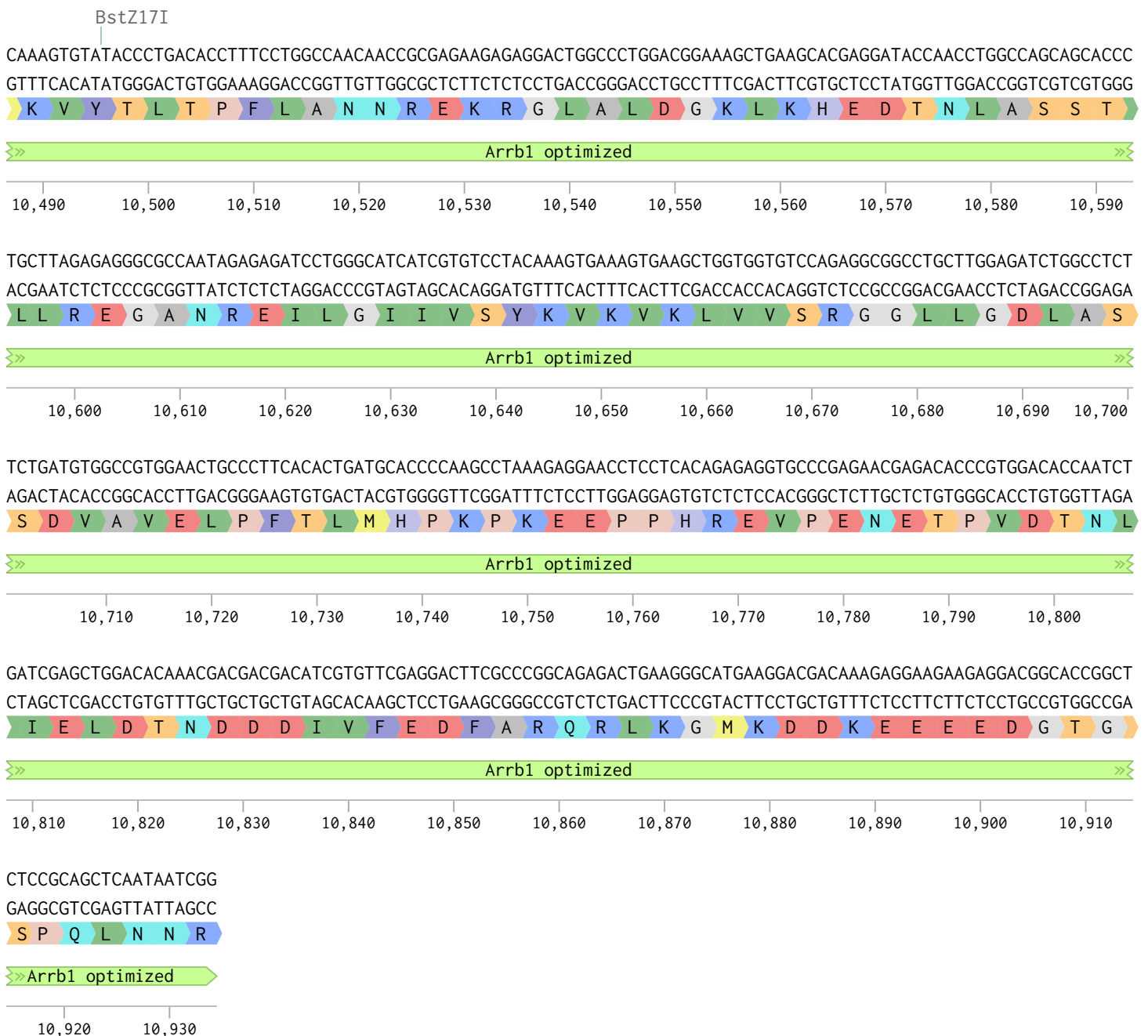
bArr1-HA-TEV219 pCDH-CuO-MCS-EF1 α -CymR-T2A-Bleo3 SparQ (10934 bp)



bArr1-HA-TEV219 pCDH-CuO-MCS-EF1 α -CymR-T2A-Bleo3 SparQ (10934 bp)

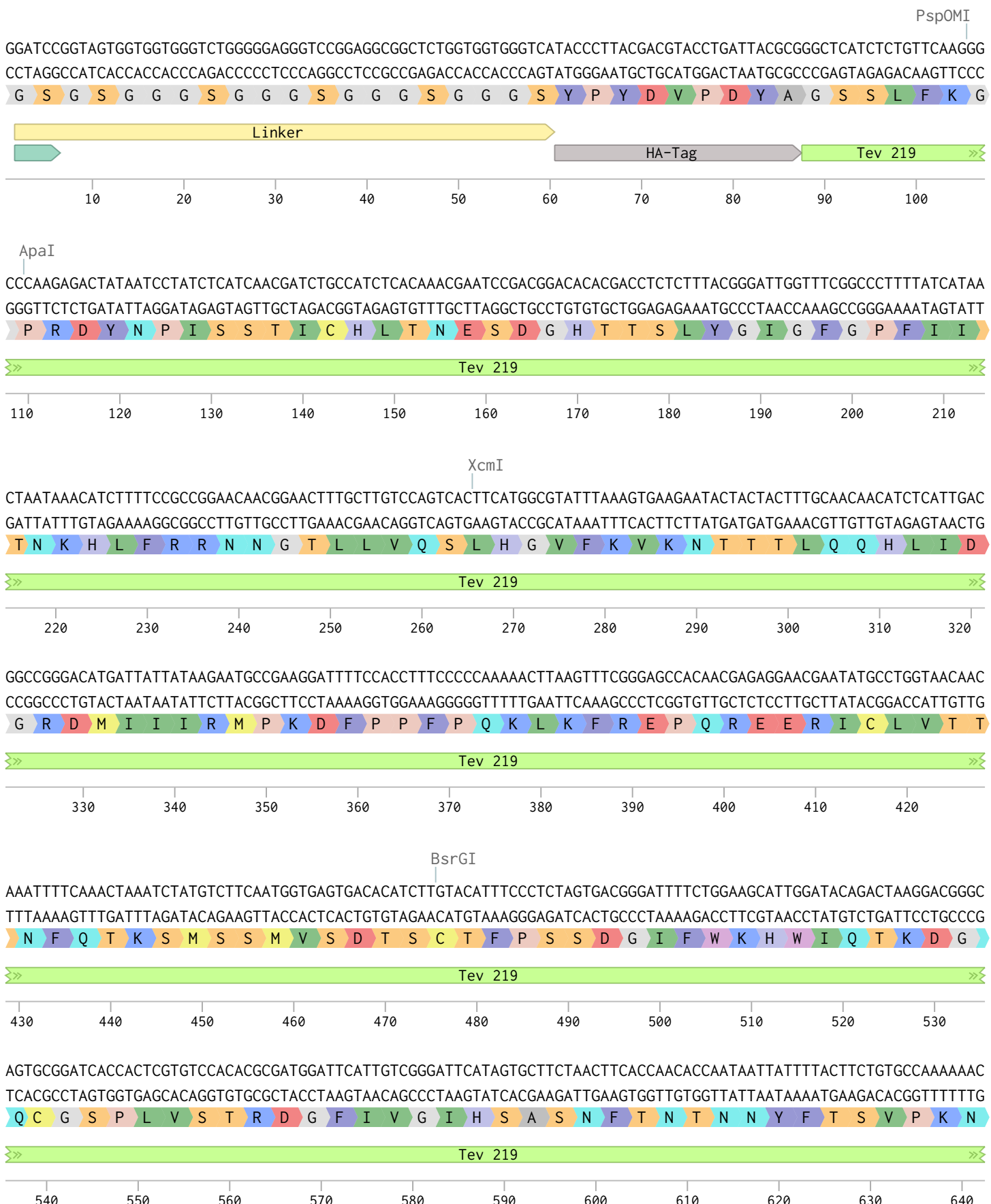


bArr1-HA-TEV219 pCDH-CuO-MCS-EF1 α -CymR-T2A-Bleo3 SparQ (10934 bp)



(from 1-642 bp)

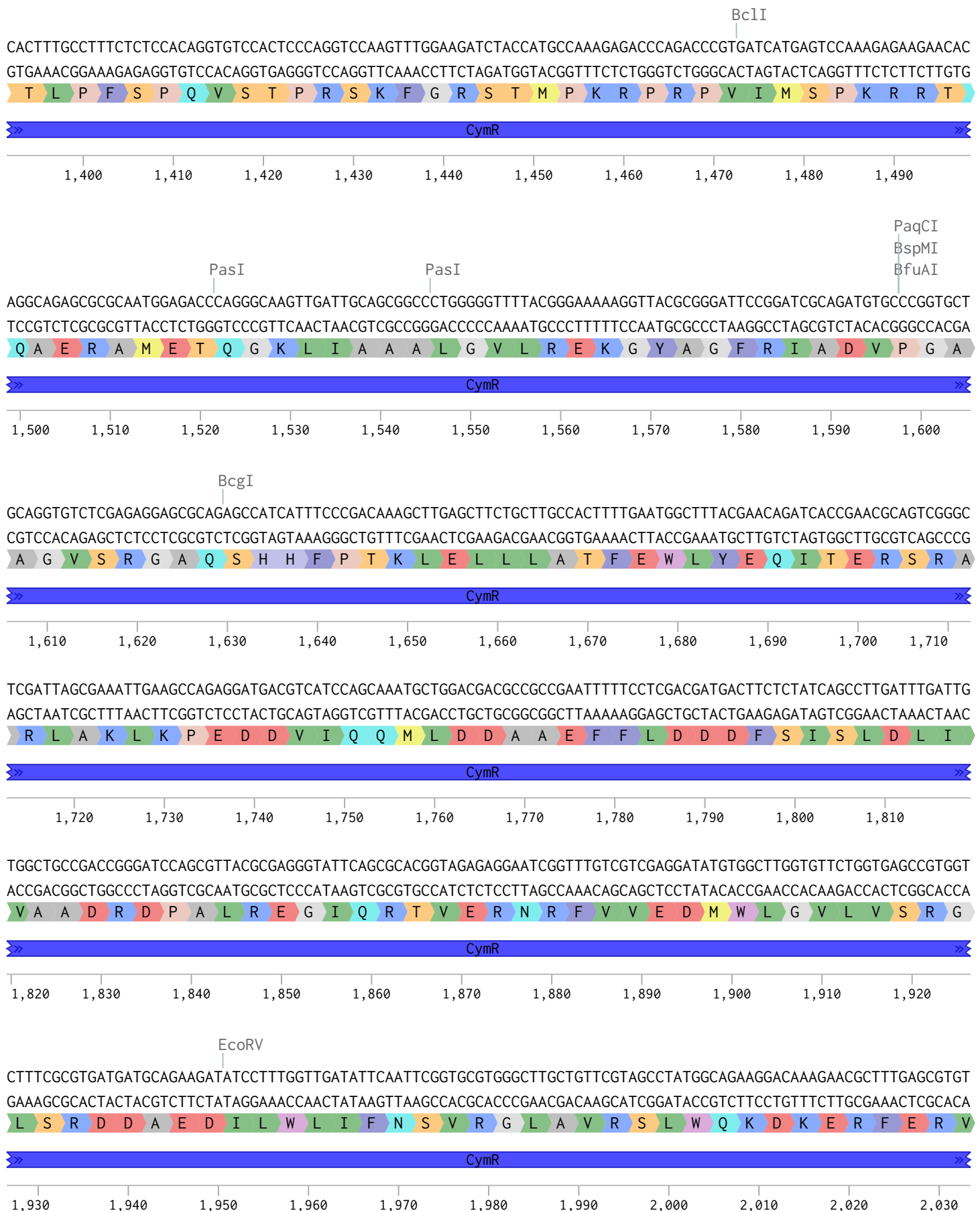
bArr2-HA-TEV219 pCDH-CuO-MCS-EF1 α -CymR-T2A-Bleo...



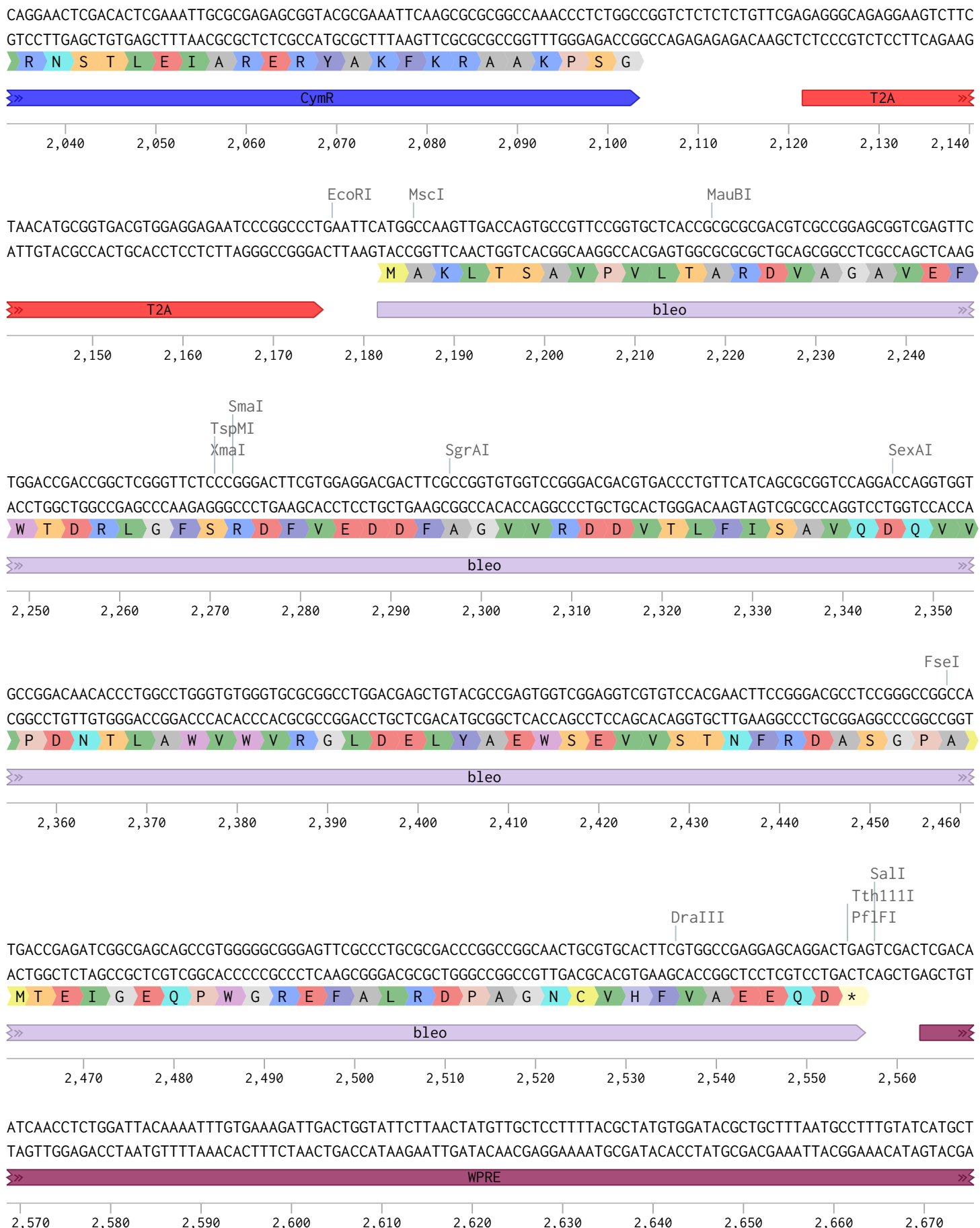
bArr2-HA-TEV219 pCDH-CuO-MCS-EF1 α -CymR-T2A-Bleo3 SparQ (10907 bp)



bArr2-HA-TEV219 pCDH-CuO-MCS-EF1 α -CymR-T2A-Bleo3 SparQ (10907 bp)



bArr2-HA-TEV219 pCDH-CuO-MCS-EF1 α -CymR-T2A-Bleo3 SparQ (10907 bp)



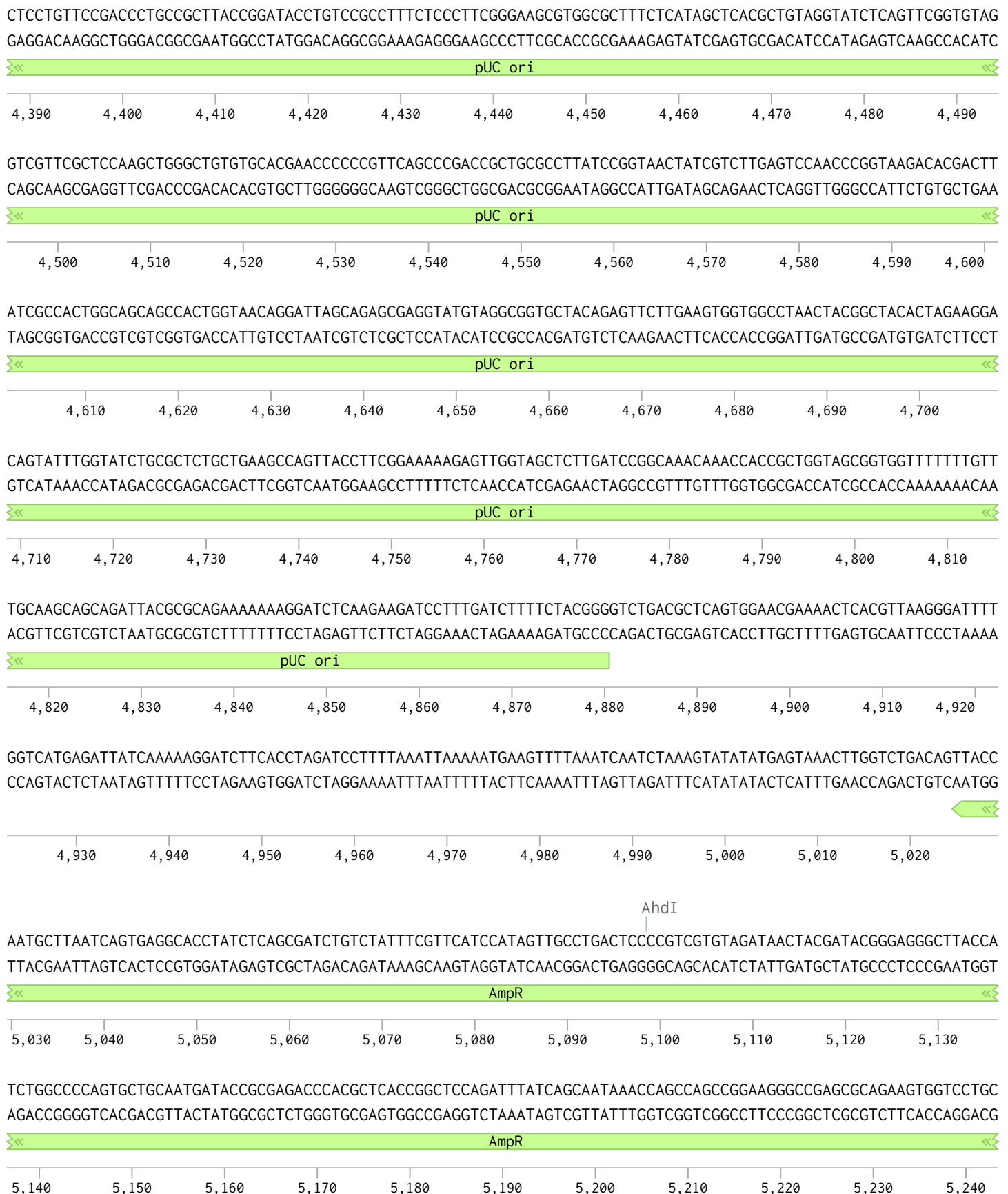
bArr2-HA-TEV219 pCDH-CuO-MCS-EF1 α -CymR-T2A-Bleo3 SparQ (10907 bp)



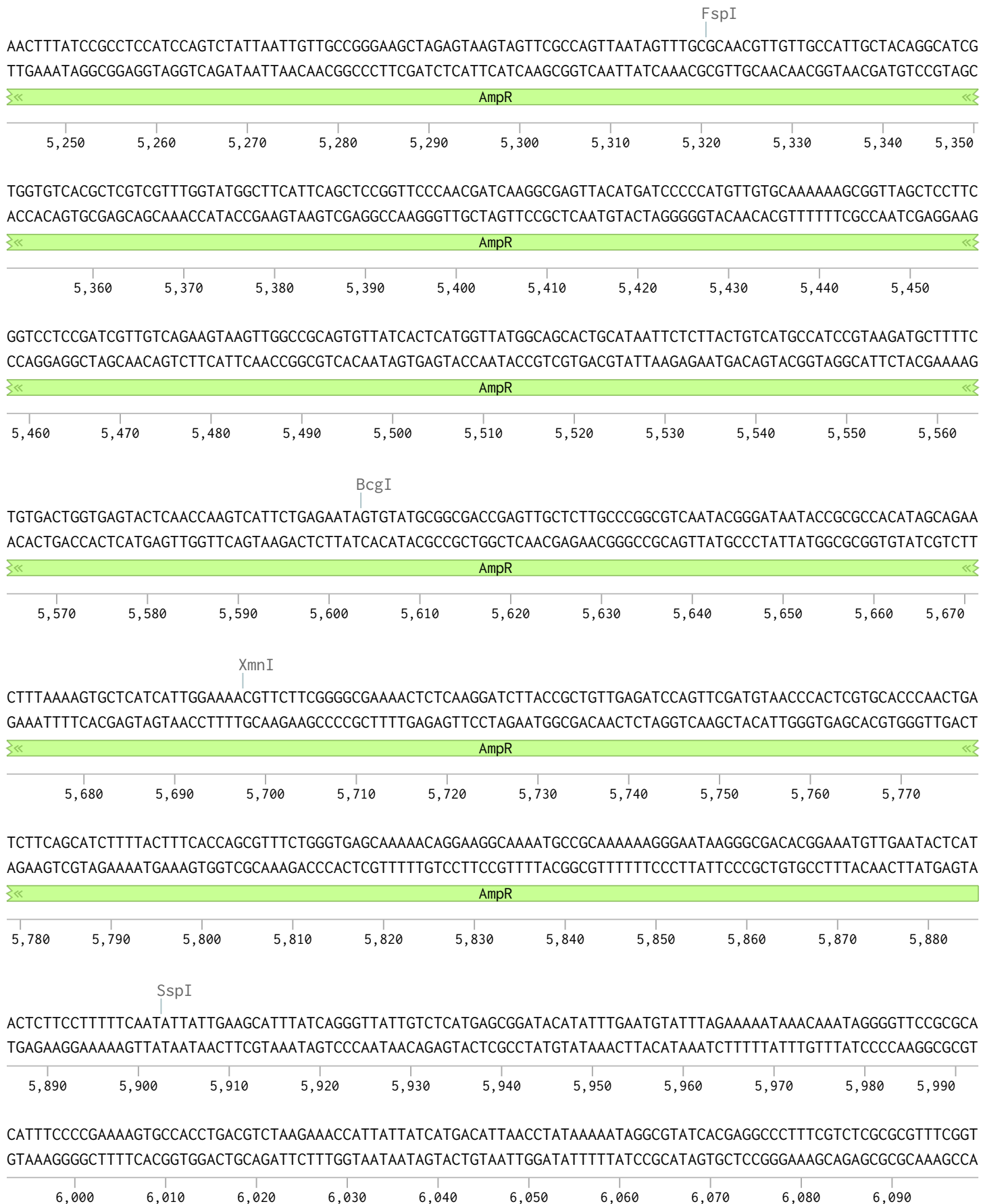
bArr2-HA-TEV219 pCDH-CuO-MCS-EF1 α -CymR-T2A-Bleo3 SparQ (10907 bp)



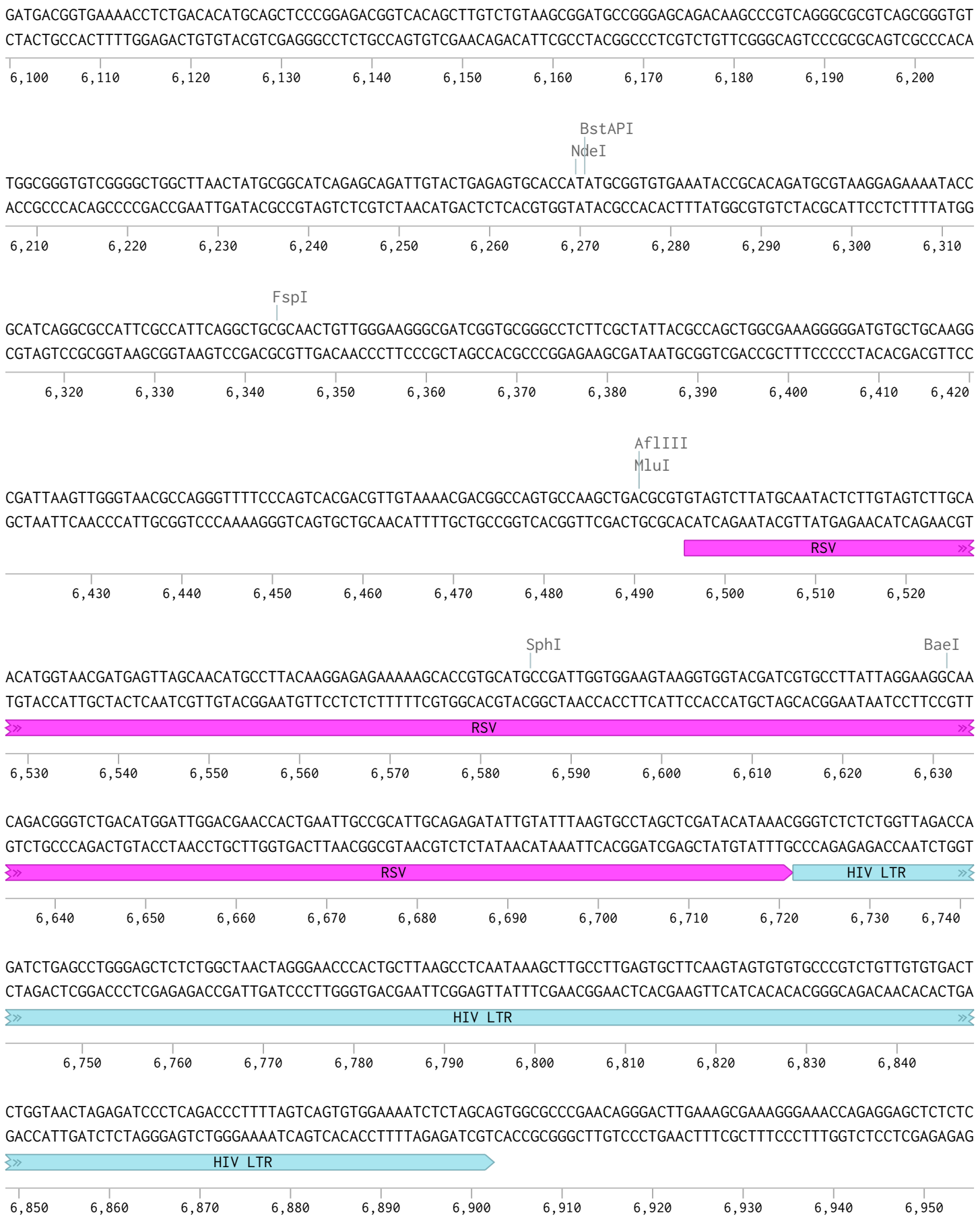
bArr2-HA-TEV219 pCDH-CuO-MCS-EF1 α -CymR-T2A-Bleo3 SparQ (10907 bp)



bArr2-HA-TEV219 pCDH-CuO-MCS-EF1 α -CymR-T2A-Bleo3 SparQ (10907 bp)



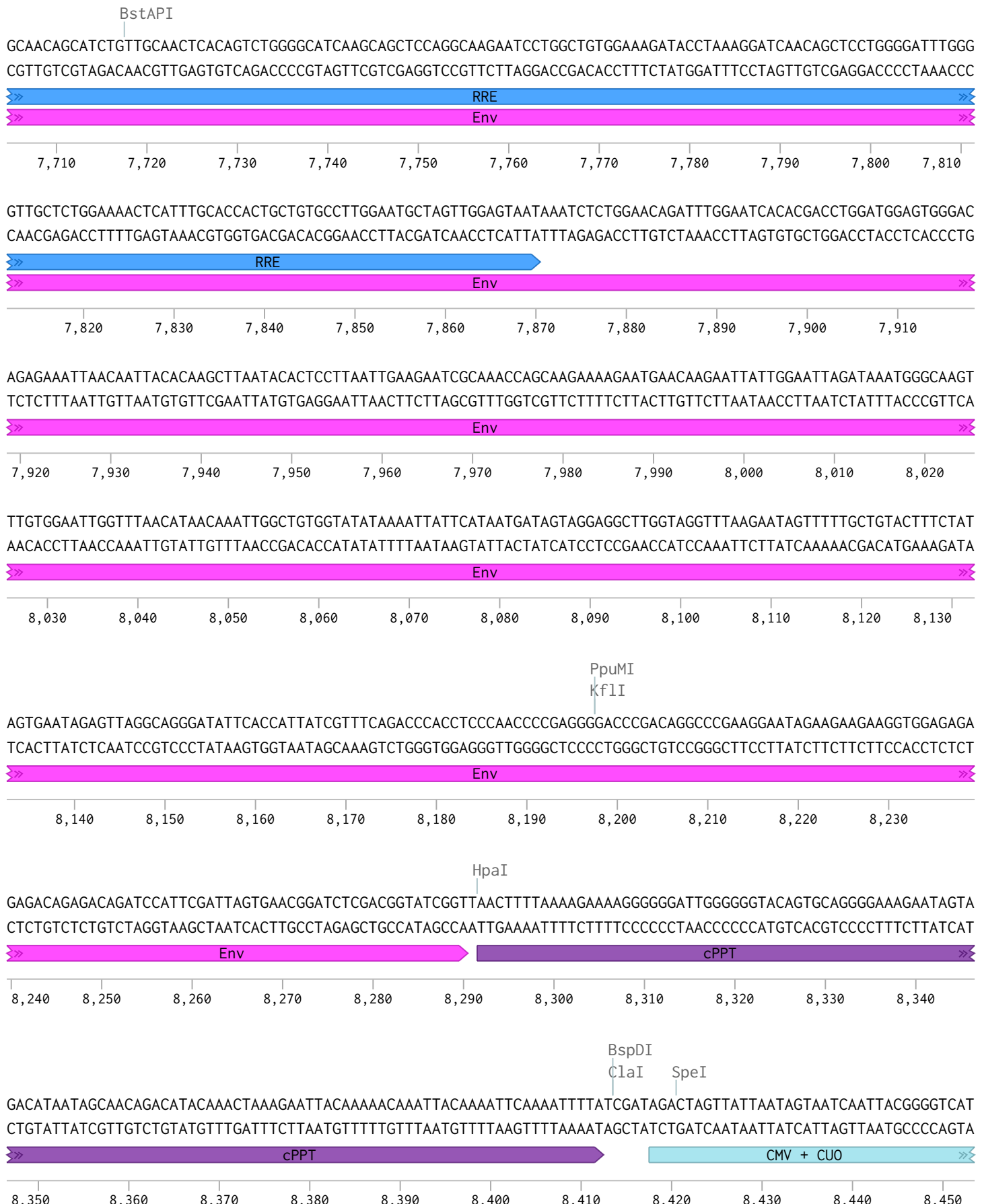
bArr2-HA-TEV219 pCDH-CuO-MCS-EF1 α -CymR-T2A-Bleo3 SparQ (10907 bp)



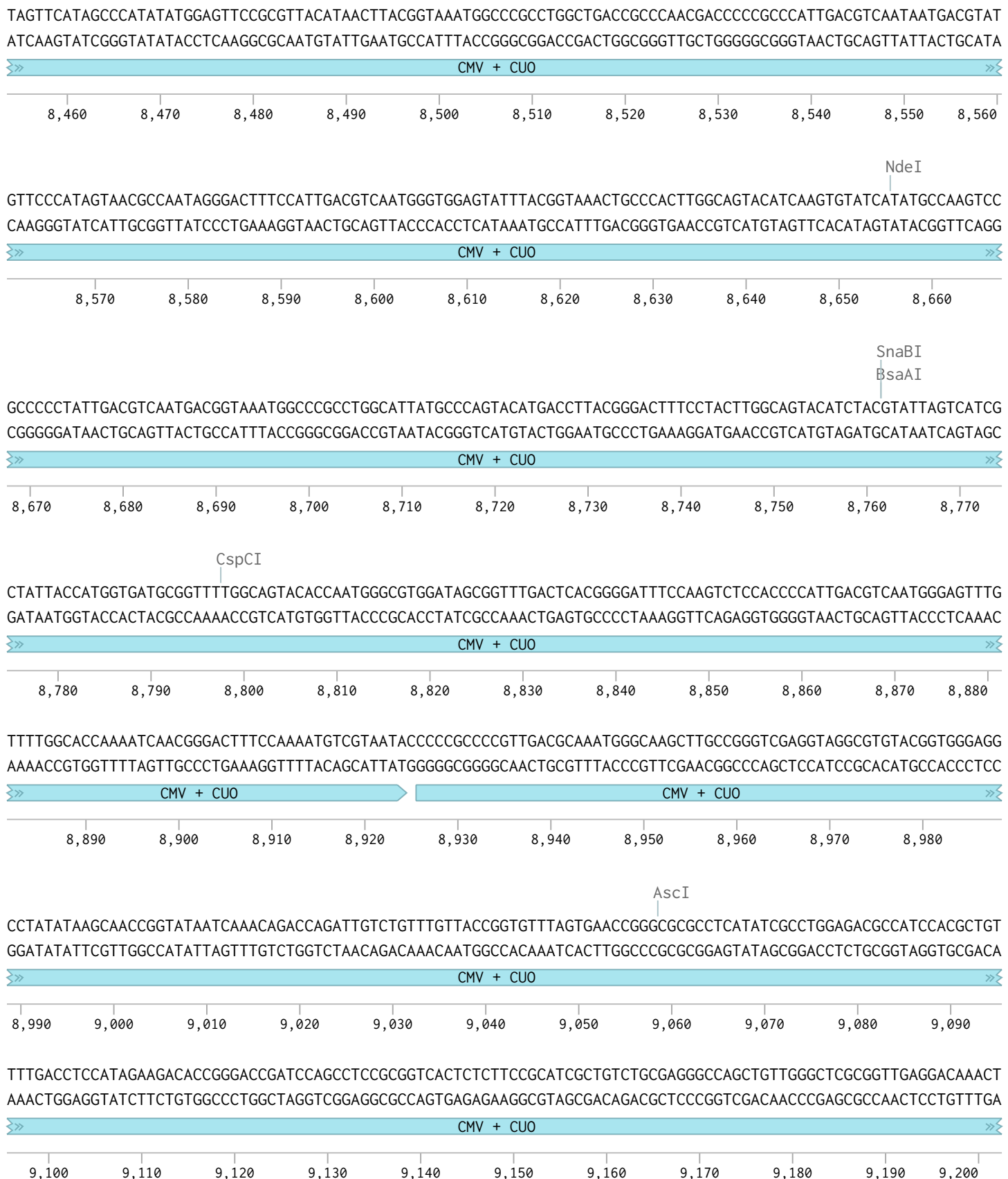
bArr2-HA-TEV219 pCDH-CuO-MCS-EF1 α -CymR-T2A-Bleo3 SparQ (10907 bp)



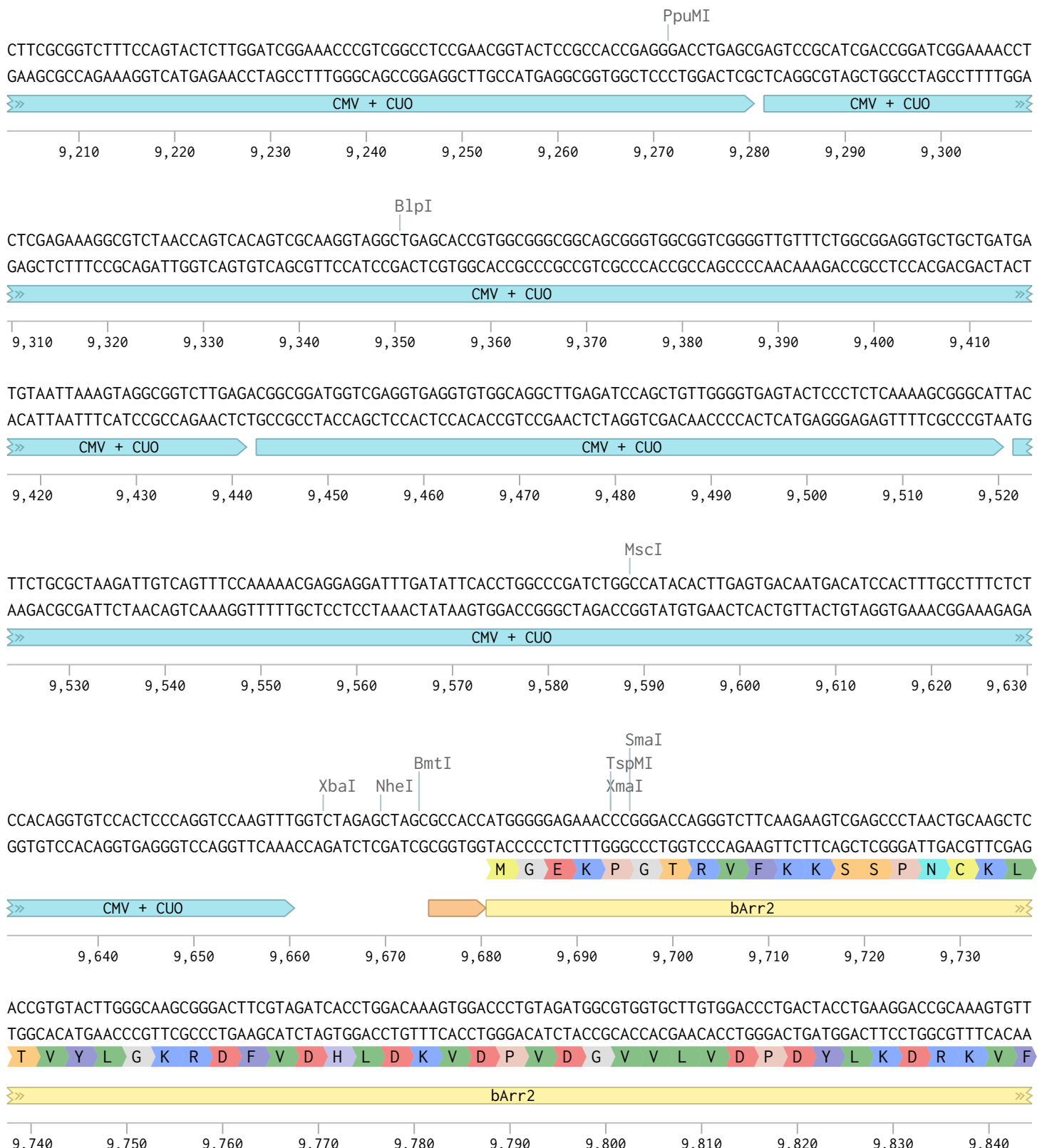
bArr2-HA-TEV219 pCDH-CuO-MCS-EF1 α -CymR-T2A-Bleo3 SparQ (10907 bp)



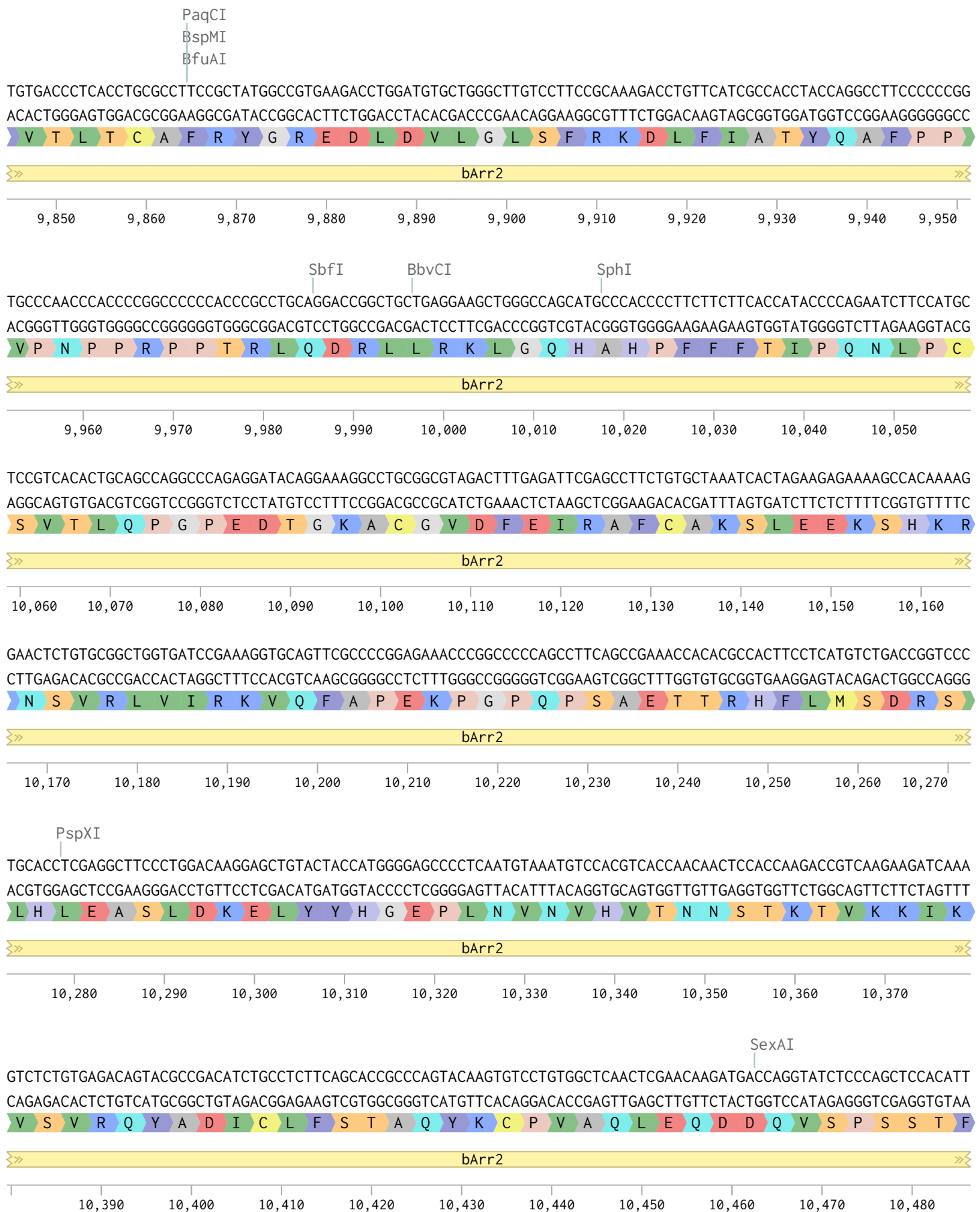
bArr2-HA-TEV219 pCDH-CuO-MCS-EF1 α -CymR-T2A-Bleo3 SparQ (10907 bp)



bArr2-HA-TEV219 pCDH-CuO-MCS-EF1 α -CymR-T2A-Bleo3 SparQ (10907 bp)



bArr2-HA-TEV219 pCDH-CuO-MCS-EF1 α -CymR-T2A-Bleo3 SparQ (10907 bp)

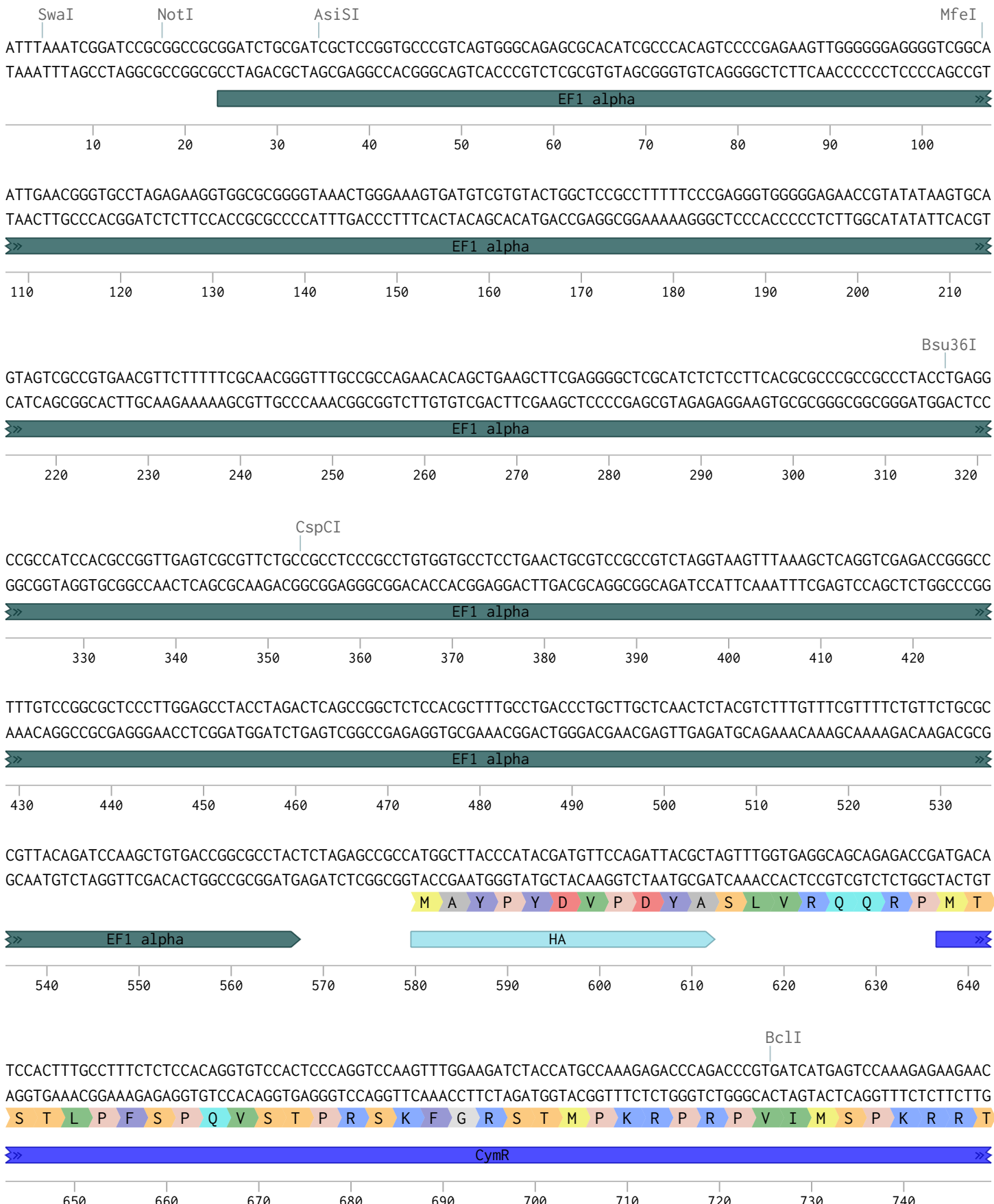


bArr2-HA-TEV219 pCDH-CuO-MCS-EF1 α -CymR-T2A-Bleo3 SparQ (10907 bp)

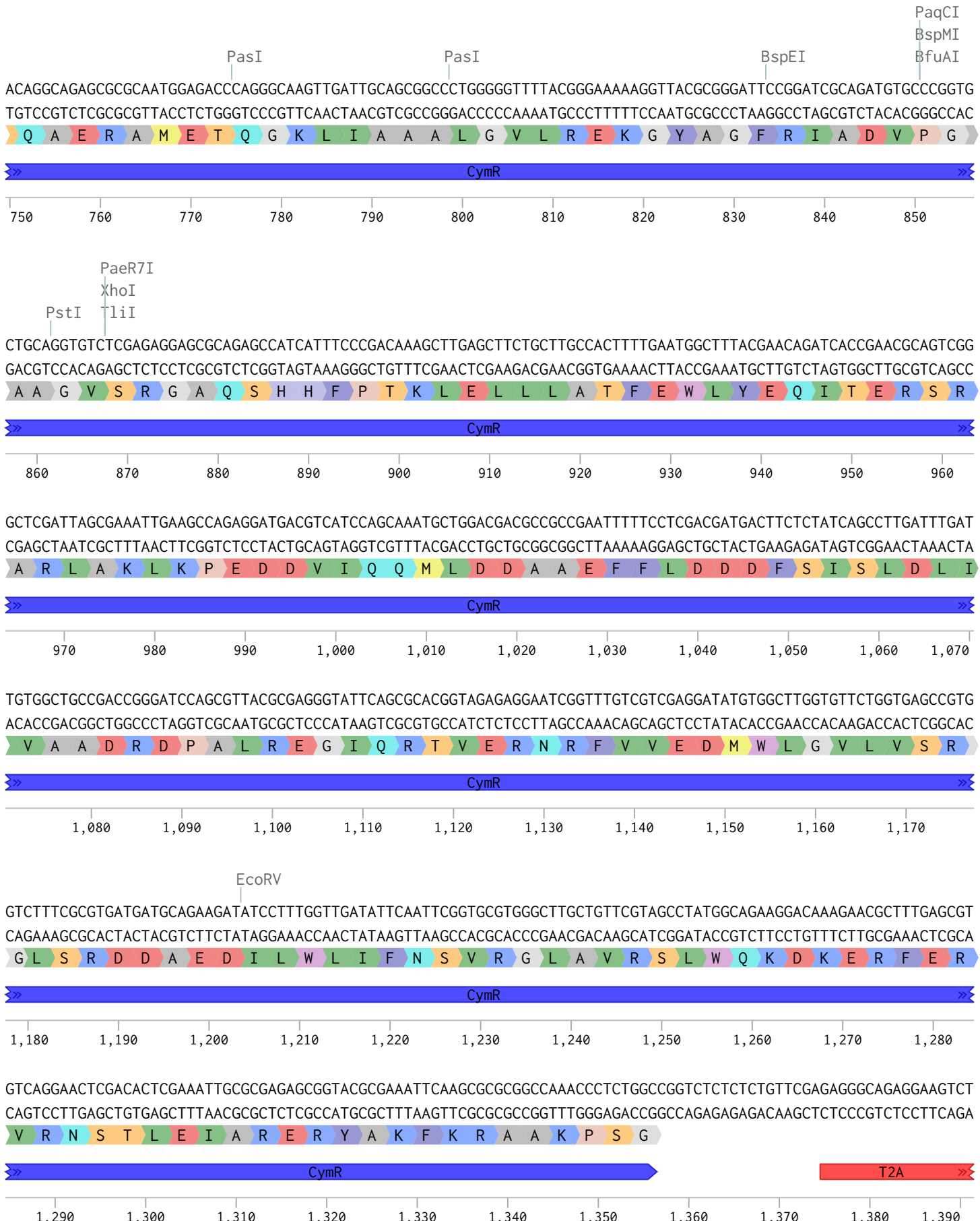


(from 1-749 bp)

Fyve-HA-TEV219 pCDH-CuO-MCS-EF1 α -CymR-T2A-Bleo3...



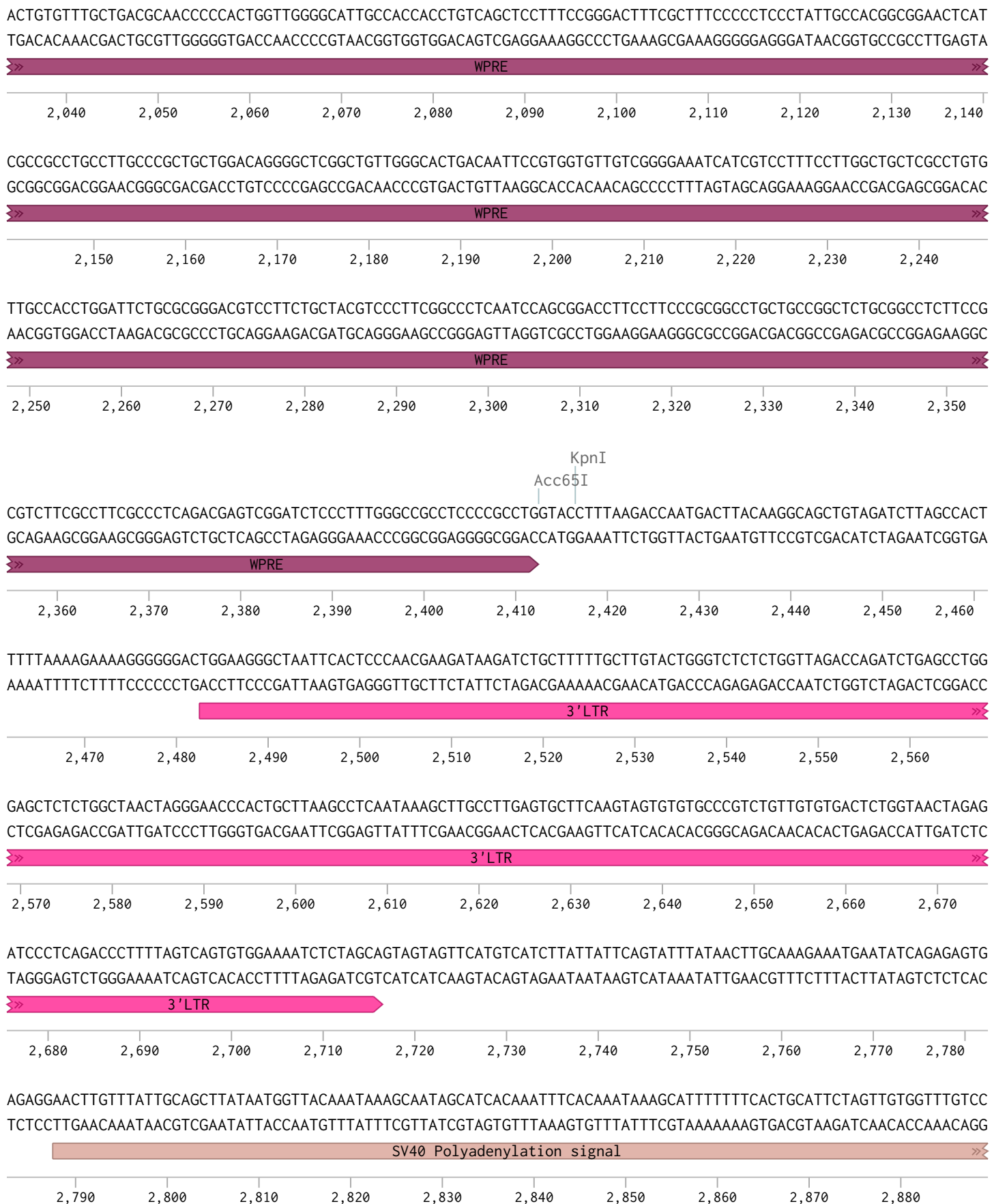
Fyve-HA-TEV219 pCDH-CuO-MCS-EF1 α -CymR-T2A-Bleo3 SparQ (10070 bp)



Fyve-HA-TEV219 pCDH-CuO-MCS-EF1 α -CymR-T2A-Bleo3 SparQ (10070 bp)



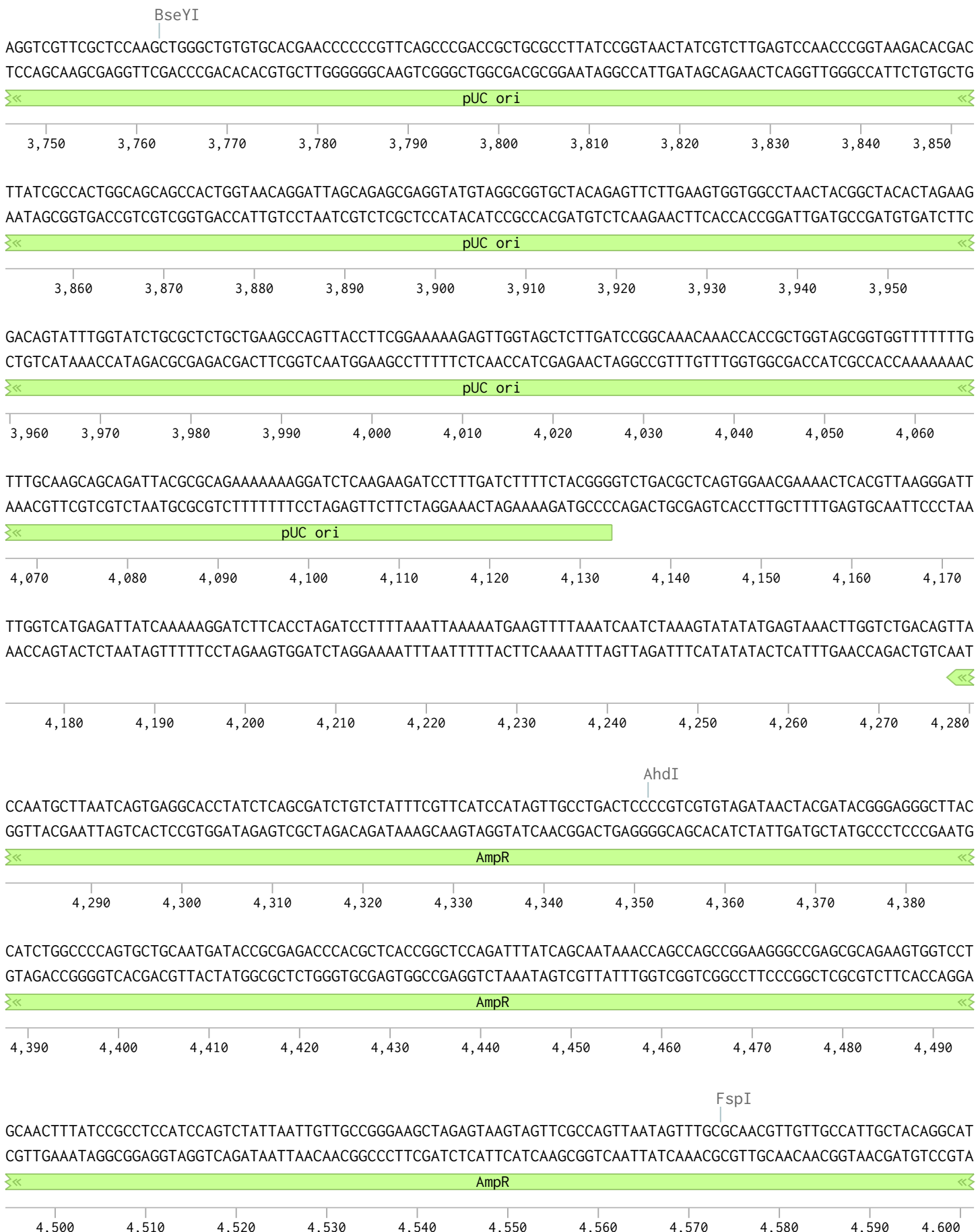
Fyve-HA-TEV219 pCDH-CuO-MCS-EF1 α -CymR-T2A-Bleo3 SparQ (10070 bp)



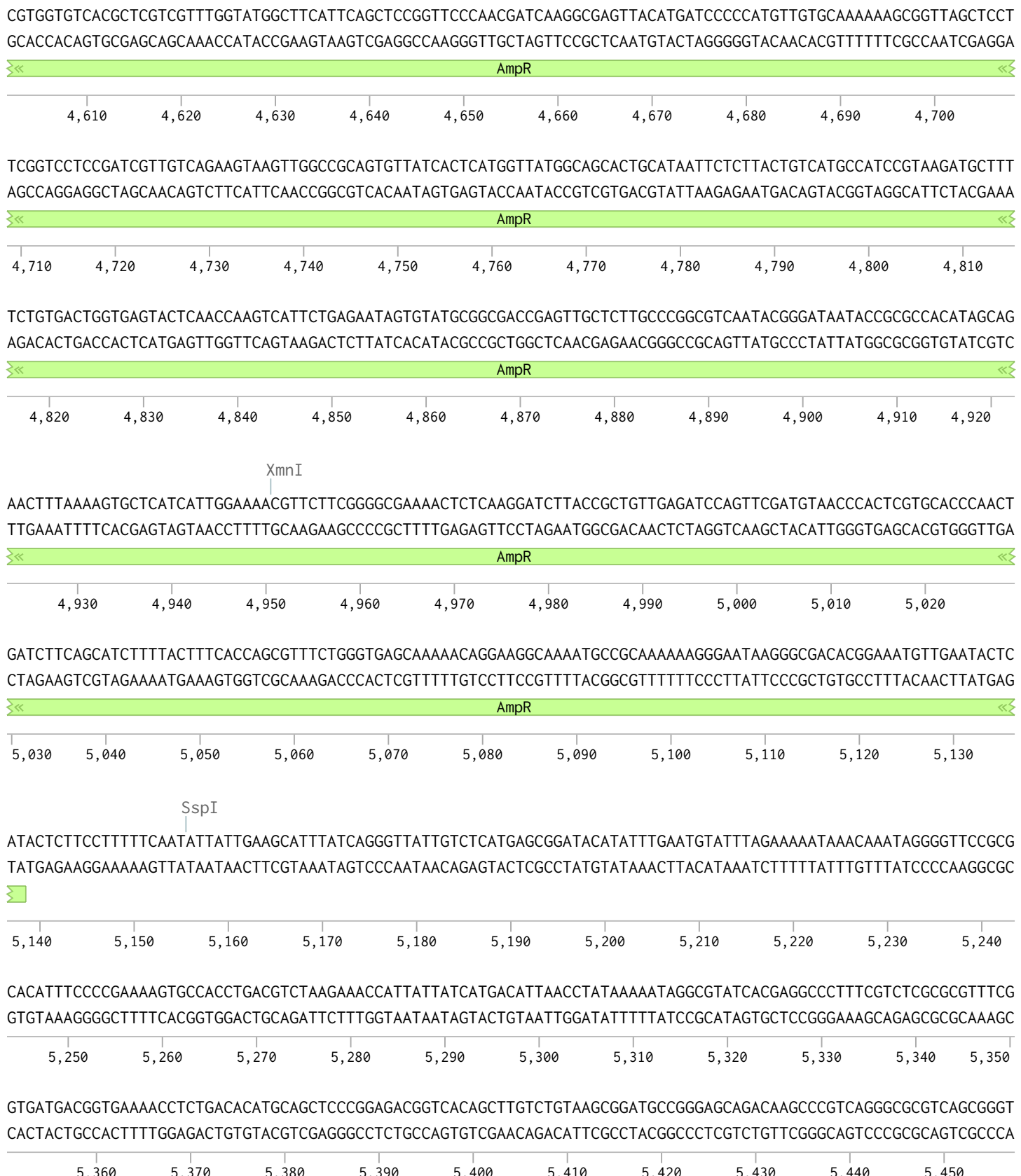
Fyve-HA-TEV219 pCDH-CuO-MCS-EF1 α -CymR-T2A-Bleo3 SparQ (10070 bp)



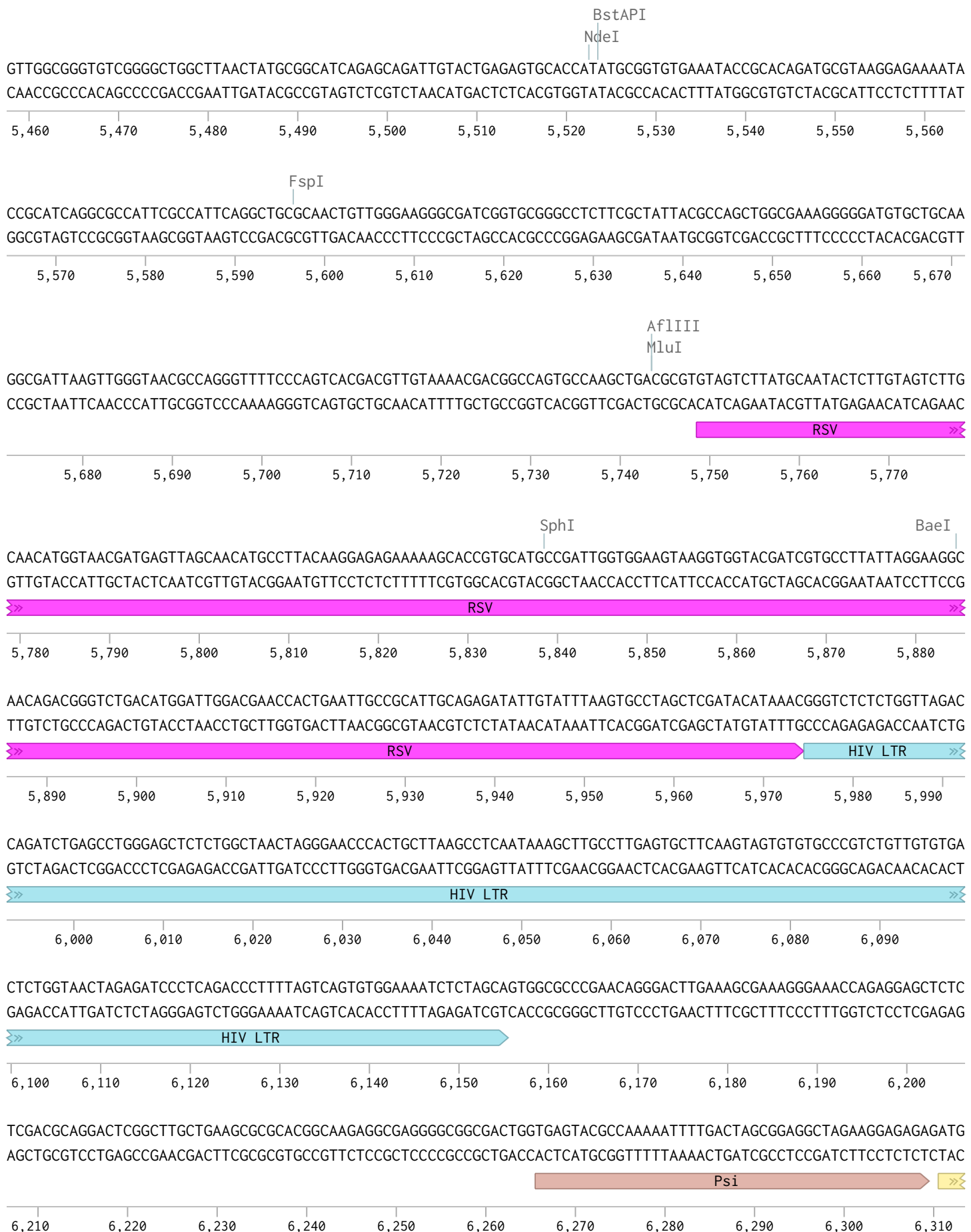
Fyve-HA-TEV219 pCDH-CuO-MCS-EF1 α -CymR-T2A-Bleo3 SparQ (10070 bp)



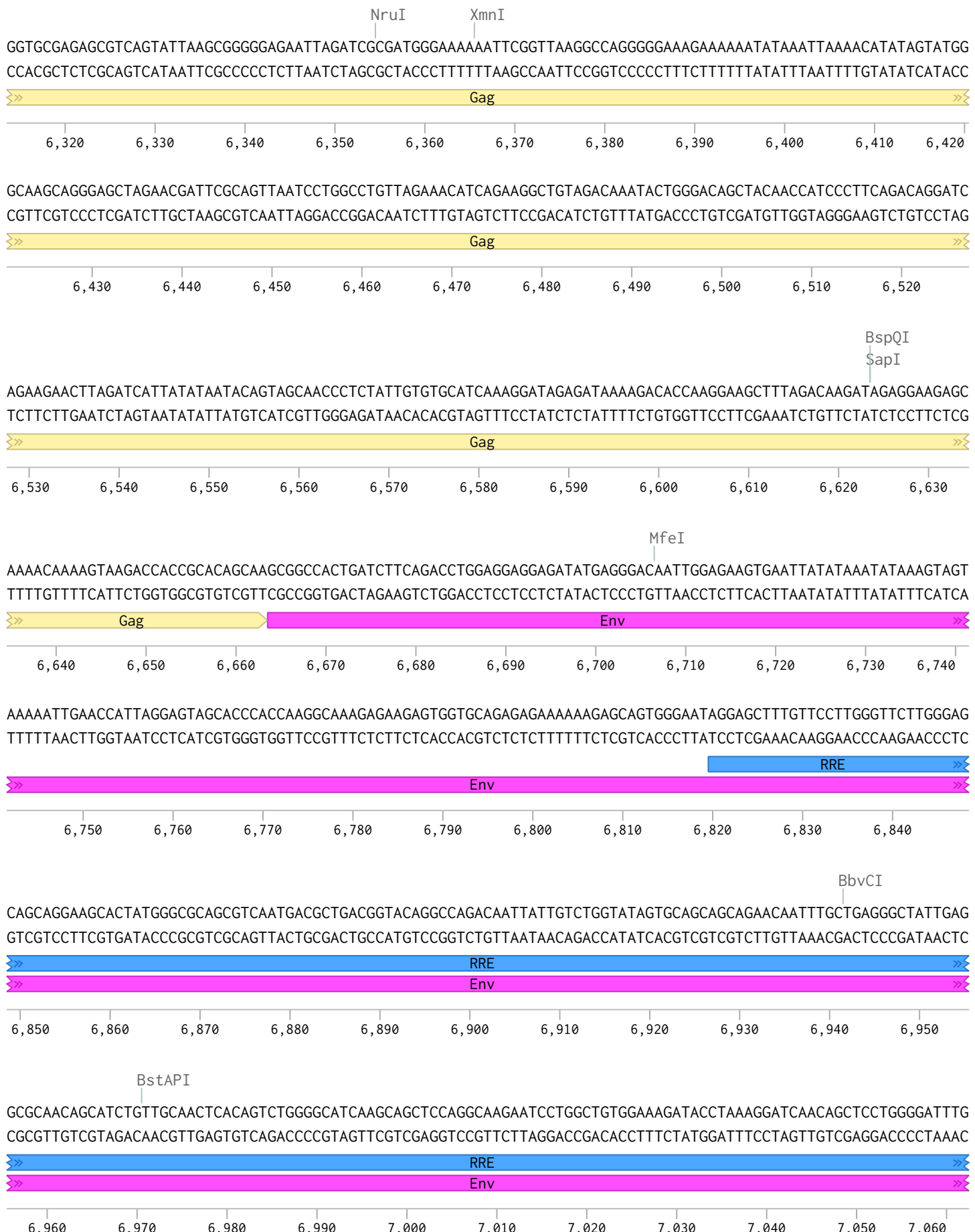
Fyve-HA-TEV219 pCDH-CuO-MCS-EF1 α -CymR-T2A-Bleo3 SparQ (10070 bp)



Fyve-HA-TEV219 pCDH-CuO-MCS-EF1 α -CymR-T2A-Bleo3 SparQ (10070 bp)



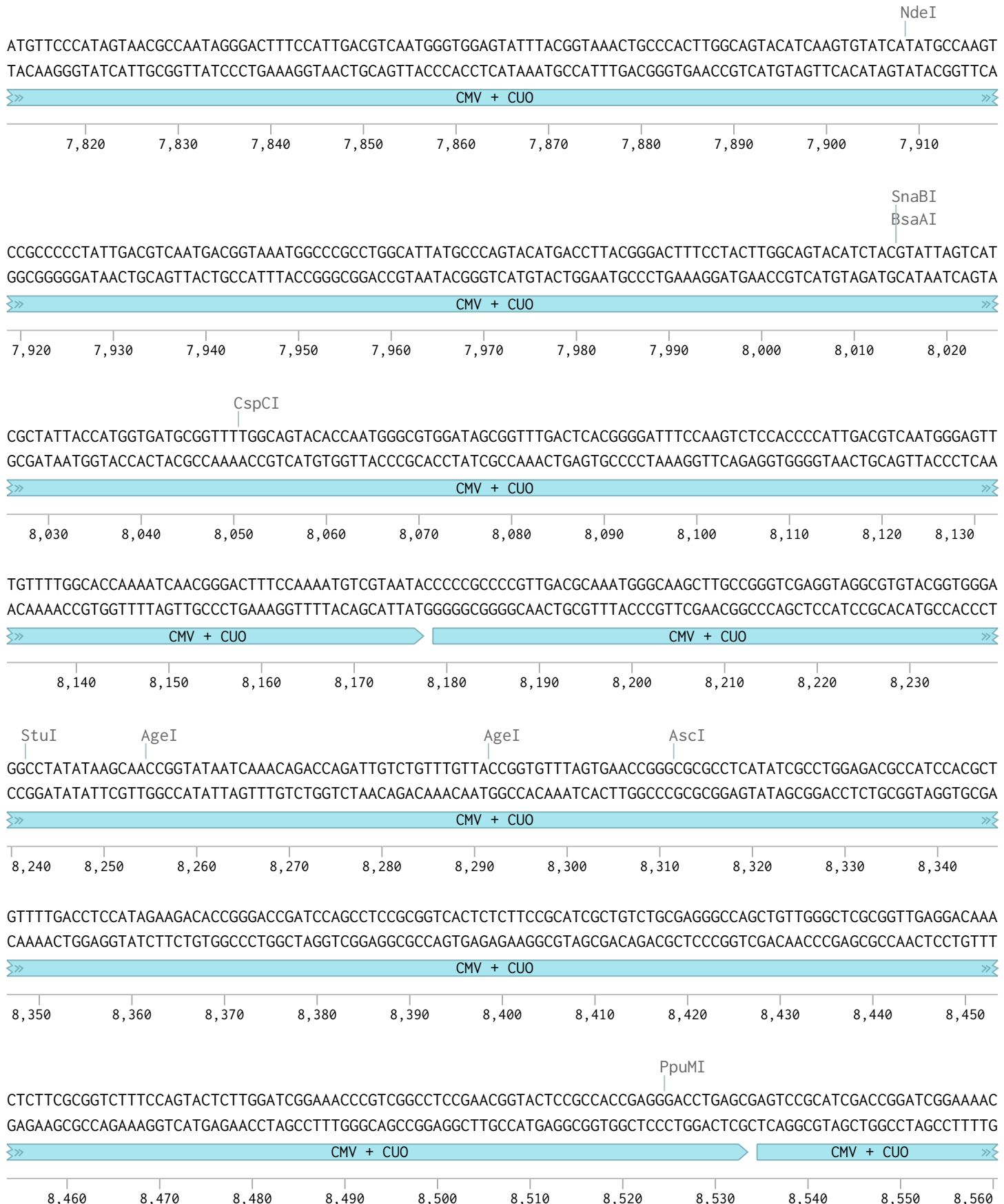
Fyve-HA-TEV219 pCDH-CuO-MCS-EF1 α -CymR-T2A-Bleo3 SparQ (10070 bp)



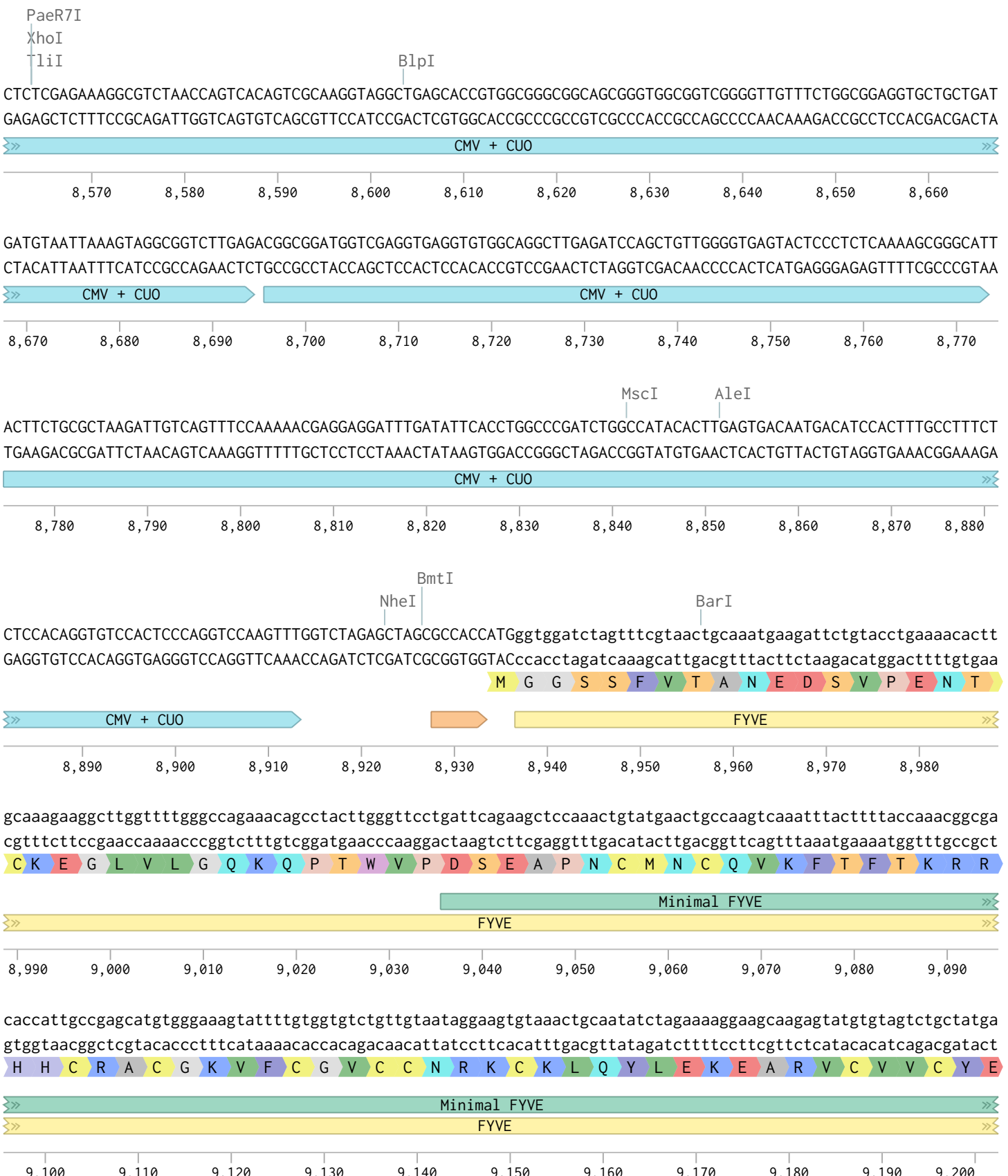
Fyve-HA-TEV219 pCDH-CuO-MCS-EF1 α -CymR-T2A-Bleo3 SparQ (10070 bp)



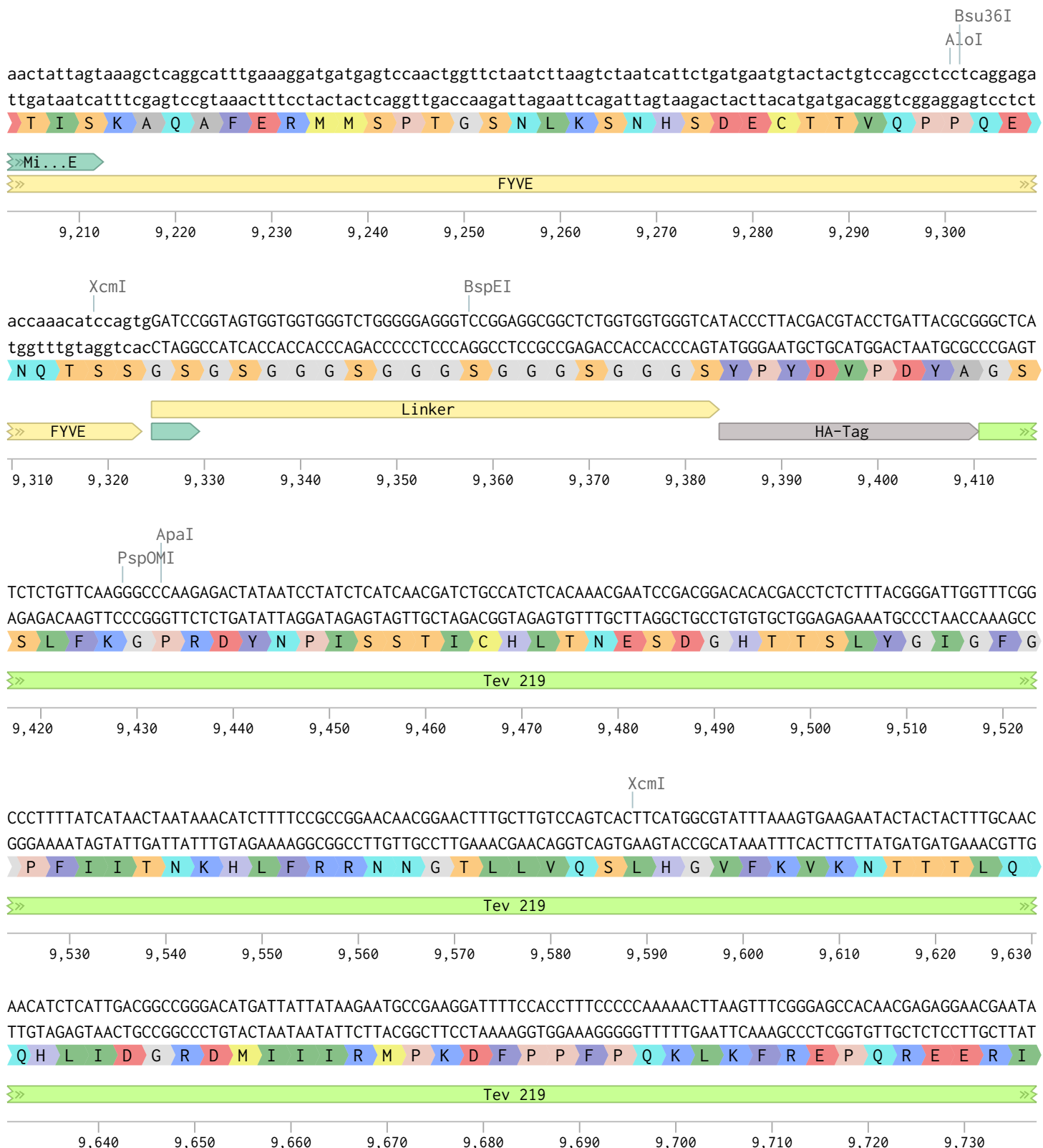
Fyve-HA-TEV219 pCDH-CuO-MCS-EF1 α -CymR-T2A-Bleo3 SparQ (10070 bp)



Fyve-HA-TEV219 pCDH-CuO-MCS-EF1 α -CymR-T2A-Bleo3 SparQ (10070 bp)



Fyve-HA-TEV219 pCDH-CuO-MCS-EF1 α -CymR-T2A-Bleo3 SparQ (10070 bp)



Fyve-HA-TEV219 pCDH-CuO-MCS-EF1 α -CymR-T2A-Bleo3 SparQ (10070 bp)

